ATOMIC HYDROGEN AND THE SURFACE OF LIQUID HELIUM

ACADEMISCH PROEFSCHRIFT

ter verkrijging van de graad van doctor
aan de Universiteit van Amsterdam,
op gezag van de Rector Magnificus
Prof. dr. P.W.M. de Meijer
in het openbaar te verdedigen in de Aula der Universiteit
(Oude Lutherse Kerk, ingang Singel 411, hoek Spui),
op dinsdag, 14 juni 1994 te 15.00 uur

door

Jacobus Johannes Berkhout

geboren te Amsterdam

Amsterdam MCMXCIV

Druk: Boek- en Offsetdrukkerij Letru, Helmond, 04920-37797

Promotor: prof. dr. J.T.M. Walraven
Commissie: prof. dr. A. Lagendijk
dr. T.W. Hijmans
prof. dr. B.J. Verhaar
prof. dr. J.J. Franse
prof. dr. A.W. Kleyn

Fakulteit der Natuur- en Sterrenkunde

The work in this thesis is part of the research program of the
Stichting voor Fundamenteel Onderzoek der Materie (FOM),
which is financially supported by the
Nederlandse Organisatie voor Wetenschappelijk Onderzoek (NWO),
and was carried out at the
Van der Waals–Zeeman Laboratorium der
Universiteit van Amsterdam
Valckenierstraat 65
1018 XE Amsterdam
The Netherlands

aan Renée

'You have employed an extraordinary mental process
to adduce what I now see to be limpid truth.'
'The process is called logic. It is not always dependable.'

— Jack Vance, *The Pnume*.

This thesis is based on the following articles:

Chapter 2:

J.J. Berkhout and J.T.M. Walraven, in *Spin-Polarized Quantum Systems*, edited by S. Stringari (World Scientific, Singapore, 1989), p. 201.

Chapter 3:

J.J. Berkhout, E.J. Wolters, R. van Roijen, and J.T.M. Walraven, Phys. Rev. Lett. **57**, 2387 (1986).

Chapter 4:

J.J. Berkhout, O.J. Luiten, I.D. Setija, T.W. Hijmans, T. Mizusaki, and J.T.M. Walraven, Phys. Rev. Lett. **63**, 1689 (1989).

Chapter 5:

J.J. Berkhout and J.T.M. Walraven, Phys. Rev. B **47**, 8886 (1993).

Chapter 6:

J.J. Berkhout, O.H. Höpfner, E.J. Wolters, and J.T.M. Walraven, in *Proceedings of the Eighteenth International Conference on Low Temperature Physics, Kyoto, Japan, 1987*, Jpn. J. Appl. Phys. **26**, Suppl. 26-3, 231 (1987).

Contents

List of Figures

Chapter 1

INTRODUCTION

"Begin at the beginning," the King said, very gravely,
"and go on till you come to the end: then stop."

— Lewis Carroll, *Alice's Adventures in Wonderland.*

In the periodic table of the elements hydrogen (H) is the first and thus the most simple. This element is the most abundant in the universe, making up about three-quarters of the mass of it. An atom of the most common hydrogen isotope consists of one proton and one electron. In interstellar space, most of this hydrogen is in the neutral atomic state. In the universe at large, atomic hydrogen is therefore a very common substance.

On earth atomic hydrogen does not exist under natural conditions. It is a chemically highly reactive substance, which may take part in lots of reactions. It even reacts with itself to form molecular hydrogen (H_2). The energy of this bond is about 52000 K (4.5 eV). The energy of the reaction from atomic to molecular hydrogen per unit mass is thus 214 MJ/kg, more than 27 times the energy per unit mass from the burning of coal, and about 17 times the energy per unit mass from the burning of molecular hydrogen. From an energetic point of view recombination of atomic hydrogen to molecular hydrogen is therefore very favorable. Low atom densities or selective population of hyperfine states may largely suppress this recombination. In interstellar space the density of the atomic hydrogen is sufficiently low (of the order of 1 atm cm^{-3})[1] for the lifetime of the atomic gas to be orders of magnitude more than the age of the universe.

Normal molecular hydrogen is an ordinary gas with a density of 0.09 $\mathrm{kg\,m}^{-3}$ at normal temperature and pressure, a melting point of 14.0 K, a boiling point of 20.4 K, and a critical temperature of 33.3 K. Atomic hydrogen is a very different substance. The difference to be expected is illustrated by the behavior of the next element in the periodic structure, helium.

While almost all substances solidify at low temperatures, the natural isotopes of helium (the common ^{4}He and the rare ^{3}He) do not, but stay liquid under their own vapor pressure down to the lowest temperature. In this liquid the atoms are bound, but not localized. This is due to the large zero-point kinetic energy compared to the attractive potential energy due to the Van der Waals interaction between atoms in a many-body system, *i.e.* it has a large De Boer parameter $\Lambda^* \equiv h/(\sqrt{m\epsilon}\sigma)$, where m is the mass of the atom, ϵ the depth of the interatomic potential, and σ the hard sphere diameter. For ^{4}He $\Lambda^* = 2.677$, while for ^{4}He $\Lambda^* = 3.084$.[2] If cooled down below the transition temperature of 2.17 K, ^{4}He displays a superfluid transition, which is a manifestation of the quantum nature of this liquid. However, because it is a liquid, the atoms in liquid ^{4}He strongly interact, making theoretical ib initio calculations impossible.

As compared to helium, hydrogen has an even larger De Boer parameter, $\Lambda^* = 4.66$. This value is larger than the critical value of $\Lambda^*_{\mathrm{crit}} \equiv 4.21$,[3] for which the ground state energy of the system is positive, and atomic hydrogen should therefore remain gaseous, even down to 0 K, where under pressures of about 80 bar[4] it would condense directly to a solid state.[3] It therefore would be a weakly interacting quantum system, in contrast to the liquid helium, and therefore much easier to describe with ab initio theory. As the H atom consists of two particles, each with spin $\frac{1}{2}$, it should observe Bose statistics as long as the atom may

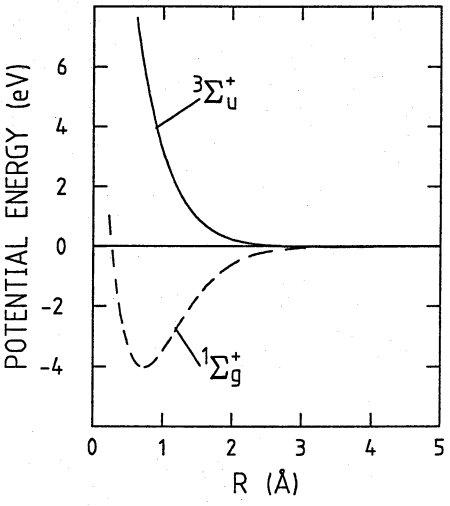

Figure 1.1:
The singlet and triplet interatomic potentials of hydrogen according to calculations of Kolos and Wolniewicz.[12–15]

be considered as an agglomerate particle. This Bose character of the hydrogen gas was experimentally verified.[5,6]

The first to point out the interesting properties of atomic hydrogen as a many-body system was Hecht in 1959, who also suggested the polarization of the electron spins of the atoms by a large magnetic field to achieve stabilization against recombination.[7] Apparently this article had not attracted attention until the early 1970's,[3,8–11] when the interest in this system was renewed because of the possible technological importance as rocket fuel.[9] However, experimental research was not possible until the conditions were found under which the atomic hydrogen did not immediately recombine to molecules.

If we neglect the hyperfine interactions, which for our purposes is justified, the interaction of hydrogen atoms may be described in terms of the singlet ($^1\Sigma_g^+$) (when the electron spins are anti-parallel), and the triplet ($^3\Sigma_u^+$) potential (when the electron spins are parallel) (see Fig. 1.1). While the singlet potential has a very deep minimum of 55100 K in which a large number of bound states exist, the triplet potential has a very shallow one (6.46 K), which does not support any bound state.[12,14,15] In first order, polarization of the electron spins therefore suppresses the recombination of the hydrogen.

The nuclear spin complicates this simple model. As may be seen in Fig. 1.2, the existence of this nuclear spin gives rise to four possible quantum states for the atoms, and thus to a hyperfine splitting. The four quantum states in order of increasing energy are:

$$\begin{aligned} |a\rangle &= \sin\theta\ |\uparrow\downarrow\rangle - \cos\theta\ |\downarrow\uparrow\rangle \\ |b\rangle &= |\downarrow\downarrow\rangle \\ |c\rangle &= \cos\theta\ |\uparrow\downarrow\rangle + \sin\theta\ |\downarrow\uparrow\rangle \\ |d\rangle &= |\uparrow\uparrow\rangle \end{aligned} \tag{1.1}$$

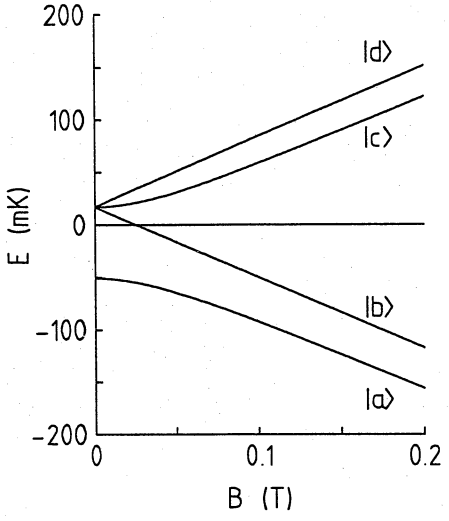

Figure 1.2:
The hyperfine energies and states of atomic hydrogen as a function of magnetic field B.

Here θ is defined by $\tan(2\theta) = a/(g_e\mu_B + g_n\mu_n)B$, where a is the hyperfine coupling constant,[16] $a/h = 1420.405751733(1)$ MHz, g_e and g_n are the electronic and nuclear g-factors, μ_B and μ_n the Bohr and nuclear magneton, and B the magnetic field. For high magnetic fields the approximation $\sin\theta = \epsilon$ and $\cos\theta = 1$ are valid, with $\epsilon = a/\{2(g_e\mu_B + g_n\mu_n)B\}$. Two of these states, the $|b\rangle$ and $|d\rangle$ states, are pure states, *i.e.* eigenstates of the free atom Hamiltonian. However, the other states ($|a\rangle$ and $|c\rangle$) are mixed: some amount of the anti-parallel electron spin state is mixed in. Recombinations involving atoms in the $|a\rangle$ state are thus not completely suppressed. A gas in which the electron spins are fully polarized is denoted by H$\downarrow$, where only the $|a\rangle$ and $|b\rangle$ are populated, or H$\uparrow$, where only the $|c\rangle$ and $|d\rangle$ states are populated.

Even if only one of the pure states is populated, recombination may still occur. Possible processes for this recombination are direct three-body recombination and two-body magnetic dipole–dipole relaxation followed by recombination.[17] The relaxation process can be nuclear dipolar relaxation or electronic dipolar relaxation. For a pure gas of $|d\rangle$ states (H$\uparrow\uparrow$) the electronic dipolar relaxation is dominant. The relaxation process is suppressed or enhanced by the factor of $e^{-\Delta/mk_BT}$, where Δ is the energy difference between the spin states. For a sufficiently high magnetic field and low temperatures the thermal energy of the atoms is less than Δ, so in a gas of pure $|b\rangle$ atoms (H$\downarrow\downarrow$) electronic relaxation is exponentially suppressed and nuclear relaxation becomes dominant. This is the reason that a H$\downarrow$-gas is more stable than a H$\uparrow$-gas.

To create a stable gas it is therefore advantageous to cool down the atoms to low temperatures. This is also necessary to trap the atoms in a walls-free geometry: the thermal energy of the atoms should then be lower than the depth of the trapping potential. Low

temperatures also are necessary to observe any quantum behavior of the atoms. However, these low temperatures pose additional problems. The binding energy of atomic hydrogen on almost all surfaces is much higher than 10 K, leading to massive adsorption of the atoms on these surfaces at low temperatures. The high surface density then leads to rapid recombination of the atoms.

The experimental work on atomic hydrogen started in earnest in 1979, when on November 1st it was first stabilized by I.F. Silvera and J.T.M. Walraven.[18] To suppress the rapid surface recombination of the hydrogen atoms they coated all surfaces of the experimental cell with superfluid liquid helium. The binding energy of the hydrogen atoms is 1 K on ^{4}He and 0.4 K on ^{3}He surfaces,[19] which is low enough to prepare a stable atomic hydrogen gas at temperatures down to below 100 mK. Since this time, a lot of research has been done on the hydrogen gas. After the initial stabilization, the recombination processes were examined in detail.[20] The binding energies on ^{4}He and ^{3}He surfaces were measured.[19] Attempts were made to achieve Bose–Einstein condensation by compressing the gas by a piston,[21] by hydrostatic pressure,[22–24] or by local magnetic compression through the use of a magnetic needle.[25] However, these attempts failed due to the increase of surface recombination with increasing density and the associated heating.

Starting in 1986, after a proposal by Hess,[26] efforts have therefore been made to trap hydrogen atoms in a surface free environment by using magnetic field gradients acting on the electron spins. Proposals were made for the construction of static magnetic traps,[26] microwave traps,[27] dynamic magnetic traps,[28] and magnetic storage rings.[29] Thus far, hydrogen has only been trapped by the confinement of atoms in the low field seeking $|c\rangle$ and $|d\rangle$ states by static magnetic traps.[30,31] The more stable high field seeking $|a\rangle$ and $|b\rangle$ states can not be trapped in a static magnetic field, as the Maxwell–Lorentz equations forbid the existence of a local magnetic field maximum in free space.[32]

Reviews of the work on atomic hydrogen have been written by Greytak and Kleppner,[33] which in particular deals with the thermodynamic properties, Silvera and Walraven,[16] concentrating on the experimental work up to 1985, Walraven,[34] dealing with the interaction of the H-atom with the liquid-helium surface, and Silvera and Reynolds,[17] who concentrate on the efforts to observe Bose–Einstein condensation and the Kosterlitz–Thouless transition.

In order to create a sample of stabilized atomic hydrogen the presence of helium-film-coated walls is of crucial importance. Below 2.17 K helium becomes superfluid. If enough helium is present in the cell, all surfaces will therefore be covered by a liquid helium film (except in the case of some unusual materials[35]). Without the use of a trap, the hydrogen atoms are in direct contact with the walls of the experimental cell, and without a liquid helium film on these walls the large binding energy on the surface leads to high surface densities and subsequently to high recombination rates.[36] With a magnetostatic trap, in order to trap the atoms some means of lowering the kinetic energy of atoms in the trap is

necessary. Usually, the trapping of neutral alkali atoms is achieved by laser-cooling. While the mechanism of laser-cooling is now available,[37] it is not possible to use it to trap atomic hydrogen for want of (semi-)continuous lasers at the Lyman-α wavelength, so all experiments up to date have used thermal accommodation with the walls and collisional exchange of kinetic energy within the trap to achieve trapping of the atoms. This mechanism is only available for atomic hydrogen, because it demands a potential energy well depth of the trap which is higher than the surface adsorption energy. The interaction of H atoms with the liquid-helium film is therefore a subject of interest for these experiments.[34]

Besides lowering the adsorption energy of all surfaces in the cell and the role played in cooling the atoms helium has been used for compression of the hydrogen as well. In the experiment in which the atomic hydrogen was first stabilized, the experimental cell had an open connection with the room temperature dissociator. In order to minimize the heat load on the cell, the helium film was removed from the surface at an intermediate cooling stage, creating a flow of helium vapor back to the cold part of the cell. This flux of helium vapor acted as a pump, moving the hydrogen atoms towards the sample space. Compression ratio's of about a factor 80 were hereby achieved.[38] This geometry is still used at present.[39,40] In the compression experiments the helium acted as confining surface for the atomic hydrogen.

The work described in this thesis concerns the interaction of the hydrogen atoms with liquid-helium surfaces. The original motivation for the experiments was the need to determine the effects of this interaction for the interpretation of the compression experiments and the realization of the magnetic field trap experiments.[22,31] However, it soon became clear that the interaction between atoms and liquid surface was itself a very interesting subject.

Scattering of particles from surfaces has been and still is an important technique in physics. Specular scattering of hydrogen and helium beams from (speculum metal) solid surfaces was first observed by Knauer and Stern[41] and Estermann and Stern[42] respectively. Subsequently molecular and atomic beams have been extensively used to study a wide range of phenomena.[43–45] The theory of scattering in the extreme low temperature limit has been of interest since the early days of quantum mechanics, as may be illustrated by the series of articles on this subject written in 1935/1936 by Lennard-Jones and co-workers.[46–49]

Most surface scattering experiments have been done with crystal surfaces. While solid state surfaces suffer from corrugations caused by adsorption of gaseous atoms or molecules and from corrugations due to imperfections in the crystal structure, liquid surfaces do not suffer from these effects. However, in general the vapor pressure above a liquid surface prevents its use in a scattering experiment. A surface which overcomes this limitation is the surface of liquid helium at low temperatures. Neutron[50] and helium atom[51] scattering from these surfaces have been studied. Neutral hydrogen atoms as scattering particles have the advantageous properties of high reflection coefficients and large thermal wavelengths, due to their low mass.

This thesis is based on articles previously published. Theory concerning the sticking and accommodation of hydrogen atoms on the ^{4}He surface is summarized in Chapter 2, together with a discussion of experimental work concerning this topic. The conclusions from theory are that the hydrogen atoms interact with the surface by exciting one ripplon on the surface, a ripplon being an elementary surface wave. For low enough temperatures, atoms either excite a ripplon and enter a bound state on the surface, the sticking process, or else just scatter (near-)elastically. As momentum parallel to the surface must be conserved, the elastic scattering leads to specular scattering. Moreover, for low enough temperatures, the sticking coefficient, that is, the probability for an atom to enter a bound state at a surface collision, scales as the square root of temperature. Thus, for $T \to 0$, the sticking coefficient should go to zero. However, at these temperatures the sticking coefficient may be largely dominated by substrate effects.[52,53]

An experiment using a capillary flow method described in Chapter 3 measured the sticking coefficient as function of temperature and found a linear dependence on T. The results show fair agreement with theory, although the temperature range in which these measurements were done was too high to observe the predicted square root dependence on temperature. Most of the discrepancy between older experiments was resolved to be the result of this linear temperature dependence.

The low value of the sticking coefficient as found in the first experiment was confirmed in the mirror reflection experiment described in Chapter 4. The experiment shows that for low enough temperatures of the atoms it is possible to construct highly reflective mirrors, which might enable some very exciting atomic interference experiments. Recently such a mirror has been applied to increase the flux in an apparatus to produce a spin-polarized hydrogen beam source to be used in high energy physics.[54] While the angular resolution of the mirror reflection experiment was small enough to in principle allow the detection of quasi-elastic scattering, the uncertainty in the value of the sticking coefficient prevented the proof or disproof of the existence of this type of scattering.

Both the capillary flow experiment and the mirror reflrection experiment are thoroughly discussed in Chapter 5. Finally, Chapter 6 describes the main detection device used in these experiments.

References

[1] A.D. Fokker and C. de Jager, in *Sterrenkunde*, vol. 4, edited by C. de Jager (Wetenschappelijke Uitgeverij Amsterdam, Amsterdam, 1969), p. 132.

[2] L.H. Nosanow, L.J. Parish, and F.J. Pinski, Phys. Rev. B **11**, 191 (1975).

[3] M.D. Miller, L.H. Nosanow, and L.J. Parish, Phys. Rev. Lett. **35**, 581 (1975).

[4] R.L. Danilowicz, J.V. Dugan, and R.D. Etters, J. Chem. Phys. **65**, 498 (1976).

[5] A. Lagendijk, G. van Yperen, and J.T.M. Walraven, J. Phys. Lett. (Paris) **45**, L-929 (1984).

[6] L.P. Lévy and A.E. Ruckenstein, Phys. Rev. Lett. **52**, 1512 (1984).

[7] C.E. Hecht, Physica **25**, 1159 (1959).

[8] J.V. Dugan, Jr. and R.D. Etters, J. Chem. Phys. **59**, 6171 (1973).

[9] R.D. Etters, J.V. Dugan, Jr., and R.W. Palmer, J. Chem. Phys. **62**, 313 (1975).

[10] W.C. Stwalley and L.H. Nosanow, Phys. Rev. Lett. **36**, 910 (1976).

[11] A.J. Berlinsky, Phys. Rev. Lett. **39**, 359 (1977).

[12] W. Kolos and L. Wolniewics, J. Chem. Phys. **43**, 2429 (1965).

[13] W. Kolos and L. Wolniewics, J. Chem. Phys. **49**, 404 (1968).

[14] W. Kolos and L. Wolniewics, Chem. Phys. Lett. **24**, 457 (1974).

[15] W. Kolos and L. Wolniewics, J. Mol. Spectrosc. **54**, 303 (1975).

[16] I.F. Silvera and J.T.M. Walraven, in *Progress in Low Temperature Physics*, edited by D.F. Brewer (North-Holland, Amsterdam, 1986), Vol. **X**, p. 139.

[17] I.F. Silvera and M. Reynolds, J. Low Temp. Phys. **87**, 343 (1992).

[18] I.F. Silvera and J.T.M. Walraven, Phys. Rev. Lett. **44**, 164 (1980).

[19] For a compilation of measurements of the binding energy og H on He see W.N. Hardy, M.D. Hürlimann, and R.W. Cline, in *Proceedings of the Eighteenth International Conference on Low Temperature Physics, Kyoto, Japan, 1987*, Jpn. J. Appl. Phys. **26**, Suppl. 26-3, 2065 (1987).

[20] For a review of the experimental work on the recombination processes see I.F. Silvera and J.T.M. Walraven, in *Progress in Low Temperature Physics*, edited by D.F. Brewer (North-Holland, Amsterdam, 1986), Vol. **X**, p. 139.

[21] D.A. Bell, H.F. Hess, G.P. Kochanski, S. Buchman, L. Pollack, Y.M. Xiao, D. Kleppner, and T.J. Greytak, Phys. Rev. B **34**, 7670 (1986).

[22] R. Sprik, J.T.M. Walraven, and I.F. Silvera, Phys. Rev. B **32**, 5668 (1985).

[23] T. Tommila, S. Jaakkola, M. Krusius, K. Salonen, and E. Tjukanov, in *Proceedings of the Seventeenth International Conference on Low Temperature Physics, LT-17, Karlsruhe, West Germany, 1984*, edited by U. Eckern, A. Schmid, W. Weber, and H. Wühl (North-Holland, Amsterdam, 1984), p. 545.

[24] J.D. Gillaspie, I.F. Silvera, and J.S. Brooks, Phys. Rev. B **38**, 9231 (1988).

[25] E. Tjukanov, A.Y. Katunin, A.I. Safonov, P. Arvela, M. Karhunen, B.G. Lazarev, G.V. Shlyapnikov, I.I. Lukashevich, and S. Jaakkola, Physica B **178**, 129 (1992).

[26] H.F. Hess, Phys. Rev. B **34**, 3476 (1986).

[27] C.C. Agosta and I.F. Silvera, in *Spin-Polarized Quantum Systems*, edited by S. Stringari (World Scientific, Singapore, 1989), p. 254.

[28] R.V.E. Lovelace, C. Mehanian, T.J. Tommila, and D.M. Lee, Nature (London) **318**, 30 (1985).

[29] D. Thompson, R.V.E. Lovelace, and D.M. Lee, J. Opt. Soc. Am. B **6**, 2227 (1989).

[30] H.F. Hess, G.P. Kochanski, J.M. Doyle, N. Masuhara, D. Kleppner, and T.J. Greytak, Phys. Rev. Lett. **59**, 672 (1987).

[31] R. van Roijen, J.J. Berkhout, S. Jaakkola, and J.T.M. Walraven, Phys. Rev. Lett. **61**, 931 (1988).

[32] W.H. Wing, Prog. Quant. Electron. **8**, 181 (1984).

[33] T.J. Greytak and D. Kleppner, in *New Trends in Atomic Physics*, vol. 2, Les Houches 1982, edited by G. Grynberg and R. Stora (North-Holland, Amsterdam, 1984), p. 1125.

[34] J.T.M. Walraven, in *Fundamental Systems in Quantum Optics*, edited by J. Dalibard, J.M. Raimond and J. Zinn-Justin (Elsevier, Amsterdam, 1992) p. 485.

[35] E. Cheng, M.W. Cole, J. Dupont-Roc, W.F. Saam, and J. Treiner, Rev. Mod. Phys. **65**, 557 (1993).

[36] J.T.M. Walraven, E.R. Eliël, and I.F. Silvera, Phys. Lett. **66A**, 247 (1978).

[37] I.D. Setija, H.G.C. Werij, O.J. Luiten, M.W. Reynolds, T.W. Hijmans, and J.T.M. Walraven, Phys. Rev. Lett. **70**, 2257 (1993).

[38] J.T.M. Walraven and I.F. Silvera, Phys. Rev. Lett. **44**, 168 (1980).

[39] M. Mertig, A.V. Levkovitch, V.G. Luppov, and Y.K. Pilipenko, Rev. Sci. Instrum. **63**, 2220 (1992).

[40] M. Cornut and P.J. Nacher, J. Low Temp. Phys. **89**, 731 (1992).

[41] F. Knauer and O. Stern, Zeits. f. Phys. **53**, 799 (1929).

[42] L. Estermann and O. Stern, Zeits. f. Phys. **61**, 95 (1930).

[43] O. Stern, in the series *Untersuchungen zur Molecularstrahlmethode aus dem Institut für physikalische Chemie der Hamburgischen Universität*, Zeitschrift für Physik, 1926 onward.

[44] R.G.J. Fraser, *Molecular Rays* (Cambridge University Press, Cambridge, 1931).

[45] N.F. Ramsey, *Molecular Beams* (Oxford University Press, London, 1985).

[46] J.E. Lennard-Jones and C. Strachan, Proc. Roy. Soc. London A **150**, 442 (1935).

[47] C. Strachan, Proc. Roy. Soc. London A **150**, 456 (1935).

[48] J.E. Lennard-Jones and A.F. Devonshire, Proc. Roy. Soc. London A **156**, 6 (1936).

[49] J.E. Lennard-Jones and A.F. Devonshire, Proc. Roy. Soc. London A **156**, 29 (1936).

[50] H.R. Glyde, J. Low Temp. Phys. **87**, 407 (1992).

[51] D.O. Edwards and W.F. Saam, in *Progress in Low Temperature Physics*, edited by D.F. Brewer (North-Holland, Amsterdam, 1978), Vol. **VIIA**, p. 283.

[52] T.W. Hijmans, J.T.M. Walraven, and G.V. Shlyapnikov, Phys. Rev. B **45**, 2561 (1992).

[53] C. Carraro and M.W. Cole, Phys. Rev. B **45**, 12930 (1992).

[54] V.G. Luppov, W.A. Kaufman, K.M. Hill, R.S. Raymond, and A.D. Krisch, Phys. Rev. Lett. **71**, 2405 (1993).

Chapter 2

STICKING AND THERMAL ACCOMMODATION OF ATOMIC HYDROGEN ON LIQUID-HELIUM SURFACES

We review the experimental results on the measurement of the sticking and thermal accommodation coefficient and outline the theory for ^{4}He surfaces.

2.1 Introduction

The interaction of hydrogen atoms with liquid-helium surfaces has important consequences for experiments with spin-polarized hydrogen at low temperature. As discussed by many authors[1] the interaction leads to surface adsorption and enables heat exchange between surface and gas. Adsorbed atoms take part in a variety of processes which often dominate the behavior of the system as a whole. The highest achievable bulk density of spin-down-polarized hydrogen (H↓) is limited by a three-body surface recombination process, while the operation of the low-temperature hydrogen maser is affected by a wall frequency shift due to adsorption. Some processes, like surface relaxation and surface recombination, are mainly sensitive for the equilibrium properties of the surface coverage. Other phenomena such as the wall shift of magnetic resonance lines and the Kapitza resistance are sensitive to the detailed kinetics of adsorption, desorption and surface scattering.

In this article we concentrate on the phenomena of sticking and thermal accommodation, which are related to the dynamics of surface scattering. The sticking coefficient s is defined as the probability of an atom colliding with the surface to enter a surface bound state. The accommodation coefficient α is defined as

$$\alpha = \lim_{T_g \to T_w} \frac{\dot{Q}_g - \dot{Q}_o}{\dot{Q}_g - \dot{Q}_w} . \tag{2.1}$$

Here $\dot{Q}_g$ is the average kinetic energy flux of the gas at temperature T_g incident on the surface, $\dot{Q}_o$ the average outgoing flux, and $\dot{Q}_w$ the average outgoing flux if all incident atoms would be thermalized on the surface at temperature T_w. For $T_g \approx T_w$ the net heat flux from gas to surface is given by

$$P \approx \alpha \Phi_g 2 k_B (T_g - T_w) , \tag{2.2}$$

with Φ_g the total incident atomic flux.

Knowledge of the value and temperature dependence of s and α for atomic hydrogen on liquid-helium surfaces is important for the interpretation of compression experiments,[2–5] and crucial for the attainment of Bose–Einstein condensation (BEC) if the H-gas is in contact with helium surfaces.[6] Knowledge of the heat exchange is also of importance for experiments aiming at BEC by confinement of spin-up-polarized atoms (H↑) in a minimum-B-field trap.[7,8] The sticking and accommodation phenomena are in itself interesting as they enable the study of scattering of atoms from a liquid surface in the extreme low temperature limit, where complete quantum reflection is expected. The values of s and α are in particular sensitive to the long-range part of the interaction potential between H and the helium surface, hence it is questionable whether they may be used to obtain detailed information about the helium surface, such as the density profile.

Up to 1986 only very incomplete data had been obtained on s and α. At present a consistent picture of all the experimental information can be presented. In Sec. 2.2 we briefly discuss the theory. In Sec. 2.3 we review the experimental information. Then we discuss the overall consistency of the available information.

2.2 Theory

Calculations of s and α are based on a model in which H atoms either scatter elastically or are adsorbed under emission of a single ripplon. The elastic collisions, in which the energy and the momentum parallel to the surface is conserved, lead to specular reflection. However, the reflection may not appear as specular with respect to the macroscopic surface due to microscopic roughness.

Inelastic processes may be divided in processes in which the atom is reflected non-specularly, and sticking processes in which the atom is scattered into a surface bound state. Thermal accommodation is sensitive to both types of inelastic collisions. According to Kagan, Shlyapnikov, and Glukhov,[9] and Castaing and Papoular,[10] the inelastic non-sticking process is less efficient by a factor of order $(\epsilon_a/k_BT)^{-1.5}$ compared to the sticking channel. The binding energy ϵ_a of H on ^{4}He is 1 K, so this process becomes quickly unimportant for temperatures below 500 mK.

In the sticking process the atoms enter a surface bound state. The adsorption potential only supports a single bound state.[11] The atoms are not localized in directions parallel to the surface and behave as a nearly free two-dimensional gas. The wave function of an adsorbed atom may therefore be written as

$$\Psi_{\vec{k}}(\vec{R}, Z) = A^{-1/2} e^{i\vec{k}\cdot\vec{R}} \phi(Z) \,, \tag{2.3}$$

in which $\vec{k}$ is the component of the wavevector parallel to the surface, $\vec{R}$ is the two-dimensional position vector and Z is the distance to the surface reference plane. As has been shown by Kagan and Shlyapnikov[6] the adsorption process is accompanied by the excitation of a single ripplon and not by phonons. In this process a substantial part of the binding energy is converted into kinetic energy of the atom in the adsorbed state. This is illustrated in Fig. 2.1, in which the dispersion curves for the ripplons on a film of 100 Å thickness and the adsorbed atoms are plotted for the case of vanishing incoming kinetic energy ($E_k \ll \epsilon_a$). At the intersection of both curves energy and momentum are conserved. This point corresponds to a ripplon with a wavelength of 42 Å and an atom with a kinetic energy equivalent to 400 mK; atom and ripplon have equal but opposite momentum. The ratio of double ripplon emission to single ripplon emission is estimated by Statt[12] to be about 0.2. After adsorption, two possible situations may occur. The atom may be evaporated by interaction with a ripplon while still in this energetic state or thermalize through ripplon

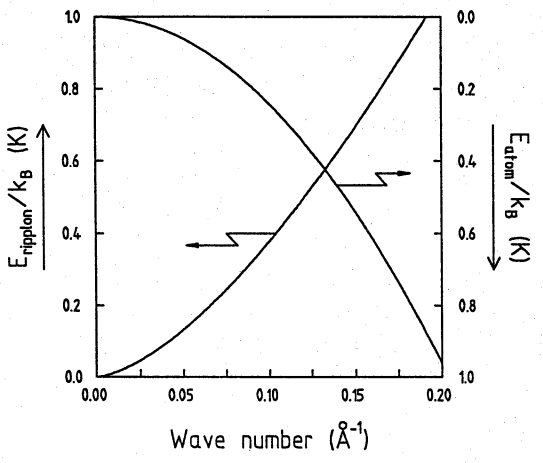

Figure 2.1:
Plot of the dispersion curves of ripplons and H atoms for a ^{4}He surface. At the intersection $\epsilon_a = E_{kin,atom} + E_{kin,ripplon} = 1$ K.

interaction before it is evaporated in a later stage. Zimmerman and Berlinsky[13] calculated the mean time between ripplon interactions for an H atom on the ^{4}He surface to range from 8.7×10^{-10} s at 400 mK to 2.4×10^{-8} s at 100 mK, much shorter than the mean residence time on the surface τ_a which ranges from 1×10^{-8} s at 400 mK to 3×10^{-4} s at 100 mK. An expression for τ_a,

$$\tau_a = 2\pi\hbar \exp(\epsilon_a/k_B T)/(s k_B T) \ , \tag{2.4}$$

is obtained by balancing the flux of sticking atoms $\phi = \frac{1}{4} s n_V \bar{v} A$ against the flux of desorbing atoms $\phi = n_S \tau_a A$, with A the surface area and $\bar{v} = (8k_B T/\pi m)^{1/2}$ the average atomic speed. The surface density n_S is related to the volume density n_V by the surface adsorption isotherm which for volume densities of practical interest may be written as[14]

$$n_S = n_V \lambda_{th} \exp(\epsilon_a/k_B T) \ , \tag{2.5}$$

where $\lambda_{th} = h/\sqrt{2\pi m k_B T}$ is the thermal wavelength.

The sticking probability has been calculated by Zimmerman and Berlinsky,[15] and Kagan and Shlyapnikov.[6] The more general problem of calculating the accommodation coefficient has been treated by Kagan, Shlyapnikov, and Glukhov,[9] Statt,[12] and Goldman.[16] In these theories the helium surface, which for the experimental temperature range is essentially in its ground state, is treated as the surface of an incompressible liquid with a sharp density

profile. The effective surface-atom interaction for an atom located at $(\vec{R}, Z)$ is given in linear approximation by

$$U(\vec{R}, Z) = U_0(Z) - \frac{1}{\sqrt{A}} \sum_{\vec{q}} h_q e^{i\vec{q}\cdot\vec{R}} \frac{\partial U_q(Z)}{\partial Z} , \tag{2.6}$$

with $U_0(Z)$ the static potential of a flat surface, $\vec{q}$ the wavevector of the ripplon, and $h_q = (\hbar q \tanh qd/2\rho_0\omega_q)^{1/2}(r_q^\dagger + r_{-q})$ the amplitude of the surface wave in terms of ripplon creation and annihilation operators. Here $\rho_0 = 145\ \mathrm{kg\,m^{-3}}$ is the ^{4}He bulk density and d the film thickness. The ripplon dispersion relation for a layer of liquid on top of a (horizontal) surface is given by[13,17]

$$\omega_q^2 = \{(g + 3\alpha/d^4)q + (\gamma/\rho_0)q^3\} \tanh(qd) , \tag{2.7}$$

with g the gravitational acceleration, $\gamma = 3.78 \times 10^{-4}\ \mathrm{J\,m^{-2}}$ the ^{4}He surface tension[18] and α the Van der Waals constant of the substrate. In the case of ^{4}He films of about 200 Å the gravitational term is 7 orders of magnitude less than the Van der Waals term. Furthermore, in the region of interest for $\vec{q}$ ($\hbar\omega_q \approx \epsilon_a$) the Van der Waals term and the thin film term $\tanh(qd)$ are not important, reducing Eq. (2.7) to $\omega_q^2 = (\gamma/\rho_0)q^3$. The interaction Hamiltonian in second quantized form is given by

$$H_{\mathrm{int}} = \frac{1}{\sqrt{A}} \sum_{\sigma',\sigma,\vec{q},\vec{k}} h_q \left\langle \sigma \left| \frac{\partial U_q(Z)}{\partial Z} \right| \sigma' \right\rangle a^\dagger_{\vec{k}-\vec{q},\sigma'} a_{\vec{k},\sigma} , \tag{2.8}$$

where σ is associated with the momentum normal to the surface and may characterize the bound state or one of the continuum states. The adsorption rate $R(E, \theta)$ per atom may be calculated using time dependent perturbation theory:[15]

$$R(E,\theta) = \frac{2\pi}{\hbar} \sum_{\vec{q}} \frac{\hbar q}{2\rho_0\omega_q} \left| \left\langle B \left| \frac{\partial U_q(Z)}{\partial Z} \right| \sigma \right\rangle \right|^2 (1 + n(\vec{q}))(1 + N(\vec{k} - \vec{q}))\delta(E - E_f) , \tag{2.9}$$

where $\langle Z|B\rangle$ is the bound state wave function and $\langle Z|s\rangle$ is the free state wave function. Far from the surface σ is the component of the wavevector normal to the surface and $E\cos^2\theta = \hbar^2\sigma^2/2m$. Further, $n(q)$ is the occupation number for ripplons with momentum $\hbar q$ [$n(q) \ll 1$] and $N(\vec{k}-\vec{q})$ the analogous function for the H atoms. The sticking probability is obtained by normalizing the transition rate to the incident flux:

$$s(E,\theta) = \frac{VR(E,\theta)}{A(E/2m)^{1/2}\cos\theta} , \tag{2.10}$$

with V the volume of the sample cell. For low temperatures ($k_B T \ll E_a$) the matrix element is proportional to σ, so in this limit $s(E,\theta) = s_0 E^{1/2}\cos\theta$ and the thermal average of s is

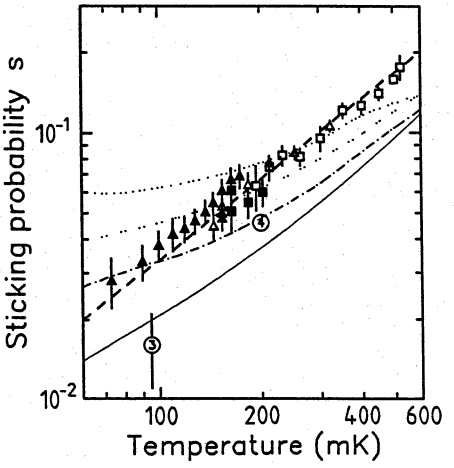

Figure 2.2:
Experimental and theoretical values for the sticking coefficient. BWRW results: open squares: ^{4}He, filled squares: ^{3}He–^{4}He (pressure gauge); open triangles: ^{4}He, filled triangles: ^{3}He–^{4}He (pump plate). UBC results: open circles. Dashed line: $s = \frac{1}{3}T$. Other lines: theoretical calculations (after Goldman).

proportional to $T^{1/2}$. However, Goldman[16] showed that s is strongly dependent on the long-range part of the interaction potential with the surface, and the low-temperature limit for some potentials is only reached for $T \ll 1$ μK. As an illustration, the results of Goldman for a Morse potential and three potentials with a $1/z^3$ behavior are shown in Fig. 2.2. For more detailed information on the potentials we refer to Ref. 16.

2.3 Experiments

2.3.1 Measurements of the sticking coefficient

The sticking coefficient was first measured by Jochemsen *et al.*,[19,20] who studied magnetic resonance of H at 1420 MHz using pure ^{4}He and pure ^{3}He surface coverages. The resonance signal shows a frequency shift $\Delta\omega$ and a decay rate $1/T_2$ that depend on the surface adsorption. For an atom resident on the surface the resonance frequency is shifted by an amount Δ_s leading to an average phase shift per sticking event $\varphi = 2\pi\tau_a\Delta_s$ where τ_a is the average residence time on the surface given in Eq. (2.4). The phase shift φ depends exponentially on temperature. If both the distribution of the residence times and that of times between wall stickings obey Poisson statistics, the frequency shift and decay rate may be given by[19]

$$\Delta\omega = \tau_b^{-1}\varphi/(1+\varphi^2) \,, \tag{2.11}$$

$$1/T_2 = \tau_b^{-1}\varphi^2(1+\varphi^2) \,, \tag{2.12}$$

with τ_b the average time between sticking events. Eqs. (2.11) and (2.12) imply a maximum frequency shift $\Delta\omega_{max} = (2\tau_b)^{-1}$ and a maximum decay rate $(T_2^{-1})_{max} = \tau_b^{-1}$, which may be

found by varying the temperature. The authors determined s by comparing the calculated (by computer simulation) mean time between wall-collisions τ_c to the observed mean time between sticking events τ_b, assuming $\tau_c/\tau_b = s(T)$. We comment on this assumption in Sec. 2.4. Jochemsen *et al.* gave $s = 0.016(5)$ for H on ^{3}He at a temperature near 95 mK and $s = 0.035(4)$ for H on ^{4}He at a temperature near 200 mK. A reanalysis by Morrow and Hardy[21] resulted in a value of $s = 0.046$ for H on ^{4}He.

The sticking coefficient was measured as a function of temperature by Berkhout, Wolters, Van Roijen, and Walraven[22] (BWRW) using a capillary-flow method. In this experiment, a buffer volume V was filled with H$\downarrow$ at a density n. The gas was then allowed to flow through a capillary to a volume kept free of H$\downarrow$ atoms[23]. The flow ϕ depends on the H$\downarrow$ flux entering the capillary and the transmission coefficient (Clausing factor) K:

$$-\frac{\mathrm{d}N}{\mathrm{d}t} = \phi = \tfrac{1}{4}n\bar{v}AK = \frac{N}{\tau}\,, \tag{2.13}$$

with N the number of atoms in the buffer volume, and A the entrance orifice. By measuring τ the Clausing factor follows from $K = \tau_0/\tau$ where $\tau_0^{-1} \equiv \frac{1}{4}\bar{v}A/V$. To determine s the relation between K and s must be known. In the Knudsen flow regime and for $s = 1$ the Clausing factor is determined purely by geometrical factors and is thus temperature-independent. In this limit we write $K = K_K$. For capillaries with large ratio of length ℓ over radius a the relation $K_K = 8a/3\ell$ holds. In the BWRW geometry $K_K = 0.0284$. For $s = 0$ the Clausing factor is 1, that is, every particle entering the capillary will scatter specularly until it leaves at the other end. Note the enormous enhancement of K for $s = 0$ in comparison to K_K. The relation between s and K for several values of interest of s was determined by a Monte Carlo computer simulation, where in line with the theoretical model presented in Sec. 2.2 the atoms were assumed to have a probability s to stick to the surface at each wall collision and $1 - s$ to scatter specularly. The BWRW results are given in Fig. 2.2. The sticking coefficient turned out to be proportional to T and may be given within 10% experimental accuracy as $s = T/T_0$ with $T_0 = 3$ K in the range $73 < T < 526$ mK. It is remarkable that within experimental error s is the same for ^{4}He surfaces and for surfaces of ^{3}He–^{4}He mixtures.

2.3.2 Measurements of the accommodation coefficient

To measure the accommodation coefficient of H$\downarrow$ on ^{4}He, several experimental methods have been used. In the first experiment, by Salonen, Silvera, Walraven, and Van Yperen,[24] ballistic heat transport was measured with a time-of-flight method. A pulsed heater was used to increase the temperature of a helium film. H$\downarrow$ atoms striking this film will on average gain some kinetic energy. This increase in kinetic energy was observed as a net heat transfer to a bolometer positioned opposite the heater. At ambient temperatures of about

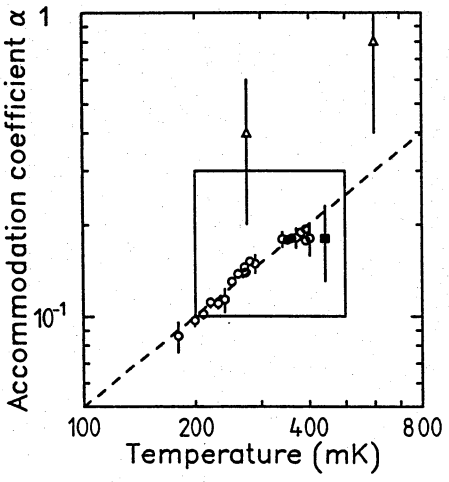

Figure 2.3:
Experimental results for the accommodation coefficient. Dashed line: $\alpha = \frac{1}{2}T$. *Big rectangle: Ref. 24, filled squares: Ref. 26, open triangles: Ref. 3, open circles: Ref. 27.*

400 mK, in addition a signal with a slower time-of-flight response due to evaporating He atoms was observed. By subtracting signals with and without H↓ in the sample cell the signal due to the H↓ itself was obtained. From the comparison of this signal with the He signal, knowing the sticking coefficient for ^{4}He atoms incident on liquid ^{4}He surfaces to be very close to 1,[25] the accommodation coefficient for H↓ was obtained. The result was given as $\alpha = 0.2(1)$ in the temperature range of 200–500 mK. Some indication of decreasing α with decreasing atomic speed was observed, but the signal-to-noise ratio did not allow any definite statement.

The heat loss of an electrically heated bolometer suspended in H↓ gas by thin wires was measured by Salonen, Jaakkola, Karhunen, Tjukanov, and Tommila.[26] The accommodation coefficient is found by applying Eq. (2.2). A difficulty of this method is the determination of the gas temperature T_g of the atoms incident on the bolometer. For a small bolometer T_g approaches the ambient temperature in the limit that the mean free path goes to infinity. The measurements were made as a function of H↓ density and extrapolated to zero density for several ambient temperatures but constant bolometer-surface temperature. By extrapolating to zero-temperature difference a value of $\alpha = 0.18(5)$ at 440 mK may be obtained. The authors interpreted their data to imply an increasing accommodation coefficient with decreasing kinetic energy of the incident atoms.

The accommodation coefficient was also measured by Bell, Hess, Kochanski, Buchman, Pollack, Xiao, Kleppner, and Greytak.[3] In this experiment the main objective was the measurement of relaxation and recombination of a sample of compressed H↓. The temperature difference was measured between both sides of a pancake-like sample bounded by a thermally floating and a rigidly pinned surface. The accommodation coefficient was obtained from a model involving heating due to surface and volume recombination, the thermal

conductivity of the gas, the accommodation process itself and the Kapitza resistance of the liquid–solid interface. The authors extracted an accommodation coefficient varying from 0.8(4) at 600 mK down to 0.4(2) at 275 mK.

The most complete determination of α was done by Helffrich, Maley, Krusius, and Wheatley (HMKW)[27]. They used a method similar to that of Salonen *et al.*,[26] but using lower H↓ densities and a better characterized bolometer. The authors present a thorough analysis of the possible systematic errors inherent to this measurement method. The HMKW results are given in Fig. 2.3. The accommodation coefficient turned out to be proportional to T and may be given within about 10% experimental accuracy as $\alpha = T/T_0$ with $T_0 = 2$ K in the range $180 < T < 400$ mK.

2.4 Discussion

For temperatures below 500 mK, where inelastic scattering is unimportant, Goldman[16] gives a simple relation between α and s:

$$\alpha(T) = s(T)\left\{1 + \frac{1}{2}\beta^2 \frac{\partial^2 \ln s(T)}{\partial \beta^2}\right\}, \tag{2.14}$$

with $\beta = (k_B T)^{-1}$. This expression enables the comparison of all experimental results discussed in the previous paragraph. For the linear temperature dependence observed in the BWRW and HMKW experiments this relation reduces to $\alpha = \frac{3}{2}s$. Using this expression both sets of data are in complete agreement. In view of this fact it is interesting to compare the other experimental results to the BWRW and HMKW (B&H) values.

We first consider the ballistic heat transport measurements of Ref. 24. As may be seen from Fig. 2.3, this result agrees within experimental error with the B&H values. However, this agreement is of limited value in view of the large error box.

The bolometric heat flux measurements done in Turku[26] extrapolated to zero-temperature difference agrees nicely with the B&H results. The temperature dependence of α as reported by the authors remains puzzling.

The values for α of Bell *et al.*[3] lie considerably above the B&H curve. The results have a large error due to a limited signal-to-noise ratio in the data most sensitive to α and the low sensitivity of the fit to the assumed value of α. In view of the complexity of the analysis it is not clear whether the deviation is significant. It should be noted that these data were obtained at densities more than 2 orders of magnitude higher than all other measurements discussed in this paper. In principle at high surface density an enhanced accommodation coefficient is expected as discussed by Collaudin, Hébral, and Papoular,[28] but such densities are not reached in this experiment.

Between the result of Jochemsen *et al.* on ^{3}He: $s = 0.016(5)$ at a temperature of 95 mK and the B&H value of 0.032(3) exists a discrepancy of a factor of 2. The deviation is smaller

for the ^{4}He results: $s = 0.046$ at about 200 mK is given by Morrow *et al.* as compared to $s = 0.066(6)$ for the B&H value. However, the analysis of the resonance experiments is based on a temperature-independent sticking coefficient. In view of the linear temperature dependence observed by B&H we analyze the consequences of a temperature-dependent sticking coefficient. We will show that the neglect of the temperature dependence of s leads to an underestimation.

As mentioned in Section 2.3 the UBC group used the assumption $\tau_b = \tau_c/s$ to extract the sticking coefficient. For H, where no inelastic non-sticking collisions occur, the speed of the atom is conserved between sticking events, and this relation is no longer valid. For perfectly rough walls, where the angle of incidence and reflection with respect to the macroscopic plane of the surface are uncorrelated, the correct relation is $\tau_b(v) = \tau_c(v)/s(v)$ with $\tau_c(v) = \tau_c\bar{v}/v$. The thermally averaged value for τ_b, which is observed, may be found from

$$\tau_b = \int \tau_b(v)\Phi(v)\mathrm{d}v / \int \Phi(v)\mathrm{d}(v) \,, \tag{2.15}$$

in which $\Phi(v)$ is the incident flux on the surface. It is easy to show $s(v)$ should equal $mv^2/4k_BT_0$ in order for s to display the observed linear T dependence $s = T/T_0$. Using this, Eq. (2.15) results in $\tau_b = 4\tau_c/s(T)$. Similarly, for $s(T) \sim T^{1/2}$ the result is $\tau_b = 1.5\tau_c/s(T)$. Therefore, the exact relation between s and τ_c/τ_b depends on the functional behavior of $s(v)$ and, if the walls are not perfectly rough, also on the geometry of the sample volume. Smooth walls tend to increase τ_b for a given value of s and τ_c. This means that the results of the UBC group are lower limits on the sticking coefficient.

Recently the BWRW results have been reanalyzed using a speed-dependent $s(v)$ as mentioned above. This reanalysis is discussed in Chapter 5. The conclusion of this reanalysis is that the result in Section 2.3.1 is a lower bound, but that the linear dependence of s on T is well established.

Summarizing we conclude that the values of s and α are fairly well known in the temperature range between 80 mK and 500 mK for the experimental results. The agreement between experimental results and theoretical calculations is reasonable. The small difference between the results on ^{4}He and ^{3}He–^{4}He mixtures deserves attention. The theoretically predicted strong specular reflection of H from the liquid helium surface has been experimentally demonstrated by the work described in Chapter 4 and thoroughly discussed in Chapter 5.

2.5 Recent developments

Since the publication of the work presented in this thesis some new developments, both theoretical and experimental, have taken place. These developments were triggered by the

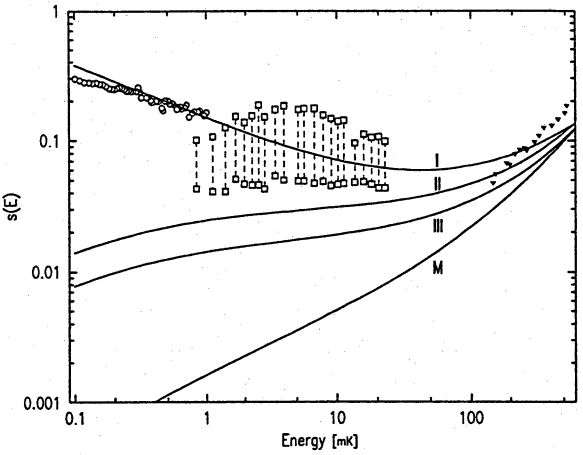

Figure 2.4:
Sticking probability vs atom energy for energies below 100 mK according to Doyle et al.[29] *The solid triangles are the results of the capillary flow experiment. The solid lines represent the predictions for s based on different potentials according to Goldman.*[16]

experiment of Doyle *et al.*,[29] who measured the sticking probability of H atoms on liquid-helium film at H atom temperatures of between 100 μK and 1 mK (see Fig. 2.4). They found s to rise from about 0.15 at 1 mK to 0.3 at 100 μK. Whereas these results are consistent with the calculations of Goldman[16] for his V_I H–He potential, which has a $-C_3 z^3$ long-range behavior, the C_3-coefficient of this potential is more than four times higher than the known value of 219.7 K Å.[30] In an article by Hijmans *et al.*[31] this unexpected rise of the sticking coefficient with decreasing temperature was attributed to the influence of the substrate beneath the helium film. This influence gives rise to an additional long-range Van der Waals attraction of the form $-C_s C_3/(z+d)^3$, where d is the film thickness and C_s+1 is the ratio between the Van der Waals attraction of the H atom due to the substrate and an infinitely thick helium film. The influence of the substrate has subsequently been calculated by Carraro and Cole.[32] Recent measurements of Yu *et al.*[33] have confirmed this dependence of s on the helium film thickness and show fair agreement with the theory of Hijmans *et al.* and Carraro and Cole.

References

[1] For reviews see:
I.F. Silvera and J.T.M. Walraven, in *Progress in Low Temperature Physics*, edited by D.F. Brewer (North-Holland, Amsterdam, 1986), Vol. **X**, p. 139;
T.J. Greytak and D. Kleppner, in *New Trends in Atomic Physics*, vol. 2, Les Houches 1982, edited by G. Grynberg and R. Stora (North-Holland, Amsterdam, 1984), p. 1125.
For a compilation of measurements of the binding energy of H on He see W.N. Hardy, M.D. Hürlimann, and R.W. Cline, in *Proceedings of the Eighteenth International Conference on Low Temperature Physics, Kyoto, Japan, 1987*, Jpn. J. Appl. Phys. **26**, Suppl. 26-3, 2065 (1987).

[2] R. Sprik, J.T.M. Walraven, and I.F. Silvera, Phys. Rev. B **32**, 5668 (1985).

[3] D.A. Bell, H.F. Hess, G.P. Kochanski, S. Buchman, L. Pollack, Y.M. Xiao, D. Kleppner, and T.J. Greytak, Phys. Rev. B **34**, 7670 (1986).

[4] T. Tommila, S. Jaakkola, M. Krusius, K. Salonen, and E. Tjukanov, in *Proceedings of the Seventeenth International Conference on Low Temperature Physics, LT-17, Karlsruhe, West Germany, 1984*, edited by U. Eckern, A. Schmid, W. Weber, and H. Wühl (North-Holland, Amsterdam, 1984), p. 545.

[5] J.D. Gillaspie, I.F. Silvera, and J.S. Brooks, Phys. Rev. B **38**, 9231 (1988).

[6] Yu. Kagan and G.V. Shlyapnikov, Phys. Lett. **95A**, 309 (1983).

[7] R. van Roijen, J.J. Berkhout, S. Jaakkola, and J.T.M. Walraven, Phys. Rev. Lett. **61**, 931 (1988).

[8] H.F. Hess, G.P. Kochanski, J.M. Doyle, N. Masuhara, D. Kleppner, and T.J. Greytak, Phys. Rev. Lett. **59**, 672 (1987).

[9] Yu. Kagan, G.V. Shlyapnikov, and N.A. Glukhov, Pis'ma Zh. Eksp. Teor. Fiz. **40**, 287 (1984) [JETP Lett. **40**, 1072 (1984)].

[10] B. Castaing and M. Papoular, J. Phys. Lett. (Paris) **44**, L537 (1983).

[11] I.B. Mantz and D.O. Edwards, Phys. Rev. B **20**, 4518 (1979).

[12] B.W. Statt, Phys. Rev. B **32**, 7160 (1985).

[13] D.S. Zimmerman and A.J. Berlinsky, Can. J. Phys. **62**, 590 (1984).

[14] I.F. Silvera and V.V. Goldman, Phys. Rev. Lett. **45**, 915 (1980).

[15] D.S. Zimmerman and A.J. Berlinsky, Can. J. Phys. **61**, 508 (1983).

[16] V.V. Goldman, Phys. Rev. Lett. **56**, 612 (1986).

[17] M.W. Cole, Phys. Rev. B **2**, 4239 (1970).

[18] H.M. Guo, D.O. Edwards, R.E. Sarwinski, and J.T. Tough, Phys. Rev. Lett. **27**, 1259 (1971).

[19] R. Jochemsen, M. Morrow, A.J. Berlinsky, and W.N. Hardy, Phys. Rev. Lett. **47**, 852 (1981).

[20] W.N. Hardy, M. Morrow, R. Jochemsen, and A.J. Berlinsky, Physica **109&110B**, 1964 (1982).

[21] M. Morrow and W.N. Hardy, Can. J. Phys. **61**, 956 (1983).

[22] J.J. Berkhout, E.J. Wolters, R. van Roijen, and J.T.M. Walraven, Phys. Rev. Lett. **57**, 2387 (1986).

[23] J.J. Berkhout, O.H. Höpfner, E.J. Wolters, and J.T.M. Walraven, in *Proceedings of the Eighteenth International Conference on Low Temperature Physics, Kyoto, Japan, 1987*, Jpn. J. Appl. Phys. **26**, Suppl. 26-3, 231 (1987).

[24] K.T. Salonen, I.F. Silvera, J.T.M. Walraven, and G.H. van Yperen, Phys. Rev. B **25**, 6002 (1982).

[25] D.O. Edwards and W.F. Saam, in *Progress in Low Temperature Physics*, edited by D.F. Brewer (North-Holland, Amsterdam, 1978), Vol. **VIIA**, p. 283.

[26] K. Salonen, S. Jaakkola, M. Karhunen, E. Tjukanov, and T. Tommila, in *Proceedings of the Seventeenth International Conference on Low Temperature Physics, LT-17, Karlsruhe, West Germany, 1984*, edited by U. Eckern, A. Schmid, W. Weber, and H. Wühl (North-Holland, Amsterdam, 1984), p. 543.

[27] J. Helffrich, M.P. Maley, M. Krusius, and J.C. Wheatley, Phys. Rev. B **34**, 6550 (1986).

[28] B. Collaudin, B. Hébral, and M. Papoular, J. Phys. (Paris) **47**, 1503 (1986).

[29] J.M. Doyle, J.C. Sandberg, I.A. Yu, C.L. Cesar, D. Kleppner, and T.J. Greytak, Phys. Rev. Lett. **67**, 603 (1991).

[30] W.C. Stwalley, Chem. Phys. Lett. **88**, 404 (1982).

[31] T.W. Hijmans, J.T.M. Walraven, and G.V. Shlyapnikov, Phys. Rev. B **45**, 2561 (1992).

[32] C. Carraro and M.W. Cole, Phys. Rev. B **45**, 12930 (1992).

[33] I.A. Yu, J.M. Doyle, J.C. Sandberg, C.L. Cesar, D. Kleppner, and T.J. Greytak, Phys. Rev. Lett. **71**, 1589 (1993).

Chapter 3

VANISHING STICKING PROBABILITIES AND ENHANCED CAPILLARY FLOW OF SPIN-POLARIZED HYDROGEN

We report on a series of capillary-flow experiments with spin-polarized hydrogen in which we observe a strong enhancement ($> 10\times$) of the flow rate in comparison to ordinary Knudsen flow. This is related to a vanishing sticking probability s for $T \to 0$ K as predicted by theory. With ^{4}He surfaces we find that $s = 0.33T$ for $145 < T < 526$ mK. Within experimental error s did not change by adding up to 50% ^{3}He at 150 mK. Results for ^{3}He–^{4}He surfaces were obtained for $73 < T < 174$ mK and are also described by $s = 0.33T$.

..., but sometimes he feels that there really is another way,
if only he could stop bumping for a moment and think of it.
And then he feels that perhaps there isn't.

— A.A. Milne, *Winnie-the-Pooh*.

The physics of scattering of hydrogen atoms from the surface of liquid helium has grown into an important subject in studies of spin-polarized hydrogen (H↓) at low temperature.[1] Inelastic scattering provides the mechanism for the exchange of heat between the bulk H↓-gas phase and the helium-covered walls of a sample cell and leads to a thermal-boundary resistance. In particular, at high H↓ densities or low temperatures, where recombination to the (solid) molecular state H_2 is most effective, substantial temperature differences may develop between gas and surface. This is recognized as a major barrier in achieving Bose–Einstein condensation in H↓ by compression methods.[2] In recent proposals to aim for Bose–Einstein condensation by pure field confinement in a magnetic trap, walls are of vital importance to provide a cooling mechanism during filling. There one has to strike a subtle balance between cooling efficiency and flux losses due to surface recombination or spin relaxation.[3]

Some experimental information is available for the sticking coefficient s, the probability per collision to be adsorbed, and for the accommodation coefficient α, characterizing the transfer of translational energy transfer per collision. The sticking coefficient was first determined by Jochemsen *et al.*[4] By means of magnetic resonance they found that $s = 0.046$ at $T \approx 200$ mK for ^{4}He-surfaces and $s = 0.016(5)$ for ^{3}He-surfaces at $T \approx 100$ mK. Salonen *et al.*[5] measured ballistic heat transport with a time-resolved method and found that $\alpha = 0.2(1)$ for H on ^{4}He. In a subsequent steady-state heat flux experiment Salonen *et al.*[6] (SJKTT) obtained $\alpha = 0.19(5)$ for $T = 440$ mK. Bell *et al.*[7] found α to decrease from $\alpha = 0.8(4)$ at 0.6 K to $\alpha = 0.4(2)$ at 0.275 K. Very recently Helffrich *et al.*[8] also found a decreasing α for decreasing temperature with an SJKTT-type experiment. We noted slightly different definitions of α by the various authors.

In this Letter we report on a series of capillary-flow experiments which are particularly suited to the estimation of s for H on liquid-helium surfaces. In comparison with ordinary Knudsen flow a dramatically reduced ($> 10\times$) flow impedance is observed which we attribute to a small value of s. The impedance is decreasing with decreasing temperature. Our results show that the earlier observed differences between sticking and accommodation coefficients are mainly due to differences in temperature of observation. We also estimate the coefficient of self-diffusion for H↓ in the gas phase.

Classically one expects s to approach unity in the zero-temperature limit. Quantum-mechanical theory predicts s to vanish as $T^{1/2}$ for $T \to 0$ K and shows excitation or de-excitation of ripplons to be the dominant mechanism of energy exchange between gas and liquid.[9–12] Also, the Kapitza conductance is calculated to vanish in the $T \to 0$ limit but the numerical values, in particular below 100 mK, vary by orders of magnitude depending on the adsorption potential and the scattering channels included in the calculation.[11–13] The experimental cell is shown schematically in Fig. 3.1. The atoms are introduced from the bottom into a buffer volume ($V_b \approx 10$ cm^3) where the pressure may be monitored

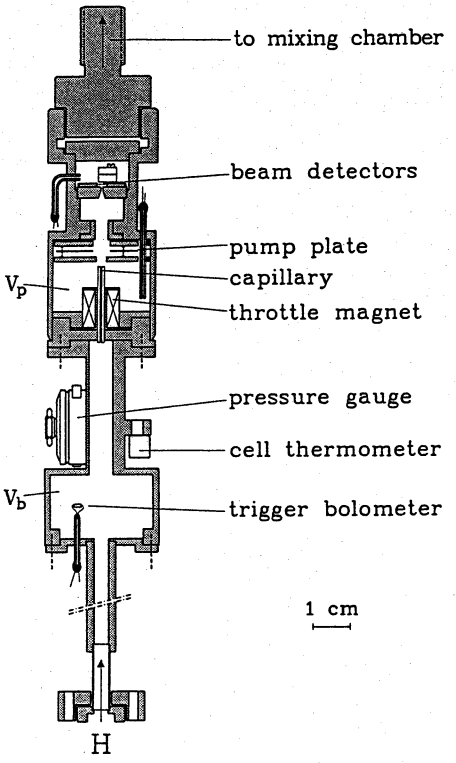

Figure 3.1:
Schematic drawing of the apparatus. For details see text.

with a capacitive pressure transducer having a sensitivity of 1.74 pF/Torr and a noise equivalent pressure of 5×10^{-7} Torr (1 standard deviation at a bandwidth of 1.25 Hz). The minimum detectable density is 1×10^{13} cm^{-3} at 500 mK. The buffer volume is connected to a pump volume (V_p) via a Pyrex capillary of length $\ell = 21.97(3)$ mm and inner radius of $a = 0.248(2)$ mm. All surfaces in the cell are covered with a film of liquid helium. To pump the H$\downarrow$ the helium film is boiled off from a copper plate of area $A_p = 7.2$ cm^2 suspended by three 16-μm-diam tungsten wires, exposing the H$\downarrow$ to a substrate offering a strong ($\gg 1$ K) binding energy and hence causing massive recombination in the pump volume. A heating power of 15 μW is needed to heat the pump plate to its operational temperature $T = 2.1(1)$ K. The whole assembly acts as a miniature atomic-beam apparatus. The beam detectors are not discussed in this article. The cell is placed in a 6-T magnetic field homogeneous to within 1:10^4 over the capillary region. The flow through the capillary may be throttled by local reduction of the field to less than 5 T with a small coil. Great care was exercised to avoid magnetic surface impurities in the buffer volume in order to minimize recombination losses.[14]

To determine s for a given temperature we measure the flow impedance of the capillary, either by using the pressure gauge or by measuring recombination heat dissipated into the pump plate. By measurement with the pressure gauge the whole cell is first filled with H$\downarrow$ up to a density $n \approx 2 \times 10^{15}$ cm^{-3}. Then the pump plate is heated to its operational temperature and one monitors, after a short (<1 s) transient due to the recombination of the gas in V_p, the exhaust of the buffer volume through the capillary. Since $A_p \gg A_0 \equiv \pi a^2$ the probability of the H$\downarrow$ atoms in returning to V_b is negligibly small ($\ll 10^{-3}$). By measurement with the pump plate one monitors the power required to stabilize the plate temperature to a fixed value of 2.1 K. The sensitivity of this method is at least 3 orders of magnitude better than that of the pressure measurements.

The flux Φ through the capillary is described by

$$-\frac{dN}{dt} = \Phi = \tfrac{1}{4} K N \bar{v} A_0 / V_b \equiv K \Phi_0 \ , \tag{3.1}$$

where N is the number of atoms in the buffer volume V_b, $\bar{v} = (8kT/\pi m)^{1/2}$ is the average atomic speed, Φ_0 is the rate at which atoms enter the capillary, and K is the Clausing factor,[15] expressing the probability for an atom to pass through the tube without returning to V_b. In the Knudsen regime for ordinary capillary flow $K = K_K \approx 8a/3\ell$, purely determined by geometrical factors and thus temperature-independent. For our geometry $K_K = 0.0284$[16]. We determine K experimentally by measuring the characteristic time $\tau \equiv \tau_0/K \equiv (\frac{1}{4} K \bar{v} A_0 / V_b)^{-1}$, typically 5–10 s, in which the buffer volume is discharged through the capillary. Here τ_0 is the characteristic time for effusion through the entrance orifice A_0. Once τ is known we extract the corresponding value for s using a computer simulation of the flow.

The nature of surface scattering only enters into Eq. (3.1) through the Clausing factor K. If one assumes the scattering to be purely diffusive (according to a cosine distribution), as was done by Clausing, one expects that $K = K_K$. On the other hand, if no momentum is transferred parallel to the surface, as in the case of specular reflection, Φ is entirely determined by the impedance of the entrance orifice and one should have $K = 1$. We simulate the capillary flow with a one-speed-test-particle Monte Carlo method.[17] At each wall collision the atom is given a probability (s_u) to scatter diffusively, otherwise the atom scatters specularly. Our results for s_u vs K were calculated to within 1% using 10^5 particles and are given within 3% by the empirical form

$$s_u = \frac{1-K}{1-K_K} \left(\frac{K_K}{K}\right)^{1/2} e^{-3.915\Delta K} \left\{1 + 4.2\Delta K^2\right\} \ , \tag{3.2}$$

where $\Delta K = K - K_K$. The model clearly represents a simplified picture of the physics involved. Our measurement is sensitive for any process that leads to momentum transfer in the direction along the axis of the capillary tube. This is most effectively done by

atoms that stick some time to the surface, but more generally results from any inelastic scattering process. Hence our model delivers an upper estimate for s. However, in view of the theoretical assertion[10–12] that the sticking channel is most effective in exchanging energy and momentum between gas and surface, it seems reasonable to assume that $s_u \approx s$. Surface roughness may also lead to non-specular reflection as is well known for ultra cold neutrons[18] and light.[19] Using a scanning electron microscope with a maximum resolution of ~ 100 Å we found the capillary inner surface to be extremely flat except for some isolated grains of loose dirt. We assume any irregularities of size <100 Å to be smoothed out by the helium film. The influence of roughness due to thermally excited ripplons appears to be small.[20]

Our simulation also allows us to study the effect of collisions between atoms in the gas phase and to extract the diffusion coefficient from the measurements. After a randomly generated collision the atoms are restarted in random directions, sampling an angular distribution chosen to be isotropic in the laboratory system. Relating the mean free path λ to n according to[21] $\lambda = (16\sqrt{2}n\sigma/9\pi)^{-1}$, where σ is the hard-sphere scattering cross section, we may describe our simulation results for the density dependence of K by

$$K \approx K_0(1 - \sigma\lambda_0 K_0 n) \; . \tag{3.3}$$

Here K_0 is the Clausing factor in the zero-density limit and $\lambda_0 \equiv 6.1$ mm is a reference length provided by the simulation. Equation (3.3) only holds in the extremely rarefied limit. At higher densities K should show a minimum before entering the viscous regime.[22] In our measurements $\lambda > 2$ cm. Once σ is known the coefficient of self-diffusion follows with $D = \frac{1}{3}\bar{v}\lambda$.[21]

With the aid of Eqs. (3.1) and (3.3) and allowing for recombination we may express the rate of loss of atoms from the buffer volume by a second-order rate equation

$$\mathrm{d}n/\mathrm{d}t = C_1 n + C_2 n^2 \; , \tag{3.4}$$

where $C_1 \equiv -K_0/\tau_0$ and $C_2 \equiv \sigma\lambda_0 K_0^2/\tau_0 - K_{\mathrm{rec}}$. K_{rec} is a rate constant accounting for recombination. Equation (3.4) is integrated and fitted to the pressure decay data to extract the first- and second-order decay constants. Data were only collected in a temperature regime where the helium-vapor pressure did not significantly impede the flow and recombination losses could be neglected, as was verified with the aid of the throttle magnet.

We note that the fraction of the atoms entering the tube over the surface is small, 4.7% for ^{4}He surfaces at $T = 145$ mK. At this temperature the adsorption time $\tau_s = (h/sk_BT)\exp(\epsilon_a/k_BT) \approx 7$ μs (h is the Planck constant, $s = 0.05$, and $\epsilon_a = 1$ K is the adsorption energy[1]), much longer than the momentum relaxation time 1.1 ns of adsorbed atoms.[23] Hence the motion of the adsorbed atoms is diffusive. The mean square displacement from the adsorption site is very small (~ 5 μm) and as such negligible.

The results for pure ^{4}He surfaces are shown in Fig. 3.2(a), where we plot K_0 vs T.

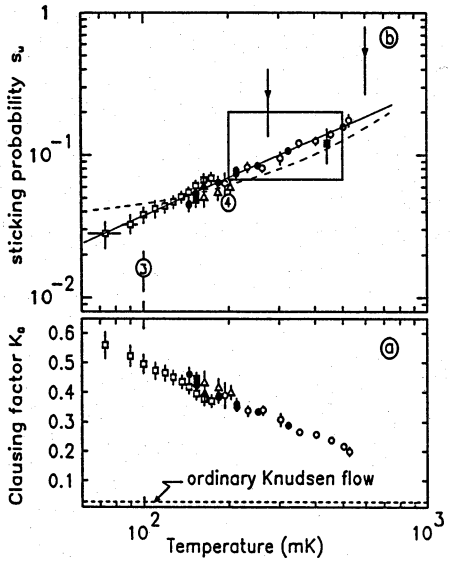

Figure 3.2:
(a) Measured values for the Clausing factor K_0 vs temperature. (b) Fraction s_u of the atoms scattered diffusively from the surface, $s_u \approx s$. Our results are the following: open circles, ^{4}He, open triangles, 0.2% ^{3}He, open triangles, 5% ^{3}He (pressure gauge); filled circles, ^{4}He, open squares, 3%–50% ^{3}He (pump plate). Other data: open circles, Ref. 4; filled squares, Ref. 6; big rectangle, Ref. 5; inverted filled triangles, Ref. 7; dashed curve, theory of Ref. 12. The solid line corresponds to $s = \frac{1}{3}T$.

The open circles are obtained from pressure-gauge measurements; the filled circles are our pump-plate results. Note the excellent agreement between both methods and the enormous enhancement in conductance in comparison to the value K_K to be expected for ordinary Knudsen flow. Each data point represents the average of at least four measurements, the error bar being the standard deviation of the results, augmented by a small systematic error.

By applying Eq. (3.2) we obtain our results for s_u, which are shown in Fig. 3.2(b). The data fit well to a straight line $s_u = 0.33T$ for $145 < T < 526$ mK. Our value for 200 mK is approximately 30% larger than the Jochemsen *et al.*[4] result [encircled 4 in Fig. 3.2(b)]. Within experimental error we find agreement with the SJKTT result at 440 mK (filled square). We also indicate in Fig. 3.2(b) the result (the large rectangle) obtained by Salonen *et al.*[5] in Amsterdam and the result of Bell *et al.*[7] (inverted filled triangle). Note that we used $s = \frac{2}{3}\alpha$ to plot the accommodation results.[12] The dashed curve in Fig. 3.2(b) corresponds to the V_{II}-curve of Goldman.[12] The straight line corresponds to $s_u = 0.33T$. In proof we note very good agreement between the recent results of Hellfrich *et al.*[8] and our ^{4}He data.

In adding a small amount of ^{3}He (0.2%) to the ^{4}He in our cell we noticed a clear reduction of the recombination rate, indicating a reduction[24] of the binding energy and implying a definite change in adsorption potential and in ripplon dispersion [the surface tension falls from $\gamma = 0.378(2)$ erg cm^{-2} to $\gamma = 0.153(4)$ erg cm^{-2} when changing from pure ^{4}He to pure ^{3}He surfaces][25]. However, within experimental error no effect was observed on K or s_u (open triangles in Fig. 3.2). After the increase of the ^{3}He fraction to 5%, a small ($\approx$10%) increase in s_u was observed at 164 mK with the pressure gauge (filled triangle). Under these

conditions we estimate the local ^{3}He concentration in the cell to be at least 30% and hence expect the H$\downarrow$ to scatter from a ^{3}He-rich phase. Most of our 5% ^{3}He results, shown as open squares in Fig. 3.2(b), were obtained with the pump plate and are in fair agreement with the 164 mK pressure-gauge result. Although the reliability of our thermometry rapidly decreases below 100 mK, the trend of decreasing sticking probabilities with decreasing temperatures clearly continues down to our lowest temperature. In comparing our 100-mK value with the ^{3}He result of Jochemsen *et al.* (encircled 3) we note that our value is a factor 2–3 larger. With the addition of 50% ^{3}He no further pressure measurements could be done as bulk liquid started to collect in the pressure gauge. With the pump plate no change was observed on s.

Values for C_2 were obtained with the pressure gauge, starting the fits at a fixed initial density $n_0 = 5 \times 10^{14}$ cm^{-3}. We found that $C_2 \times 10^{17} = 6.2(15) - 8(14)[T - 0.27]$ cm^3/s which leads to a diffusion constant which is temperature-independent within experimental error. Averaging over all data we find that $Dn = 1.3(5) \times 10^{18}$ cm^{-1} s^{-1}, in good agreement with the theoretical value of Lhuillier,[26] $Dn = 1.5 \times 10^{18}$ cm^{-1} s^{-1}. In view of the large experimental error in C_2 no effort was made to refine the treatment of diffusion in our simulation.

Our results show that earlier observed differences between sticking and accommodation coefficients are largely due to differences in temperature of observation [see Fig. 3.2(b)]. Differences between our results and those of Bell *et al.*[7] may not be significant in view of their large experimental error. The surface densities in their experiments are not sufficiently high to cause enhanced sticking through the mechanism of Collaudin, Hébral, and Papoular.[27] The discrepancy with the ^{3}He result of Jochemsen *et al.*[4] remains unexplained. Remarkable is the small, <10%, change in s when one adds ^{3}He into the cell.

The authors wish to thank O.H. Höpfner for technical support, J. Koelman for pointing out an inconsistency in our computer simulation, and I.D. Setija, I. Lunding, and J. Mosk for assistance with the measurements and data analysis. We profited from discussions with H. Beijerinck, A. Lagendijk, M. Papoular and R. Sprik. The financial support of the Stichting FOM is gratefully acknowledged.

References

[1] I.F. Silvera and J.T.M. Walraven, in *Progress in Low Temperature Physics*, edited by D.F. Brewer (North-Holland, Amsterdam, 1986), Vol. **X**, p. 139.

[2] R. Sprik, J.T.M. Walraven, and I.F. Silvera, Phys. Rev. Lett. **51**, 479, 942(E) (1983); H.F. Hess, D.A. Bell, G.P. Kochanski, R.W. Cline, D. Kleppner, and T.J. Greytak, Phys. Rev. Lett. **51**, 483 (1983);
T.J. Tommila, S. Jaakkola, M. Krusius, I. Krylov, and E. Tjukanov, Phys. Rev. Lett. **56**, 941 (1986).

[3] H.F. Hess, Bull. Am. Phys. Soc. **30**, 854 (1985);
R.V.E. Lovelace, C. Mehanian, T.J. Tommila, and D.M. Lee, Nature (London) **318**, 30 (1985);
H.F. Hess, Phys. Rev. B **34**, 3476 (1986);
T.J. Tommila, Europhys. Lett. **2**, 789 (1986).

[4] R. Jochemsen, M. Morrow, A.J. Berlinsky, and W.N. Hardy, Phys. Rev. Lett. **47**, 852 (1981); we use the result of the reanalysis by M. Morrow and W.N. Hardy, Can. J. Phys. **61**, 956 (1983).

[5] K.T. Salonen, I.F. Silvera, J.T.M. Walraven, and G.H. van Yperen, Phys. Rev. B **25**, 6002 (1982).

[6] K. Salonen, S. Jaakkola, M. Karhunen, E. Tjukanov, and T. Tommila, in *Proceedings of the Seventeenth International Conference on Low Temperature Physics, LT-17, Karlsruhe, West Germany, 1984*, edited by U. Eckern, A. Schmid, W. Weber, and H. Wühl (North-Holland, Amsterdam, 1984), p. 543.

[7] D.A. Bell, H.F. Hess, G.P. Kochanski, S. Buchman, L. Pollack, Y.M. Xiao, D. Kleppner, and T.J. Greytak, Phys. Rev. B **34**, 7670 (1986).

[8] J. Helffrich, M.P. Maley, M. Krusius, and J.C. Wheatley, Phys. Rev. B **34**, 6550 (1986).

[9] D.S. Zimmerman and A.J. Berlinsky, Can. J. Phys. **61**, 508 (1983).

[10] B.W. Statt, Phys. Rev. B **32**, 7160 (1985).

[11] Yu. Kagan, G.V. Shlyapnikov, and N.A. Glukhov, Pis'ma Zh. Eksp. Teor. Fiz. **40**, 287 (1984) [JETP Lett. **40**, 1072 (1984)].

[12] V.V. Goldman, Phys. Rev. Lett. **56**, 612 (1986).

[13] B. Castaing and M. Papoular, J. Phys. Lett. (Paris) **44**, L537 (1983).

[14] R. Sprik, J.T.M. Walraven, G.H. van Yperen, and I.F. Silvera, Phys. Rev. B **34**, 6172 (1986).

[15] P. Clausing, Ann. Phys. (Leipzig) **12**, 961 (1932).

[16] R.J. Cole, Prog. Astronaut. Aeronaut. **51**, 261 (1977).

[17] G.A. Bird, *Molecular Gas Dynamics* (Clarendon, Oxford, 1976). For another method see K. Yamamoto, J. Hara, and K. Hirose, J. Phys. Soc. Jpn. **51**, 3729 (1982).

[18] M. Brown, R. Golub, and J.M. Pendlebury, Vacuum **25**, 61 (1975).

[19] J.M. Elson and J.M. Bennet, J. Opt. Soc. Am. **69**, 31 (1979).

[20] D.O. Edwards and P.P. Fatouros, Phys. Rev. B **17**, 2147 (1978).

[21] J.O. Hirschfelder, C.F. Curtiss, and R.B. Bird, *Molecular Theory of Gases and Liquids* (Wiley, New York, 1954).

[22] M. Knudsen, Ann. Phys. (Leipzig) **28**, 75 (1908).

[23] D.S. Zimmerman and A.J. Berlinsky, Can. J. Phys. **62**, 590 (1984).

[24] A.P.M. Matthey, J.T.M. Walraven, and I.F. Silvera, Phys. Rev. Lett. **46**, 668 (1981).

[25] D.O. Edwards and W.F. Saam, in *Progress in Low Temperature Physics*, edited by D.F. Brewer (North-Holland, Amsterdam, 1978), Vol. **VIIA**, p. 283.

[26] C. Lhuillier, J. Phys. (Paris) **44**, 1 (1983).

[27] B. Collaudin, B. Hébral, and M. Papoular, J. Phys. (Paris) **47**, 1503 (1986).

Chapter 4

QUANTUM REFLECTION: FOCUSING OF HYDROGEN ATOMS WITH A CONCAVE MIRROR

We use a concave spherical mirror to focus on a 18-mm-diam beam of H atoms down to 0.5 mm. The mirror consists of a fused-quartz substrate polished to optical precision and coated with a liquid-^{4}He film to obtain high reflectivity. The temperature dependence of the focused beam intensity enables us to study the influence of the dynamic surface roughness on the reflection of the H atoms. Both zero-point fluctuations and thermal excitations turn out to be of importance. A monolayer of ^{3}He does not significantly affect the results.

Hydrogen atoms (H) colliding with the surface of liquid ^{4}He are particularly well suited to study the quantum regime of atom-surface scattering. This arises from the small mass of the H atom, the weak interaction between H and helium, and the possibility to cool H gas to sub-Kelvin temperatures. Moreover helium is easily purified and liquid-^{4}He surfaces are highly reproducible and can be accurately described in terms of elementary excitations. For vanishingly low incident energy theory predicts H atoms to scatter elastically from the helium surface with a probability approaching unity.[1] This is a purely quantum-mechanical reflection phenomenon, which suggests the feasibility of a near-perfect atomic mirror. Classically, under similar conditions the atoms should stick to the surface as surface excitation is unavoidable.

Quantum reflection of both ^{4}He and ^{3}He beams at the liquid–vacuum interface of liquid helium has been observed by various authors,[2] in particular, by Edwards and collaborators who studied the energy dependence of the effect. However, high reflectivity was not achieved except at grazing incidence (20% at an angle of 87.5°) due to absorption of the beams by the liquid even at the lowest operating temperatures.[3]

In this Letter we demonstrate for the first time focussing of a highly divergent beam of cold ($T < 0.5$ K) hydrogen atoms by the use of a hemispherical concave substrate of optical quality coated with a film of superfluid helium to obtain high reflectivity. At normal incidence we measure a lower limit of 80% for the specular reflectivity. We discuss how static surface roughness due to the substrate and dynamic surface roughness due to the helium film limit this reflectivity. Mirror and diaphragm enable us to study the specularly reflected beam within an acceptance angle of about 10 mrad. By measuring the specular reflectivity as a function of temperature we obtain for the first time experimental evidence for direct inelastic scattering induced by thermal ripplons.

The theory for scattering of low-energy H atoms from the surface of liquid ^{4}He is the subject of several papers in the literature.[4–9] The H–He interaction is extremely weak and gives rise to a surface adsorption potential which only supports a single bound state.[10] Quantum reflection arises since at low energy the scattering amplitude for scattering by zero-point fluctuations or thermal ripplons is small.

Indirect evidence for the occurrence of quantum reflection of H from liquid-helium surfaces has been obtained experimentally by measurements of the sticking coefficient s,[11–13] the probability for surface adsorption, as well as measurements of the accommodation coefficient α,[14–17] a measure for the efficiency of energy transfer in atom-surface collisions. The coefficients s and α may be related using the important theoretical result that sticking is the dominant channel for heat exchange below 0.5 K[7–9]. If s depends linearly on temperature, this leads to the relation $\alpha = \frac{3}{2}s$[9].

The most complete set of data for the sticking coefficient was obtained by Berkhout *et al.*,[13] who observed a linear temperature dependence, $s/T = 0.33(3)$ K^{-1}, both for the

surface of pure ^{4}He beween 145 and 526 mK and for surfaces of ^{3}He–^{4}He mixtures between 73 and 174 mK. The results for ^{4}He surfaces are in fair agreement with theory[4,5] if the Morse potential is adjusted to yield a 1-K binding energy. Further support for the theoretical model is obtained by comparing the results for the sticking coefficient with the data of Helffrich *et al.*[17] for the accommodation coefficient of H atoms on ^{4}He surfaces between 180 and 400 mK. On the basis of the relation $\alpha = \frac{3}{2}s$, both sets of experimental data are in full agreement (3% level) with one another.

The measurements of s and α enable an estimate for the specular reflectivity at normal incidence $R_\perp$ using the *Ansatz* $R_\perp = 1 - s_\perp$. The experimental values for s and α represent an average over all angles of incidence. Theory[4] may be used to relate the sticking probability at angle of incidence θ, $s(\theta)$, to the angular-average s, yielding $s(\theta) = 1.5s\cos(\theta)$. Using this, the sticking at normal incidence as implied by our previous results[13] is given by $s_\perp = \gamma_1 T$ with $\gamma_1 = 0.50(5)$ K^{-1}. We thus calculate $R_\perp \approx 0.95$ at $T = 100$ mK.

To obtain direct experimental evidence for high specular reflectivity we designed the experimental cell shown in Fig. 4.1. H atoms are produced in an RF dissociator operated at 600 mK and situated in the 0.25-T fringe field of a 6-T superconducting magnet. Under the influence of field gradients spin-down-polarized atoms (H$\downarrow$) are driven downward to the center of the magnet and collected in a buffer reservoir with volume $V_b \approx 10$ cm^3 which is entirely contained in a larger volume, the pumping volume. Atoms escaping through an orifice of 0.5 mm diam in the 0.05-mm-thick bottom of the buffer reservoir give rise to a highly divergent atomic beam in the pumping volume. A small quantity of liquid helium, typically 0.02 cm^3, assures the presence of a saturated film on all surfaces. The gas originating from the beam is continually removed by a "pumping plate" H-flux detector[18] mounted around the neck of the buffer reservoir. All dimensions are chosen to assure that the probability for an atom to reach the pump is about 50× larger than the probability to reenter the buffer volume. The main component of the cell is a concave spherical mirror facing the beam and mounted in the pumping volume. This mirror consists of a helium covered fused-quartz substrate ground to optical precision into a hemispherical shape with radius of curvature 9 mm. A push and pull mechanism driven by an inchworm motor at room temperature enables vertical positioning of the mirror with a resolution of 0.5 μm.

The principle of the experiment is to observe the influence of the position of the mirror on the density decay time of the H gas in the buffer reservoir. If the center of the mirror coincides with the center of the orifice, the atoms in the beam will be specularly reflected back into the reservoir. The net flux through the diaphragm may be expressed as $-\mathrm{d}N/\mathrm{d}t = \frac{1}{4}n\bar{v}A\chi$, with n the density in the buffer volume, $\bar{v}$ the average atomic speed, A the area of the orifice, and χ a loss factor representing the probability that the atoms are *not* scattered back into the buffer volume. For our mirror 100% reflectivity would correspond to $\chi_g = 0.042$, as limited by geometrical factors such as spherical aberration. For

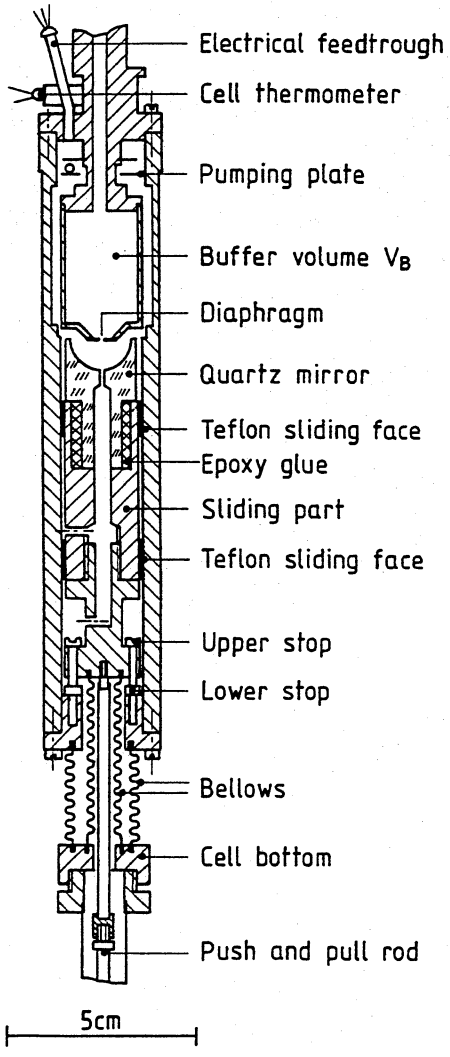

Figure 4.1:
The experimental cell.

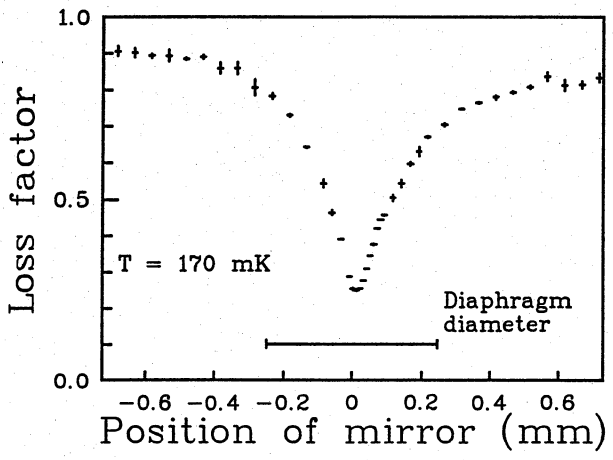

Figure 4.2:
The loss factor as a function of the vertical mirror position.

densities up to $n = 10^{14}$ cm^{-3} interatomic collisions in the beam are completely negligible. This analysis implies that the leakage from the reservoir may be largely suppressed with the mirror.

A typical measurement is shown in Fig. 4.2. We plot the observed loss factor $\chi \equiv \tau_0/\tau \approx -(\tau_0/N)\mathrm{d}N/\mathrm{d}t$ as a function of the vertical position of the mirror. Here $\tau_0 \equiv 4V_b/\bar{v}A$ is the first-order decay time in the absence of the mirror and τ the measured first-order decay time. The results clearly demonstrate the occurrence of specular reflection of the atoms. With the mirror far from focusing conditions, the decay time is only slightly larger than that expected in the absence of a mirror. As the mirror is moved to bring the diaphragm into focus, the decay time starts to increase dramatically. From each position scan we may extract the minimal χ value (χ_{min}) for a given temperature and film thickness. As seen from the figure, an axial displacement of the mirror over 150 μm suffices to reduce the maximum effect by a factor of 2, while the mirror must be positioned with an accuracy of better than 30 μm to determine the maximum effect.

A summary of our results for χ_{min} as a function of temperature is shown in Fig. 4.3. The triangles represent our data for a saturated ^{4}He film of estimated thickness 11.5 nm.[19] For ideal alignment of the optics ($\chi_g = 0.042$) the temperature dependence of χ_{min} predicted on the basis of our earlier results[13] for s is indicated by the dotted line. Here we use for the lossfactor due to sticking $\chi_s = s_\perp = \gamma_1 T$ with $\gamma_1 = 0.5$ K^{-1}. Most of the discrepancy with the data may be explained by assuming a lateral misalignment of the mirror or by residual roughness due to surface imperfections of the quartz substrate. Both effects cause

References

[1] For a review, see J.J. Berkhout and J.T.M. Walraven, in *Spin-Polarized Quantum Systems*, edited by S. Stringari (World Scientific, Singapore, 1989), p. 201.

[2] A first measurement was reported by D.T. Meyer, H. Meyer, W. Hallidy, and C.F. Kellers, Cryogenics **3**, 150 (1963). For a review, see D.O. Edwards and W.F. Saam, in *Progress in Low Temperature Physics*, edited by D.F. Brewer (North-Holland, Amsterdam, 1978), Vol. **VIIA**, p. 283.

[3] V.U. Nayak, D.O. Edwards, and N. Masuhara, Phys. Rev. Lett. **50**, 990 (1983).

[4] D.S. Zimmerman and A.J. Berlinsky, Can. J. Phys. **61**, 508 (1983).

[5] Yu. Kagan and G.V. Shlyapnikov, Phys. Lett. **95A**, 309 (1983).

[6] B. Castaing and M. Papoular, J. Phys. Lett. (Paris) **44**, L537 (1983).

[7] Yu. Kagan, G.V. Shlyapnikov, and N.A. Glukhov, Pis'ma Zh. Eksp. Teor. Fiz. **40**, 287 (1984) [JETP Lett. **40**, 1072 (1984)].

[8] B.W. Statt, Phys. Rev. B **32**, 7160 (1985).

[9] V.V. Goldman, Phys. Rev. Lett. **56**, 612 (1986).

[10] I.B. Mantz and D.O. Edwards, Phys. Rev. B **20**, 4518 (1979).

[11] R. Jochemsen, M. Morrow, A.J. Berlinsky, and W.N. Hardy, Phys. Rev. Lett. **47**, 852 (1981).

[12] W.N. Hardy, M. Morrow, R. Jochemsen, and A.J. Berlinsky, Physica **109&110B**, 1964 (1982).

[13] J.J. Berkhout, E.J. Wolters, R. van Roijen, and J.T.M. Walraven, Phys. Rev. Lett. **57**, 2387 (1986).

[14] K.T. Salonen, I.F. Silvera, J.T.M. Walraven, and G.H. van Yperen, Phys. Rev. B **25**, 6002 (1982).

[15] K. Salonen, S. Jaakkola, M. Karhunen, E. Tjukanov, and T. Tommila, in *Proceedings of the Seventeenth International Conference on Low Temperature Physics, LT-17, Karlsruhe, West Germany, 1984*, edited by U. Eckern, A. Schmid, W. Weber, and H. Wühl (North-Holland, Amsterdam, 1984), p. 543.

[16] D.A. Bell, H.F. Hess, G.P. Kochanski, S. Buchman, L. Pollack, Y.M. Xiao, D. Kleppner, and T.J. Greytak, Phys. Rev. B **34**, 7670 (1986).

[17] J. Helffrich, M.P. Maley, M. Krusius, and J.C. Wheatley, Phys. Rev. B **34**, 6550 (1986).

[18] J.J. Berkhout, O.H. Höpfner, E.J. Wolters, and J.T.M. Walraven, in *Proceedings of the Eighteenth International Conference on Low Temperature Physics, Kyoto, Japan, 1987*, Jpn. J. Appl. Phys. **26**, Suppl. 26-3, 231 (1987).

[19] We purified our ^{4}He with a superleak. The ^{3}He content is ≈ 0.2 ppm. To estimate the film thickness we use the formula $mgh = V(d)$ with $V(d) = m\alpha(d)d^{-3}$. For $d = 0$ we use $\alpha = 2.42 \times 10^{-24}$ m^5 s^{-2} [G.D.L. Webster, M. Chester, E. Webster, and T. Oestereich, J. Low Temp. Phys. **40**, 207 (1980)], while we assume $\alpha(115\text{Å}) \approx 0.75\alpha(0)$ [D.F. Brewer, in *The Physics of Liquid and Solid Helium*, edited by K.H. Bennemann and J.B. Ketterson (Wiley, New York, 1978), Part II, p. 584].

[20] As pointed out to us by M. Papoular, static roughness with a needlelike shape and a diameter comparable to the thermal wavelength of the atoms may also result in a temperature dependence. The presence of this type of surface roughness is unlikely in view of the polishing procedure employed.

[21] T.W. Hijmans and G.V. Shlyapnikov, Phys. Lett. A **142**, 45 (1989).

[22] E. Tiesinga, H.T.C. Stoof, and B.J. Verhaar , Phys. Rev. B **41**, 8886 (1990). See also Ref. 6.

[23] D.W. Keith, M.L. Schattenburg, H.I. Smith, and D.E. Pritchard, Phys. Rev. Lett. **61**, 1580 (1988).

Chapter 5

SCATTERING OF HYDROGEN ATOMS FROM LIQUID-HELIUM SURFACES

We analyze in detail experiments in which we study the interaction of atomic hydrogen with liquid-helium surfaces. A theoretical background and a description of the experimental setup is given. A first experiment measured the transmission of hydrogen atoms through a capillary in the temperature interval of $145 < T < 526$ mK for ^{4}He surfaces and $73 < T < 174$ mK for ^{3}He surfaces. To extract the thermally averaged sticking probability s we need a model relating the atomic sticking coefficient $s(\vec{v})$ to the capillary transmission K. We analyze our data with a model based on a fixed $s(\vec{v})$, resulting in $s = 0.33(3)T$, and a model based on a speed-dependent $s(\vec{v})$, resulting in $s = 0.65(6)T$. The data show s to be linearly dependent on temperature. We do not observe any significant difference in s between ^{4}He and ^{3}He surfaces. In a second experiment we used a hemispherical liquid-helium-covered quartz mirror to focus a hydrogen atom beam. The resolution of our setup is about 10 mrad, which is sufficient to study direct near-elastic scattering, providing precision data for the sticking coefficient is available.

Als wetenschappelijker denk ik eerst wanneer
een duchtiger onderzoeking aangevangen geworden is geweest.

— Prof. dr. Prlwytzkofsky, *PRAW! der Hemeldonderweder.*

5.1 Introduction

Scattering hydrogen atoms from the surface of liquid helium has attracted interest from a variety of physical fields.[1–5] The topic originates in studies of (spin-polarized) hydrogen at low temperature, where inelastic scattering processes provide the mechanism to exchange heat between bulk H gas and helium-covered walls of a sample cell. In particular at high gas densities or at low temperatures, where recombination to the (solid) molecular state H_2 is most effective, substantial temperature differences may develop between gas and surface. This issue arises in experiments aimed at achieving Bose–Einstein condensation in electron spin-down-polarized hydrogen (H↓) by compression methods.[6–12] In experiments to accumulate electron spin-up-polarized hydrogen (H↑) using pure field confinement in a magnetic trap, walls provide a cooling mechanism during filling.[13–17] There one has to strike a subtle balance between cooling efficiency and flux losses due to surface recombination or spin relaxation.[18–20] From a more general point of view the scattering of hydrogen atoms from the surface of liquid helium may be regarded as a model system to study the low energy limit of atom surface scattering. Apart from beam-type scattering experiments experimental information may be extracted from data for the sticking coefficient s, defined as the probability that a colliding atom will be scattered into a surface bound state, or from the accommodation coefficient α, characterizing the energy transfer per collision.

In this article we analyze two series of experiments in which we addressed the scattering of neutral hydrogen atoms from the surface of liquid helium in the temperature regime where quantum effects dominate the physics. First we studied the effect of sticking on the flow of H gas through a capillary.[21] This capillary-flow (CF) experiment proved that the average momentum of the atoms parallel to the capillary axis is largely conserved in the flow, which was interpreted to imply the presence of substantial specular reflection on the capillary surface. The second series of experiments were done to obtain additional support for this interpretation and to look for the presence of direct (non-sticking) inelastic scattering using an atomic mirror.[22] As the results of the CF-experiment showed that reflection of H atoms at a surface turns out to be high and the influence of substrate roughness is not too important, the feasibility of this mirror reflection (MR) experiment became clear. Generally, information about the atom–surface collisions is best obtained by angularly resolved measurements of single atom–surface scattering for the whole range of angles of incidence. In the MR experiment the effect of individual collisions of atoms incident along the surface normal were observed by using the reflection of atoms at a mirror surface to focus an atomic beam. An experimental advantage of this approach is the relatively easy detection due to the large integrated intensity. In these experiments for the first time focusing of an atomic beam by means of a solid mirror could be demonstrated.

This article is organized as follows. First we summarize the theoretical and experimental

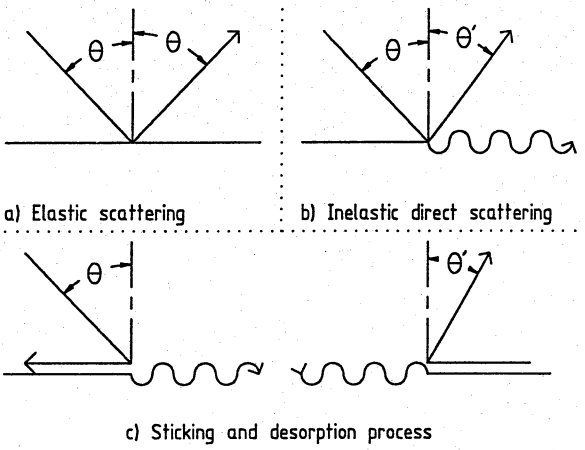

Figure 5.1:
Scattering of H atoms from a liquid-helium surface may be elastic (a), inelastic non-sticking (b), or inelastic by sticking and desorption (c); θ is the angle of incidence of the atom, θ' the angle of reflection.

background. Then we discuss the principle of our experiments and describe the detailed experimental setups. Section 5.5 deals with the measurements and their interpretation. The conclusions are given in Sec. 5.6.

5.2 Background

If an H-atom collides with a liquid-helium surface, in general three types of scattering processes may occur, two of which are inelastic; the third channel is elastic (see Fig. 5.1).

The elastic collisions, in which the energy and the momentum parallel to the surface is conserved, lead to specular reflection, be it that microscopic roughness may cause the reflection to appear as non-specular with respect to the macroscopic substrate.

Inelastic scattering may be divided in direct inelastic processes in which the atom is reflected non-specularly without adsorption, and sticking processes where the atom scatters into a surface bound state. In principle heat transfer is sensitive to both types of inelastic collisions. However, the direct inelastic channel is less efficient in this respect by a factor of order $(\epsilon_a/k_BT)^{-1.5}$ compared to the sticking channel (here ϵ_a is the surface adsorption energy and k_B is the Boltzmann factor).[23,24] For H on ^{4}He $\epsilon_a = 1.00(2)$ K,[25] so the energy transfer of this process becomes quickly unimportant for temperatures below 500 mK. Also the momentum transfer parallel to the surface will become very small, so its influence

on the capillary flow will be negligible. Nevertheless, as we shall argue in this paper the probability for near-elastic scattering may remain important at lower temperatures for experiments discriminating between elastic and near-elastic scattering. This view is supported by calculations.[26,27]

Experimentally the sticking process is characterized by the sticking coefficient s, defined as the probability that a colliding atom will enter a surface bound state. The heat transfer is characterized by the accommodation coefficient α which is defined as

$$\alpha = \lim_{T_g \to T_w} \frac{\dot{Q}_g - \dot{Q}_o}{\dot{Q}_g - \dot{Q}_w} , \tag{5.1}$$

where $\dot{Q}_g$ is the average kinetic energy flux (heat flux) carried by the incident gas atoms, T_g is the gas temperature, $\dot{Q}_o$ the outgoing heat flux, and $\dot{Q}_w$ the outgoing heat flux if all incident atoms would be thermalized on the surface at temperature T_w. For $T_g \approx T_w$ the net heat flux from gas to surface is given by

$$P \approx \alpha \Phi 2 k_B (T_g - T_w) , \tag{5.2}$$

with Φ the total incident atomic flux.

For a thermal gas of hydrogen atoms s was first determined by Jochemsen *et al.*[28,29] Using magnetic resonance they found $s = 0.046$ at $T \approx 200$ mK for ^{4}He surfaces and $s = 0.016(5)$ for ^{3}He surfaces at $T \approx 100$ mK. Salonen *et al.* measured ballistic heat transport with a time-resolved method and found $\alpha = 0.2(1)$ for H on ^{4}He.[30] In a subsequent steady-state heat flux experiment Salonen *et al.* (SJKTT) obtained $\alpha = 0.19(5)$ for $T = 440$ mK.[31] Bell *et al.* found α to decrease from $\alpha = 0.8(4)$ at 600 mK to $\alpha = 0.4(2)$ at 275 mK.[9] Helffrich *et al.* also found a decreasing α for decreasing temperature in the range 180–400 mK with an SJKTT-type experiment.[32] Recently Doyle *et al.* extended the temperature range studied by three orders of magnitude. They observed an increasing sticking coefficient with decreasing temperature up to a value of $s = 0.30$ at $T = 100$ μK.[33] We noted slightly different definitions of α by the various authors.

The interpretation of the experiments mentioned in the previous paragraph is primarily based on a model in which H atoms either scatter elastically or enter a surface bound state (the sticking process) under emission of a single ripplon. The adsorption potential only supports a single bound state.[34,35] The adsorbed atoms are not localized in directions parallel to the surface but behave as the atoms of a nearly free two-dimensional gas.[36] The wave function of an adsorbed atom may therefore be written as

$$\Psi_{\vec{k}}(\vec{R}, Z) = A^{-1/2} \exp(i\vec{k} \cdot \vec{R}) \phi(Z) , \tag{5.3}$$

in which $\vec{k}$ is the component of the wave vector parallel to the surface, $\vec{R}$ is the two-dimensional position vector, Z is the distance to the surface reference plane with area A,

and $\phi(Z)$ is a function describing the Z dependence of the wave function. The sticking of the atoms leads to a surface density n_S which in thermal equilibrium is related to the volume density n_V by the surface adsorption isotherm. For volume densities of practical interest in our experiments this surface adsorption isotherm may be written as[37]

$$n_S = n_V \lambda_{th} \exp(\epsilon_a / k_B T) , \tag{5.4}$$

where $\lambda_{th} = (2\pi\hbar^2/mk_BT)^{1/2}$ is the thermal wavelength (m is the mass of the hydrogen atom). As was first pointed out by Kagan and Shlyapnikov the adsorption process is accompanied by the excitation of a single ripplon and not significantly by the excitation of phonons.[38] The ratio of double ripplon emission to single ripplon emission for the adsorption process was estimated by Statt to be about 0.2.[39] The dispersion relation for the ripplons on a layer of helium covering a horizontal substrate is given by[40,41]

$$\omega_q{}^2 = \left[\left(g + \frac{3\alpha}{m_{He} d^4}\right) q + \frac{\gamma}{\rho_0} q^3\right] \tanh(qd) , \tag{5.5}$$

with ω_q the ripplon frequency, q the ripplon wave number, g the gravity acceleration, α the Van der Waals attractive constant (which is of the order of 2×10^{-50} J m^3),[42] d the helium-film thickness, $\gamma = 3.54 \times 10^{-4}$ J m^{-2} the ^{4}He surface tension at $T < 0.5$ K,[43,44] and $\rho_0 = 145$ kg m^{-3} the ^{4}He bulk density. Except for ^{4}He layers thicker than approximately 1 μm the Van der Waals contribution dominates the gravity contribution in Eq. (5.5). For typical ^{4}He films of about 100 Å thickness the gravity contribution is 8 orders of magnitude smaller than the Van der Waals contribution. The Van der Waals attraction also dominates over capillarity for ripplon wavelengths of order 4000 Å and larger. The hyperbolic tangent incorporates the effect of the film thickness on the ripplon dispersion. Ripplons with wavelengths comparable to or smaller than this thickness behave as those on bulk liquid.

In the adsorption process a substantial part of the binding energy is converted into kinetic energy of the atom in the adsorbed state. This is illustrated in Fig. 5.2, in which the dispersion curves for ripplons and adsorbed atoms are plotted for the case of vanishing incoming kinetic energy ($E_k \ll \epsilon_a$). At the intersection of these curves both the momentum parallel to the surface and the energy are conserved, atom and ripplon having equal but opposite momentum. The intersection point corresponds to a ripplon with a wavelength $\lambda_r = 47$ Å and an atom with a kinetic energy $E^*/k_B = 423$ mK. Thus, for the sticking process on a typically 100 Å thick film the gravitational acceleration, the Van der Waals term and the thin film factor $\tanh(qd)$ are not important, reducing Eq. (5.5) to

$$\omega_q{}^2 = (\gamma/\rho_0) q^3 . \tag{5.6}$$

After adsorption, two possible situations may occur. The atom may be evaporated by interaction with a ripplon while still in the energetic state E^* or thermalize through ripplon

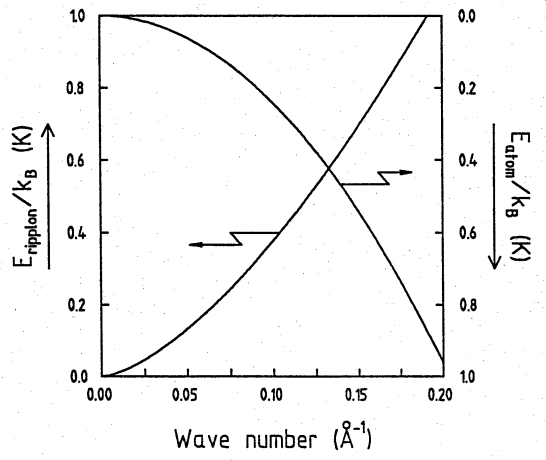

Figure 5.2:
Plot of the dispersion relations of ripplons on a ^{4}He surface (left axis) and H atoms (right axis). At the intersection the sum of the kinetic energies of the H-atom and the ripplon equals the binding energy of the H-atom on the helium surface.

interaction before it is evaporated at a later stage. Zimmerman and Berlinsky calculated the mean time between ripplon interactions for an H-atom on the ^{4}He surface to range from 8.7×10^{-10} s at 400 mK to 2.4×10^{-8} s at 100 mK, much shorter than the mean residence time on the surface τ_a which ranges from 1×10^{-8} s at 400 mK to 3×10^{-4} s at 100 mK.[40] An expression for τ_a,

$$\tau_a = \frac{2\pi\hbar}{sk_BT} \exp(\epsilon_a/k_BT) \ , \tag{5.7}$$

is obtained by balancing the flux of sticking atoms $\Phi_s \equiv s\Phi$ against the flux of desorbing atoms $\Phi_d = n_S A \tau_a^{-1}$ for thermal equilibrium conditions. Here $\Phi = \frac{1}{4} n_V \bar{v} A$ is the total incident flux of atoms with A the surface area and $\bar{v} = (8k_BT/\pi m)^{1/2}$ is the average atomic speed.

The sticking probability was first calculated by Zimmerman and Berlinsky[36] and Kagan and Shlyapnikov.[38] Recent calculations by Hijmans, Walraven and Shlyapnikov[45] and Carraro and Cole[46] discuss the sticking probability on helium films, taking into account the effects of the substrate. The more general problem of calculating the accommodation coefficient has been addressed by Kagan *et al.*,[23] Statt,[39] and Goldman.[47] In these theories the helium surface is treated as the surface of an incompressible liquid with a sharp density

profile

$$\rho(\vec{r},z)=\rho_0\theta[z+h(\vec{r})]\ . \tag{5.8}$$

Here $\vec{r}$ is the two-dimensional position vector in the plane of the surface, z the coordinate perpendicular to the surface, and $\theta(z)$ is the unit step function. Note that for a surface with a smooth density profile the use of the error function instead of the unit step function is more appropriate. The height fluctuations of the surface $h(\vec{r})$ may be expressed in terms of the elementary surface excitations, the ripplons, using a normal mode decomposition:

$$h(\vec{r})=\frac{1}{\sqrt{A}}\sum_{\vec{q}}h_{\vec{q}}\,e^{i\vec{q}\cdot\vec{r}}\ , \tag{5.9}$$

with $\vec{q}$ the ripplon wave vector. The ripplon amplitude $h_{\vec{q}}$ is expressed in terms of the ripplon creation $r^\dagger_{\vec{q}}$ and annihilation $r_{\vec{q}}$ operators as

$$h_{\vec{q}}=\left[\frac{\hbar q\tanh(qd)}{2\rho_0\omega_q}\right]^{1/2}(r^\dagger_{\vec{q}}+r_{-\vec{q}})\ . \tag{5.10}$$

The effective surface–atom interaction for an atom at position $(\vec{R},Z)$ with $\vec{R}$ the two-dimensional vector along the surface is given in linear approximation by

$$U(\vec{R},Z)=U_0(Z)-\frac{1}{\sqrt{A}}\sum_{\vec{q}}h_{\vec{q}}\exp(i\vec{q}\cdot\vec{R})\frac{\partial U_q(Z)}{\partial Z}\ , \tag{5.11}$$

with $U_0(Z)$ the static potential of a flat surface, and $U_q(Z)$ defined as

$$U_q(Z)=n_{\rm He}\int e^{i\vec{q}\cdot\vec{r}}\int V(\{r^2+[Z-z]^2\}^{1/2})\theta(z)\mathrm{d}z\mathrm{d}^2r\ , \tag{5.12}$$

where $n_{\rm He}$ is the helium-atom density. The interaction Hamiltonian in second quantized form is given by

$$H_{\rm int}=\frac{1}{\sqrt{A}}\sum_{\sigma\prime,\sigma,\vec{q},\vec{k}}h_{\vec{q}}\left\langle\sigma\left|\frac{\partial U_q(Z)}{\partial Z}\right|\sigma\prime\right\rangle a^\dagger_{\vec{k}-\vec{q},\sigma\prime}a_{\vec{k},\sigma}\ , \tag{5.13}$$

where σ is associated with the momentum of the H-atom normal to the surface and may characterize the bound state or one of the continuum states. Far from the surface σ is the component of the wave vector normal to the surface and $E\cos^2\theta=\hbar^2\sigma^2/2m$. The adsorption rate $R(E,\theta)$ per atom may be calculated using first order time dependent perturbation theory:[36]

$$\begin{aligned}R(E,\theta)=\frac{2\pi}{\hbar A}\sum_{\vec{q}}\quad&\frac{\hbar q\tanh(qd)}{2\rho_0\omega_q}\left|\left\langle B\left|\frac{\partial U_q(Z)}{\partial Z}\right|\sigma\right\rangle\right|^2\\&\times[(1+n_{\vec{q}})(1+N_{\vec{k}-\vec{q}})\delta(E+\epsilon_{\rm a}-E_{\rm f}-\hbar\omega_q)\\&+n_{\vec{q}}(1+N_{\vec{k}+\vec{q}})\delta(E+\epsilon_{\rm a}-E_{\rm f}+\hbar\omega_q)]\ ,\end{aligned} \tag{5.14}$$

with $\langle Z|B\rangle$ the bound-state wave function of the atom with kinetic energy E_f and $\langle Z|\sigma\rangle$ the free-state wave function. Further, $n_{\vec{q}}$ is the occupation number for ripplons with momentum $\hbar\vec{q}$ and $N_{\vec{k}-\vec{q}}$ ($\ll 1$) the analogous function for the H atoms. As the wavelength of the ripplons involved in the transition from free- to bound-state of the H atoms (47 Å) is smaller than the wavelength of thermal ripplons (typically 100 Å at 200 mK) the thermal occupation of these states is vanishing ($n_{\vec{q}} \ll 1$). For the adsorption process the surface therefore may be considered to be in its ground state over the temperature range covered by our experiments. The sticking probability is obtained by normalizing the transition rate to the incident flux:

$$s(E,\theta) = \frac{VR(E,\theta)}{A(E/2m)^{1/2}\cos\theta} , \tag{5.15}$$

with V the volume of the sample cell. For low temperatures ($k_B T \ll \epsilon_a$) the matrix element is proportional to σ, so in this limit

$$s(E,\theta) = s_0 E^{1/2}\cos\theta \tag{5.16}$$

or

$$s(\vec{v}) = s_0(\tfrac{1}{2}mv^2)^{1/2}\cos\theta , \tag{5.17}$$

where s_0 is a proportionality constant. The thermally averaged sticking coefficient for incoming atoms at an angle θ with the normal on the surface, $s(T,\theta)$, and the overall thermally averaged sticking coefficient, $s(T)$, follow from integrating $s(\vec{v})P_{in}(T,\vec{v})d\vec{v}$, in which $P_{in}(T,\vec{v})$ is the normalized velocity distribution of the incoming atomic flux at temperature T. For a Maxwell–Boltzmann gas we find

$$P_{in}(T,\vec{v})d\vec{v} = \left(\frac{m}{k_B T}\right)^2 \frac{v\cos\theta\exp(-mv^2/2k_B T)}{2\pi} d\vec{v} . \tag{5.18}$$

By calculating $s(T,\theta)$ and $s(T)$ we find for the angular dependence

$$s(T,\theta) = \tfrac{3}{2}s(T)\cos\theta . \tag{5.19}$$

As found by Zimmerman and Berlinsky the dependence of $s(E,\theta)/\cos\theta$ continues to be weakly dependent on θ even for higher temperatures, so Eq. (5.19) holds for higher temperatures as well.[36] Equation (5.16) also leads to the thermal average of s, $s(T)$, being proportional to $T^{1/2}$ in the low-temperature limit. However, Goldman showed that s is strongly dependent on the long-range part of the interaction potential with the surface, and due to resonant enhancement of the sticking process the low-temperature limit for some potentials is only reached for $T \ll 1$ μK.[47] For helium films such resonances may be induced by the substrate potential as discussed by Hijmans *et al.*[45] and Carraro and Cole.[46]

In the regime where direct inelastic scattering is unimportant, that is for temperatures below 500 mK, Eq. (5.1) may be used to relate the accommodation coefficient to the sticking coefficient. From the Boltzmann distribution follows

$$\dot{Q}_{\mathrm{g}} = 2k_{\mathrm{B}}T_{\mathrm{g}}\Phi \tag{5.20}$$

and

$$\dot{Q}_{\mathrm{w}} = 2k_{\mathrm{B}}T_{\mathrm{w}}\Phi \ , \tag{5.21}$$

where Φ is the total incoming flux of atoms. The average outgoing heat flux $\dot{Q}_{\mathrm{o}}$ depends on the distribution of incoming atoms $P_{\mathrm{in}}(T_{\mathrm{g}}, \vec{v})$ and that of the desorbing atoms $P_{\mathrm{out}}(T_{\mathrm{w}}, \vec{v})$. To find the velocity distribution of the desorbing atoms, we apply the principle of detailed balance: the incoming atomic flux $\Phi_{\mathrm{in}}(\vec{v})\mathrm{d}\vec{v}$ must, in equilibrium conditions, exactly equal the outgoing flux $\Phi_{\mathrm{out}}(\vec{v})\mathrm{d}\vec{v}$. The incoming flux follows from Eq. (5.18):

$$\Phi_{\mathrm{in}}(\vec{v})\mathrm{d}\vec{v} = \Phi P_{\mathrm{in}}(T, \vec{v})\mathrm{d}\vec{v} \ . \tag{5.22}$$

The outgoing flux consists of two contributions:

$$\Phi_{\mathrm{out}}(\vec{v})\mathrm{d}\vec{v} = \Phi_{\mathrm{in}}(\vec{v})[1 - s(\vec{v})]\mathrm{d}\vec{v} + P_{\mathrm{out}}(T, \vec{v})\mathrm{d}\vec{v} \int s(\vec{v})\Phi_{\mathrm{in}}(\vec{v})\mathrm{d}\vec{v} \ , \tag{5.23}$$

the first part being the flux due to the specularly scattered atoms and the second part being due to the desorbed surface atoms. As, by definition,

$$s(T) = \frac{\int s(\vec{v})\Phi_{\mathrm{in}}(\vec{v})\mathrm{d}\vec{v}}{\int \Phi_{\mathrm{in}}(\vec{v})\mathrm{d}\vec{v}} \ , \tag{5.24}$$

this balance leads to the relation

$$s(\vec{v})\Phi_{\mathrm{in}}(\vec{v})\mathrm{d}\vec{v} = s(T)\Phi P_{\mathrm{out}}(T, \vec{v})\mathrm{d}\vec{v} \ , \tag{5.25}$$

or

$$s(\vec{v})P_{\mathrm{in}}(T, \vec{v})\mathrm{d}\vec{v} = s(T)P_{\mathrm{out}}(T, \vec{v})\mathrm{d}\vec{v} \ . \tag{5.26}$$

Like the outgoing atom flux the average outgoing heat flux $\dot{Q}_{\mathrm{o}}$ also consists of two parts:

$$\dot{Q}_{\mathrm{o}} = \Phi \int \tfrac{1}{2}mv^2 P_{\mathrm{in}}(T_{\mathrm{g}}, \vec{v})[1 - s(\vec{v})]\mathrm{d}\vec{v} + \Phi s(T_{\mathrm{g}}) \int \tfrac{1}{2}mv^2 P_{\mathrm{out}}(T_{\mathrm{w}}, \vec{v})\mathrm{d}\vec{v} \ . \tag{5.27}$$

Substitution of Eqs. (5.20), (5.21) and (5.27) in Eq. (5.1) results in

$$\alpha = \lim_{T_{\mathrm{g}} \to T_{\mathrm{w}}} \frac{1}{2k_{\mathrm{B}}(T_{\mathrm{g}} - T_{\mathrm{w}})} \times \left[\int \tfrac{1}{2}mv^2 P_{\mathrm{in}}(T_{\mathrm{g}}, \vec{v}) s(\vec{v})\mathrm{d}\vec{v} - s(T_{\mathrm{g}}) \int \tfrac{1}{2}mv^2 P_{\mathrm{out}}(T_{\mathrm{w}}, \vec{v})\mathrm{d}\vec{v} \right] \ . \tag{5.28}$$

Using Eq. (5.26) this results in

$$\alpha = \frac{s(T_w)}{2k_B} \left.\frac{d}{dT}\right|_{T=T_w} \frac{1}{s(T)} \int \tfrac{1}{2} m v^2 s(\vec{v}) P_{in}(T, \vec{v}) d\vec{v} \, . \tag{5.29}$$

To reduce this expression we find an expression for $\frac{1}{2} m v^2 P_{in}(T, \vec{v})$ by differentiating Eq. (5.18) with respect to T:

$$\tfrac{1}{2} m v^2 P_{in}(T, \vec{v}) = 2k_B T \left[P_{in}(T, \vec{v}) + \tfrac{1}{2} T \frac{d}{dT} P_{in}(T, \vec{v}) \right] \, . \tag{5.30}$$

By substituting this result in Eq. (5.29) and using Eq. (5.24) we find

$$\alpha = s(T_w) \left.\frac{d}{dT}\right|_{T=T_w} \frac{T}{s(T)} \left[s(T) + \tfrac{1}{2} T \frac{d}{dT} s(T) \right] \, , \tag{5.31}$$

or, after some straightforward differentiation:

$$\alpha(T) = s(T) \left[1 + \tfrac{1}{2} \frac{d \ln s(T)}{d \ln T} + \tfrac{1}{2} \frac{d^2 \ln s(T)}{(d \ln T)^2} \right] \, . \tag{5.32}$$

This expression enables the comparison of all experimental results on the sticking coefficient with those on the accommodation coefficient. For the linear temperature dependence of s observed in our experiments this relation reduces to $\alpha(T) = \frac{3}{2} s(T)$. An equivalent form of this expression has been given by Goldman.[47]

The theory as described above may also be used to calculate the amount of direct inelastic scattering. The direct inelastic scattering rate may be found by replacing $\langle Z|B\rangle$ with $\langle Z|\sigma I\rangle$ in Eq. (5.14), taking $N(\vec{k})$ to be the density of bulk atom states and adapting the sum over final states to bulk instead of bound states. For direct inelastic scattering over small angles the density of states of thermal ripplons is not negligible. Furthermore, the ripplons involved in this type of scattering have large wavelengths, so both the Van der Waals term and the thin film factor in Eq. (5.5) have to be taken into account and the use of the reduced Eq. (5.6) is not allowed anymore. A calculation by Hijmans and Shlyapnikov shows that for atoms perpendicularly incident on the surface the probability for direct inelastic scattering becomes greater than the probability for sticking for scattering angles less than about 0.2 rad at 500 mK down to 0.1 rad at 100 mK.[26]

5.3 Experimental setup

In the CF-experiment the aim was to determine $s(T)$. We use two volumes connected by a capillary (see Fig. 5.3). At the start of a measurement, one of the volumes, the buffer volume, contains a quantity of H gas. The second volume, the pump volume, is kept empty of H atoms at all times (by recombining them to H_2 molecules). The atoms travel through

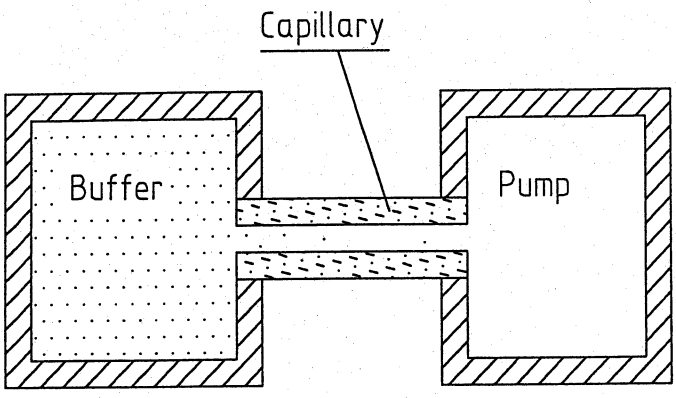

Figure 5.3:
The principle of capillary-flow experiment.

the capillary from the buffer volume to the pump volume. As the mean free path of the atoms is much larger than the dimensions of the capillary, the atomic flux Φ is determined by the capillary impedance, which should depend on the sticking coefficient. We extract the sticking coefficient either from the time constant of the resulting density decrease in the buffer volume or the time constant of the decreasing flux through the capillary.

The aim of the MR experiment was to determine the fraction of atoms reflected specularly from a surface after a single collision per atom. Again a geometry with a buffer volume and a pump volume was used (see Fig. 5.4). Atoms are loaded into the buffer volume, from which they may escape to the pump volume through a small diaphragm. In this pump volume a concave mirror is situated which acts to reflect all specularly scattering atoms back through the diaphragm into the buffer volume. In the ideal case with unit probability of specular reflection, this results in the absence of a density decrease in the buffer volume. In the actual situation, the decay of the stagnant density allows us to extract information about the scattering process.

5.4 Experimental apparatus

5.4.1 General cryogenic system

Our experiments are carried out in an Oxford Instruments 1000 (1000 μmol/s maximum circulation) dilution refrigerator[48] with a maximum cooling power of 500 μW at a mixing chamber temperature of 100 mK and an unloaded base temperature of 4.5 mK (see Fig. 5.5). The sample cells were placed in the center of a 6 T superconducting magnet (Thor Cryogenics

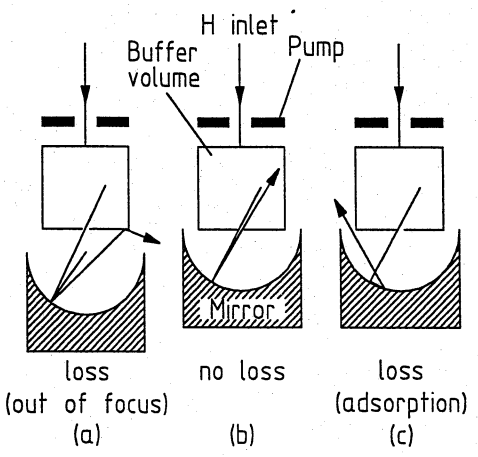

Figure 5.4:
The principle of mirror reflection experiment.

Ltd., 35 mm bore) with a homogeneity in the center of $1{:}10^4$ in a volume of at least 1 cm^3.

5.4.2 The capillary-flow cell

A schematic drawing of the capillary-flow cell used in the CF-experiment is shown in Fig. 5.6. The cell body has been made of a low magnetic impurity type copper and is connected to the mixing chamber by a 20 × 20 mm copper rod. The H atoms are produced by a room-temperature discharge and fed into the cell from the bottom through a thin-walled german silver filling tube of 5.6 mm inner diameter. On their way to the cell the atoms pass two intermediate cooling stages, the accommodator, running at about 7 K, and the HEVAC, running at about 650 mK.[8] The H$\downarrow$ atoms are driven to the high magnetic field region by field gradients and fluxing helium vapor and are collected in a buffer volume (V_b). Because of the difference in magnetic field between the dissociator (almost no field) and the cell (6 T) only high field seeking atoms enter the cell. Due to the relatively low concentration of magnetic impurities, some double polarization by preferential recombination of $|a\rangle$ states may occur. (The ground-state hyperfine levels are labeled $|a\rangle$, $|b\rangle$, $|c\rangle$, and $|d\rangle$ in order of increasing energy.) However, any double polarization and subsequent change in relaxation rates is completely unimportant in this series of experiments in view of the relevant time scales involved.

All inner surfaces at cell temperature are covered with a liquid-helium film. An upper limit of 110 Å for the thickness of this film is calculated by assuming the helium content

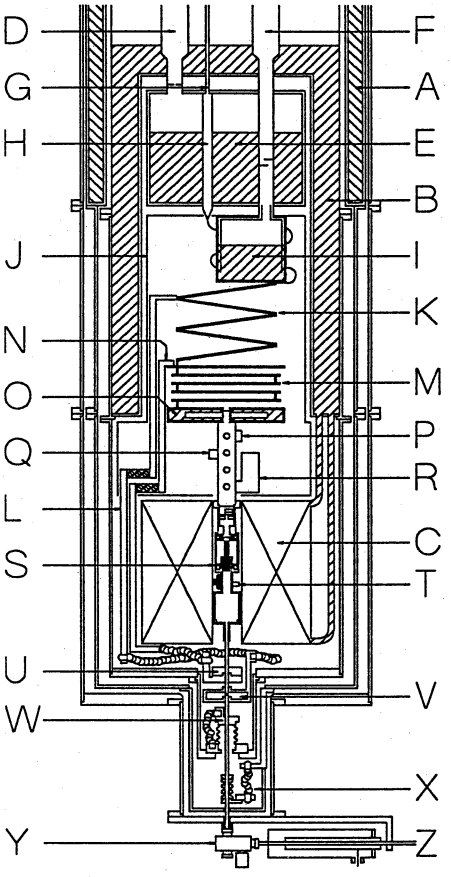

Figure 5.5:
Schematic view of our dilution refrigerator cryostat. Explanation of symbols: A: Liquid nitrogen bath (77 K); B: Main He bath (4.2 K); C: Main magnet; D: He pump line; E: Pumped He bath (1.2 K); F: Mixture pump line; G: Mixture return line; H: Condensor and condenser capillary; I: Still; J: Shield (800 mK); K: Continuous heat exchanger; L: Pinning (600 mK); M: Discrete heat exchanger; N: Pinning (200 mK); O: Mixing chamber; P: Cell heater; Q: Upper cell thermometer; R: NBS fixed point device; S: CF cell; T: Lower cell thermometer; U: Thermal platform (about 300 mK); V: HEVAC (about 650 mK); W: Accommodator (about 7 K); X: Pinning (about 80 K); Y: Teflon valve Z: Room-temperature dissociator;

of the cell to be just short of being capable to form bulk liquid. This corresponds to the maximum allowed quantity of helium before its evaporation at higher temperatures in the fill tube gives rise to unacceptable heat loads on the cell.

The buffer volume contains a doped germanium bolometer[49] and a capacitive pressure transducer. The pressure gauge, which was previously used by Van Yperen *et al.*,[50] has a sensitivity of 1.74 pF/Torr and a noise equivalent pressure of 5×10^{-7} Torr (1 standard deviation at a bandwidth of 1.25 Hz) which corresponds to a minimum detectable density of 1×10^{13} cm^{-3} at 500 mK. The noise was due mainly to voltage noise originating in our General Radio capacity bridge. The pressure gauge also displayed long term drift, induced by changes in the magnetic field. The buffer volume was etched and thoroughly cleaned to free it from magnetic impurities, thereby reducing impurity relaxation (and subsequent

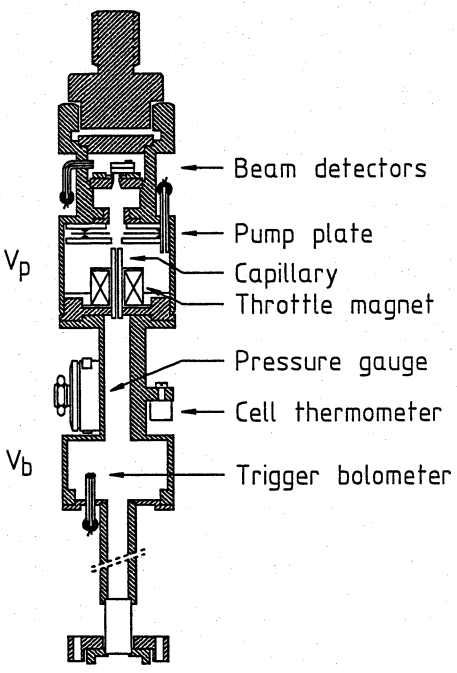

Figure 5.6:
The experimental cell for the capillary-flow experiment.

recombination).[51] The effective volume of this compartment, defined as

$$V_b \equiv \int_V [n(\vec{r})/n_0] \mathrm{d}\vec{r} = \int_V \exp\left(\frac{\mu_B[B(\vec{r}) - B_0]}{k_B T}\right) \mathrm{d}\vec{r}\,, \tag{5.33}$$

ranges from $V_b = 5.3(4)$ cm^3 at 70 mK to 10.0(1) cm^3 at 500 mK. Here B_0 and $B(\vec{r})$ are the magnetic fields at the entrance of the capillary and at position $\vec{r}$ respectively, n_0 and $n(\vec{r})$ are the corresponding atom densities, μ_B is the Bohr magneton, and T the gas temperature.

Atoms will move from the buffer volume to the pump volume through the capillary, where they are subsequently removed by a pump plate (PP) which also serves as a flux detector. The PP detection method is described in detail elsewhere.[52] The flow capillary has a length of 21.97(3) mm, an inner diameter of 0.496(3) mm, and 1.1(1) mm outer diameter. Aiming for a smooth inner surface we used a commercial Pyrex capillary tube which was ground down to the specified outer diameter to fit inside the bore of a small superconducting magnet in the cell to throttle the capillary flow as described below. The main field is homogeneous to within 1:10^4 over the capillary region. The capillary is glued into a copper plate using Stycast 1266 epoxy.[53] To account for the difference in thermal contraction between the pyrex and the copper, the thickness of the Stycast is chosen such that the combined thermal contraction of the pyrex and the epoxy matches the thermal contraction of the copper closely over the whole temperature range from room temperature

down to our operating temperature. A sufficiently accurate rule of thumb turns out to be $d = r/3$ (d the thickness of the epoxy between pyrex and copper and r the radius of the capillary). Before gluing, the capillary was sealed off at one end, which enabled us to test the bond to the copper plate for leaks before cutting the capillary to its proper length and assembling the cell as a whole. The joint was found to be vacuum tight to temperatures below the lambda point, even after repeated cycling between room temperature and helium temperatures. It proved essential to roughen and clean the outer surface of the pyrex thoroughly to obtain a good bond. For roughening the grinding procedure turned out to be sufficient, provided not too fine a grade was used. Cleaning was done ultrasonically using ethanol, acetone and freon.

The flow through the capillary may be throttled by locally reducing the field to less than 5 Tesla with a small magnet coil mounted around the capillary in the upper compartment. The coil has been wound with 12,500 turns of NIOMAX CN superconducting wire[54] with thickness of about 60 μm (including insulation) on a copper former with a bore of 1.2 mm. To reduce eddy currents, the former had a radial slit of 0.3 mm width, filled with Stycast 1266 epoxy. The turns were impregnated with Cyanolit 201. The Cyanolit cracks if cooled down, thereby enabling the liquid helium in the cell to cool the windings. The outer diameter of the coil was 11.8 mm. It is capable of producing a field of 1.3 T at a current of 1 A. By applying this field in the direction opposite to the main field, an energetic barrier for the H$\downarrow$ atoms is created, thereby effectively isolating the lower part of the cell from the upper part. For a temperature of 200 mK we calculate a reduction of the atomic flux to about 9% due to the throttling field if we assume a sticking coefficient $s = 0$, and even to 3% if we assume $s = 1$. By observing the pressure decay with and without the throttling field we were able to verify that the intrinsic recombination in the cell was mostly due to recombination in the upper compartment. This pressure decay was completely dominated by the loss of atoms through the capillary when the PP detector was activated.

An assembly of two additional bolometers was also placed in the upper part. As these detectors were not used in the actual measurements, we omit further description in the current context.

5.4.3 The mirror cell

The cell used in the MR experiment is shown in Fig. 5.7. In this case the buffer volume is separated from the pump volume by a diaphragm. The surfaces of the cell were again covered with a film by admitting into the cell a quantity of typically 0.02 cm^3 of liquid helium. This cell was connected to the mixing chamber by a 22 $\times$ 22 mm copper rod.

To produce the H atoms we changed over to a cryogenic RF dissociator operated at 600 mK and situated above the cell just outside the same 6 Tesla superconducting magnet

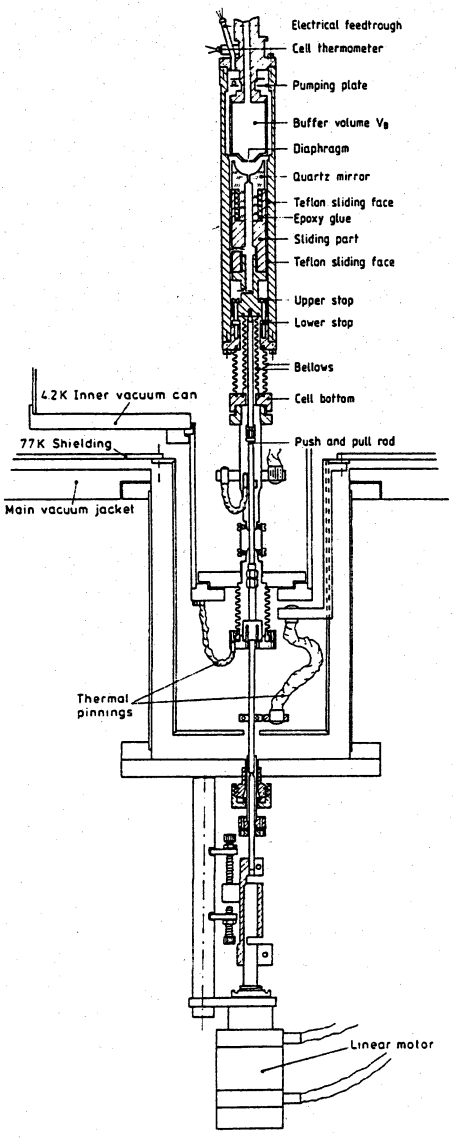

Figure 5.7:
The experimental cell for the mirror reflection experiment.

as used in the CF-experiment. The dissociator was used in an earlier experiment by our group[14] except for the helix, which was replaced by a helix of thicker copper wire in order to improve cooling. This four-turn helix was 13.5(5) mm in height with an outer diameter of 9.1(1) mm and a pitch of 0.33 mm^{-1} and was made from 1.55(5) mm diameter uninsulated commercial copper wire. It was glued with Eccoshield VSM silver filled epoxy[53] into a pothole drilled in the dissociator flange. To couple the RF power into the helix, a one turn coupling loop from copper wire 0.75(5) mm diameter and an outer diameter of 8.6(1) mm was glued to the end of the inner conductor of the RF feed line with Eccoshield VSM. Loop and helix were wound in opposite sense for optimal coupling.[55] This resulted in a dissociator with resonance frequency of 773.2 MHz and a Q-factor of 460 at room temperature. At 4.2 K the resonance had shifted to 776.5 MHz and the Q-factor rose to 725. The H$\downarrow$ flux entering the cell reached 1×10^{14} at/s with an input peak power of 32 mW during a pulse of 120 μs and a repetition rate of 150 Hz. As the dissociation energy of H_2 is 4.5 eV this corresponds to a dissociator efficiency of 6%. Crucial to starting the discharge proved a magnetic field exceeding 34 mT.

The dissociator is connected by a thin-walled stainless steel tube of 6 mm diameter and 11 mm length to an intermediate cooling stage at about 200–400 mK, depending on the cell temperature. To effectively cool the atoms and to recondense the helium vapor coming from the dissociator, this cooling stage is configured as a labyrinth with four right turns in the path of the atoms. Just before this labyrinth a germanium trigger bolometer is located in order to enable quick removal of any atoms remaining in the dissociator region after filling the buffer volume.

The high field seeking atoms ($|a\rangle$ and $|b\rangle$ states) are forced into the buffer volume by the magnetic gradient of the main coil. In order to minimize recombination losses great care was exercised to avoid magnetic surface impurities in the buffer volume by using a low magnetic impurity type copper[56] and careful etching and cleaning. Soldered to the bottom of the buffer compartment is a 50 μm thick copper foil containing a 0.25 mm radius orifice through which the atoms can escape to the pump volume. The effective buffer volume V_b (according to Eq. (5.33) with $B(0)$ at the diaphragm) ranges from 10.12 cm^3 at 80 mK to 10.39 cm^3 at 400 mK and is thus only very weakly dependent on temperature.

The pump volume contains a concave hemispherical fused quartz mirror with a radius of 9 mm, ground to optical precision. If this mirror is perfectly aligned with the orifice, an angle of reflection of an atom of about 1° with respect to the normal is sufficient to let the reflecting atom miss the orifice. The mirror is mounted in a copper sliding piece using Stycast 1266. To account for thermal contraction, the thickness of the Stycast layer has been matched to the thickness of the mirror stem with the method described above. While the epoxy was cured, the position of the focus was aligned to the vertical axis of the sliding piece by a laser system to an accuracy of better than 50 μm. The sliding piece fits into the

cell with a tolerance of less than 5 μm and can be moved up and down over a distance of about 4.8 mm.

At first the sliding surfaces were made of polished copper, but as this resulted in severe damage after moving the piece up and down several times before the start of the experiment, we changed the sliding surface to teflon rings of about 0.5 mm thickness, fitting tightly on the copper substrate and fixed in position by a rim of Stycast 1266. To ensure smooth operation at low temperature, it proved essential to polish the teflon surface to a high finish. The sliding piece was connected to a push and pull mechanism extending to an inchworm motor situated at room temperature. This inchworm motor may be positioned with an accuracy of 0.5 μm relative to the cryostat outer shield. To prevent damage to mirror and diaphragm, the displacement of the sliding piece was limited by stops also functioning as internal reference points for the mirror position. To prevent the occurrence of a pool of liquid helium at the bottom of the mirror a 1.1 mm hole was drilled at the axis of the mirror. This channel is also used to insure efficient evacuation of the lower part of the cell.

The atoms not reflected back into the buffer volume will travel randomly in the pump volume and may reach a PP detector through a slit between the outer wall of the buffer compartment and the inner cell wall. This annular slit is 0.5 mm wide over a length of 1.2 mm, followed by a 2.5 mm wide section over 35 mm. The probability for an atom moving randomly in the pump volume to reenter the buffer volume is calculated to be at most 2% of that to reach the pump plate.

The pump plate used in the MR experiment is mounted around the neck of the buffer volume. The design deviates slightly from that described in Ref. 52. The plate is cut out of 50 μm thick copper foil and is suspended by three 16 μm tungsten wires. To try to reduce microphonic noise these wires were put under tension with stainless steel springs exerting a force of 100–200 N at room temperature. This design turned out to be fairly shockproof. The operating temperature of the pump plate was 1.1 K with a heating power of typically 16 μW.

5.4.4 Surface roughness

Crucial to both experiments is the quality of the scattering surface, the inner surface of the capillary in the CF-experiment and the mirror surface in the MR-experiment. In order to estimate this quality we used a scanning electron microscope with a maximum resolution of about 100 Å.

To determine the smoothness of the inner surface of the capillary used in the CF-experiment, we put a sample of the same rod from which this capillary was made under the microscope. The results show a very smooth inner surface with no noticeable roughnesses of more than 100 Å in height except for some isolated grains of dirt and some scratches.

For the test sample the total area of damaged or dirty surface was less than 1% of the total surface area. The nature of the scratches leads us to believe that they were the result of the mechanical abrasion necessary to prepare the test sample. Therefore, to our estimate, less than 0.1% of the inner surface of the capillary used in the cell was not smooth.

The mirror surface was itself checked for microscopic roughness. This required the evaporation of a layer of chromium (about 50 Å) followed by a layer of gold (about 200 Å) on the surface. The surface was found to be very smooth, except for some pores with typical dimensions 1 μm not exceeding 0.3% of the total area. These holes possibly are an intrinsic property of the type of fused quartz from which the mirror was made. We estimate that not more than 1% of the atoms are lost from the specular beam due to static surface irregularities, which is negligible to the loss due to other geometrical factors such as the coma of the mirror. As the metallic layer on the quartz was damaged chemically by H_2 gas in a preliminary stage of the experiment, we repeated the final polishing stages on the surface, using the bare quartz surface in the experiment.

We assume any irregularities of size less than 100 Å to be smoothed out by the helium film. To support this assumption, we numerically analyzed the behavior of a helium film over a solitary cylindrical obstacle with a radius of 100 Å and a height of 100 Å on top of an otherwise perfectly smooth surface. We assume the substrate potential to result from addition of pair interaction of a test particle with the individual substrate atoms. In our model we treated the substrate as a homogeneous mass distribution. If the contribution to the total Van der Waals potential due to a volume element d^3x in the substrate is given by

$$\mathrm{d}U_{\mathrm{vdW}} = -\frac{6\alpha}{\pi r^6}\mathrm{d}^3x \ , \tag{5.34}$$

integration over a half-infinite three-dimensional substrate results in the usual expression for the Van der Waals potential $U_{\mathrm{vdW}} = -\alpha/d^3$. We numerically integrated Eq. (5.34) to obtain the Van der Waals potential $U_{\mathrm{vdW}}(\vec{r}, z)$ for any position above our model substrate. The hydrostatic pressure p in an incompressible liquid covering this substrate is given by:

$$p_{\mathrm{vdW}}(\vec{r}, z) = -\rho_0[U_{\mathrm{vdW}}(\vec{r}, z) - U_{\mathrm{vdW}}(\mathrm{ref})] \ , \tag{5.35}$$

where $U_{\mathrm{vdW}}(\mathrm{ref})$ is the Van der Waals potential at the surface of the liquid at infinity (above the flat plane reference). The surface tension also contributes to the hydrostatic pressure. At the liquid–vapor interface this pressure is given by

$$p_\gamma = \gamma\left(\frac{1}{R_1} + \frac{1}{R_2}\right) \ , \tag{5.36}$$

where R_1 and R_2 are the principal radii of curvature of the interface. As the gas and vapor pressures are negligible the total hydrostatic pressure at the surface has to be zero. The shape of the surface is therefore obtained from

$$p_{\mathrm{vdW}}(\vec{r}, z) + p_\gamma(\vec{r}, z) = 0 \ , \tag{5.37}$$

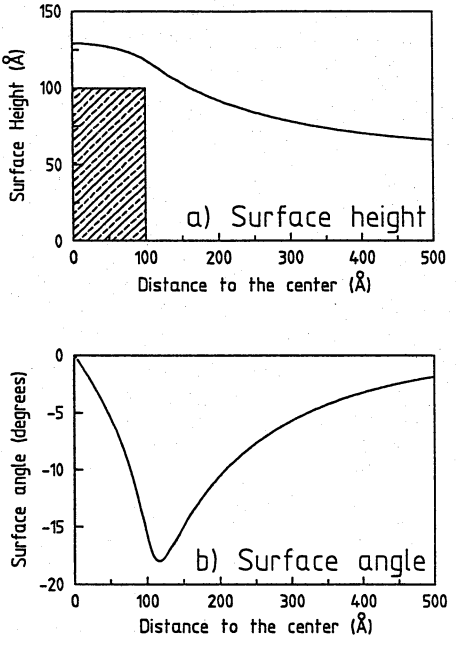

Figure 5.8:
a) Surface height of a ^{4}He film of 60 Å above a cylindrical obstacle of 100 Å as a function of the distance to the center of the obstacle; b) Angle of this film surface with respect to the plane of the surface.

resulting in

$$\rho_0[U_{\mathrm{vdW}}(\vec{r}, z) - U_{\mathrm{vdW}}(\mathrm{ref})] = \gamma \left(\frac{1}{R_1} + \frac{1}{R_2}\right) . \tag{5.38}$$

We calculated this shape numerically by relaxing the surface to zero total hydrostatic pressure for several film thicknesses. Figure 5.8(a) shows an example of a plot of the surface height as a function of distance to the center of the cylindrical obstacle for a film thickness of 60 Å. The angle of the film surface with respect to the plane of the substrate for this surface is shown in Fig. 5.8(b). The results for the maximum angle of the film surface with respect to the plane of the surface are given in Fig. 5.9 for several film thicknesses. For film thicknesses greater than about 120 Å this maximum angle, which is only reached in a small area, is smaller than 3°. A deviation of 3° for a specularly reflecting atom means that only after some tens of collisions an appreciable amount of momentum transfer parallel to the surface is achieved. We conclude that this amount of surface roughness is unimportant in the CF-experiment for the temperature regime studied. As the resolution of the MR-experiment is about 0.6°, this type of deviation might be of importance in this experiment. However, we believe that the total area thus affected is small enough to reduce the effect to a completely unimportant level. This assumption is supported by the observed reflectivity of the mirror as described below.

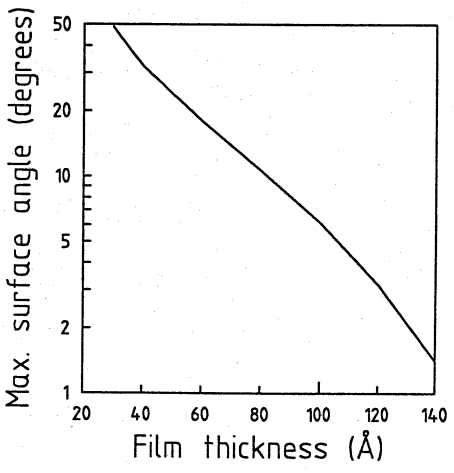

Figure 5.9:
Maximum angle with respect to the plane of the substrate of the film surface above a cylindrical obstacle as a function of film thickness.

5.4.5 Thermometry

The temperature of each cell was monitored by two separate carbon resistors (Matsushita 200 Ω). One of these thermometers was situated on the copper connection rod between cell and mixing chamber, in a region were the stray field of the 6-T coil was reduced to less than 0.1 T. The other thermometer was placed on the buffer compartment of the cell. The zero field values of these thermometers were calibrated in previous runs against ^{3}He vapor pressure and an NBS SRM 768 fixed point superconducting device providing five separate reference temperatures consisting of the transition temperatures between normal and superconducting state of samples of $AuIn_2$ (with transition temperature of 205.4 mK), $AuAl_2$ (162.53 mK), Ir (98.7 mK), Be (23.6 mK), and W (15.3 mK). Only the upper three reference points were actually used.

The Matsushita thermometer values were checked again in the CF-experiment against the NBS device and in the MR experiment against a ^{3}He melting line thermometer and turned out to be correct within 3 mK over the whole temperature range of interest. While calibrating these thermometers, we discovered an error in our previous assumptions regarding the NBS device. The transition temperature of the superconducting materials are specified for zero magnetic field and shift to lower temperatures with increasing field. The magnetic field also causes hysteresis, that is the temperature of the transition going from lower to higher temperature is higher than the temperature of the transition while going from higher to lower temperature. This difference in temperature has a known linear relation to the magnetic field for low fields, and as the shift in critical temperature has a known linear relation to the field too, the true critical temperature may be obtained by determining the magnetic field from the hysteresis and correcting the critical temperature for this field. However, for sufficiently high magnetic fields, the hysteresis saturates, but the critical

temperature keeps shifting. This leads to an underestimation of the actual magnetic field and thus to an underestimation of the shift in critical temperature. For the $AuIn_2$ transition, which shows the largest hysteresis of all five transitions, this saturation was found to occur at a field of the order of 23 μT. In our cryostat it turned out not to be possible to cancel the field sufficiently to enter the linear regime. We estimate that due to this effect our thermometry has an additional uncertainty of about 1 mK, which is small compared to the other sources of error. The field dependence of the thermometer calibrations was determined by comparing the thermometer in near-zero field to the thermometer in high field.

To facilitate the use of our melting line thermometer, we put additional temperature pinning points in the filling capillary. From the melting line thermometer itself at cell temperature, the capillary was pinned first to a point connected to the cold plate of the dilution refrigerator, then to a point having the temperature of the cell and then to the cold plate pinning again. By including this last pinning point, it is not necessary anymore to let the cell temperature cross the temperature of the cold plate pinning point at exactly the temperature of the minimum in the melting line in order to avoid motion of the solid plug in the capillary. Instead, as long as the cold plate pinning point is kept lower in temperature than the cell until the latter passes the melting line minimum temperature, a strong solid plug in some part of the capillary (though not always the same part) is assured at any time.

5.5 Measurements

5.5.1 Capillary-flow experiments

In the CF-experiments we determined the sticking probability as a function of temperature by measuring the capillary-flow impedance by observing either the density decay (with the pressure gauge) or the hydrogen atom flux (with the PP detector).

Measuring with the pressure gauge the whole cell is first filled with H$\downarrow$ up to a density $n \approx 2 \times 10^{15}$ cm^{-3}. Then the pump plate is heated to its operational temperature and one monitors, after a short (<1 s) transient due to the recombination of the gas in the pump volume, the exhaust of the buffer volume through the capillary. Since the area of the pump plate is much larger than the area of the entrance orifice of the capillary, the probability of the H$\downarrow$ atoms to return to the buffer volume is negligibly small ($\ll 10^{-3}$). A typical pressure decay measurement is shown in Fig. 5.10.

Measuring with the pump plate one monitors the H flux during filling and decay. The sensitivity of this method is at least 3 orders of magnitude better than that of the pressure measurements. A typical pump plate measurement is shown in Fig. 5.11.

Neglecting recombination and gas collisions the flux Φ of atoms escaping V_b through the

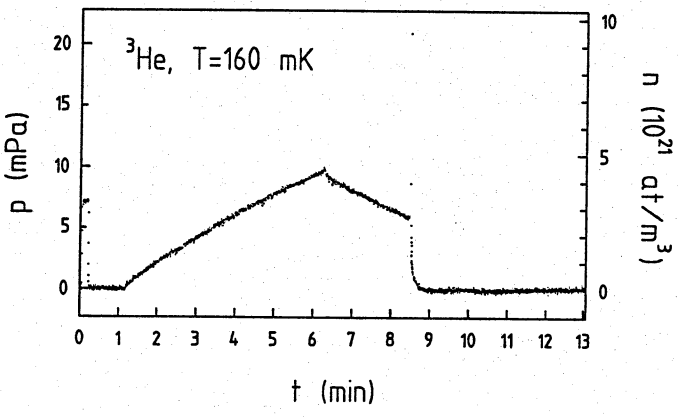

Figure 5.10:
A typical pressure decay measurement.

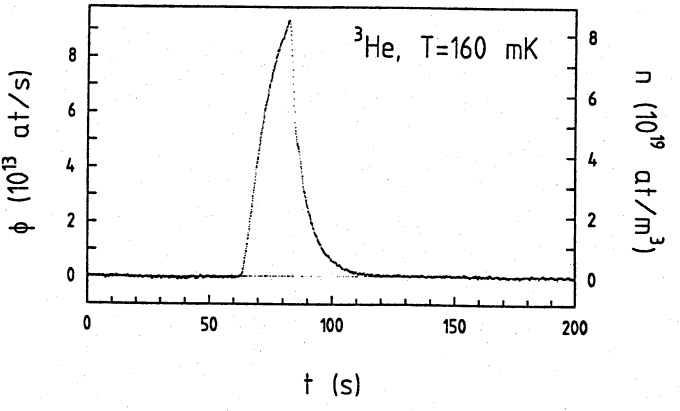

Figure 5.11:
A typical flux decay measurement.

capillary is given by

$$\Phi = \tfrac{1}{4} n \bar{v} A K \ , \tag{5.39}$$

with n the density in the buffer volume, $A = \pi a^2$ the area of the entrance orifice of the capillary of radius a and K the transmission coefficient. This flux equals the rate of change of the number of atoms N in the buffer volume, leading to the density decay:

$$\mathrm{d}n/\mathrm{d}t = -\tfrac{1}{4} K n \bar{v} A / V_\mathrm{b} = -n/\tau_1 \ , \tag{5.40}$$

with τ_1 the time constant of the density decay. From our measurements we determined the time constants of the decay by a computer analysis. To correct for recombination in the buffer volume and collisions in the gas phase, we included a second order decay term in the equation to be fitted:

$$\mathrm{d}n/\mathrm{d}t = -c_1 n - c_2 n^2 \ , \tag{5.41}$$

with $c_1 \equiv {\tau_1}^{-1}$ and c_2 the first and second order decay constants. As c_1 is dominant, the flux depends linearly on the density and an equation of the form of Eq. (5.41) may be written for the flux decay as well. Equation (5.41) is integrated analytically and the result is fitted to the pressure or flux decay data to extract c_1 and c_2. Data were only collected in a temperature regime where the helium-vapor pressure did not significantly impede the flow and recombination losses could be neglected.

We note that the fraction of the atoms entering the tube over the surface is small, 4.7% for ^{4}He surfaces at $T = 145$ mK. At this temperature the residence time τ_a is about 7 μs, which is much longer than the momentum relaxation time 1.1 ns of the adsorbed atoms.[40] Hence the motion of the adsorbed atoms is diffusive and the mean square displacement from the adsorption site is negligibly small (about 5 μm).

Throughout this paper we neglect the effects associated with the finite transmission time through the capillary. This transmission time may be estimated by

$$\tau_\mathrm{tr} = \frac{2 N_\mathrm{c} a}{\bar{v}} \ , \tag{5.42}$$

where N_c is the average number of wall collisions a transmitted particle has undergone. For purely diffusive flow $N_\mathrm{c} = \ell^2/(8a^2)$,[57] where ℓ is the length of the capillary, we find τ_tr ranges from 12 ms at 77 mK to 5 ms at 500 mK, much less than the observed density decay time constants. In the specular limit $N_\mathrm{c} = \ell/a$ and τ_tr is even smaller.

The role of wall collisions only enters into Eq. (5.40) through the transmission coefficient K. Assuming the atoms to scatter purely diffusively according to a cosine distribution (which corresponds to a sticking probability of one), one obtains the transmission coefficient

calculated by Clausing (K_C). An accurate fitting formula for K_C is given by Berman:[58] defining $F \equiv \ell/a$, $G \equiv (F^2+4)^{1/2}$, and $H \equiv \ln([F+G]/2)$, then

$$K_C = 1 + \tfrac{1}{4}F(F-G) - \frac{[(8-F^2)G + F^3 - 16]^2}{72FG - 288H} \,. \tag{5.43}$$

This coefficient K_C is purely determined by geometrical factors and thus temperature independent. In the Knudsen regime for long capillaries the Clausing factor is given by:[59]

$$K_C \approx K_K = \frac{8a}{3\ell} \,. \tag{5.44}$$

The decay time constant τ_1 for $K = K_K$ would be

$$\tau_1 = \tau_{max} = \frac{3\ell V_b}{2Aa\bar{v}} \,. \tag{5.45}$$

In the absence of momentum transfer parallel to the surface, as in the case of specular reflection, the transmission coefficient of the capillary becomes 1 and the decay time constant τ_1 becomes

$$\tau_1 = \tau_0 \equiv \frac{4V_b}{A\bar{v}} \,. \tag{5.46}$$

For our capillary $\ell/a = 88.6(6)$ and therefore $K_C = 0.0284$, resulting in a maximum possible enhancement of the decay time by a factor of 35. The transmission coefficient K in the experiment follows as $K = \tau_0/\tau_1$. The observed decay times τ_1 typically are 5 to 10 s. The experimental results for K are given in Table 5.1.

As the aim of this experiment is the determination of the sticking coefficient s we need to know the relation between K and s. In the case of $s = 0$, K remains 1 even for infinite capillary lengths, but for $s = 1$ the transmission coefficient K becomes the Clausing factor K_C and approaches the asymptote K_K. The relation $K(s)$ is given by De Marcus as approximately[60]

$$K(s) = K_C \frac{(K_C - 1)s + 2}{(1 - K_C)s + 2K_C} \,. \tag{5.47}$$

Inversion of this relation results in

$$s(K) = \frac{2K_C(1-K)}{(K + K_C)(1 - K_C)} \,. \tag{5.48}$$

Unfortunately, the use of this inverted formula may result in large relative errors in s for K close to 1. We therefore simulated the flow through the capillary by a one-speed test particle Monte Carlo computer simulation[61,62] in which we assumed the atom to have a probability s to stick to the surface and to scatter specularly otherwise. This assumption is justified in section 5.2. We calculated K as function of ℓ/a for several values of s (see Fig. 5.12). We show in Fig. 5.13 the results of K vs s according to De Marcus and our simulation, calculated to within 1% using 10^5 particles. Our results are described within 3% by the

Table 5.1: *The experimental results of the CF-experiment for K vs T obtained with the pressure gauge and the PP detection method for all different helium contents of the cell.*

Method	Cell contents	T (mK)	K
Pressure gauge	Pure ^{4}He	193(3)	0.391(32)
		213(3)	0.360(17)
		233(3)	0.338(14)
		263(3)	0.340(13)
		303(3)	0.309(17)
		353(3)	0.264(9)
		403(3)	0.258(11)
		453(3)	0.240(8)
		503(3)	0.236(6)
		528(3)	0.200(15)
Pressure gauge	0.2% ^{3}He	163(3)	0.459(29)
		182(3)	0.420(22)
		203(3)	0.391(22)
Pressure gauge	5% ^{3}He	164(3)	0.422(26)
PP method	Pure ^{4}He	146(3)	0.463(23)
		155(3)	0.429(19)
		164(3)	0.407(18)
		183(3)	0.387(17)
		213(3)	0.353(13)
		253(3)	0.334(11)
		323(3)	0.290(8)
PP method	5% ^{3}He	77(7)	0.551(55)
		92(6)	0.518(41)
		101(5)	0.495(34)
		110(5)	0.472(30)
		119(4)	0.466(27)
		128(4)	0.453(24)
		137(3)	0.437(22)
		146(3)	0.421(20)
		155(3)	0.422(20)
		164(3)	0.379(18)
		173(3)	0.374(17)

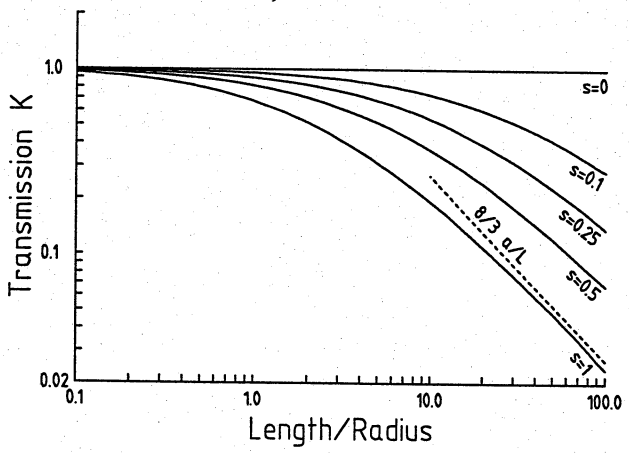

Figure 5.12:
The transmission coefficient K as function of the length over radius quotient ℓ/a for several fixed atomic sticking probabilities.

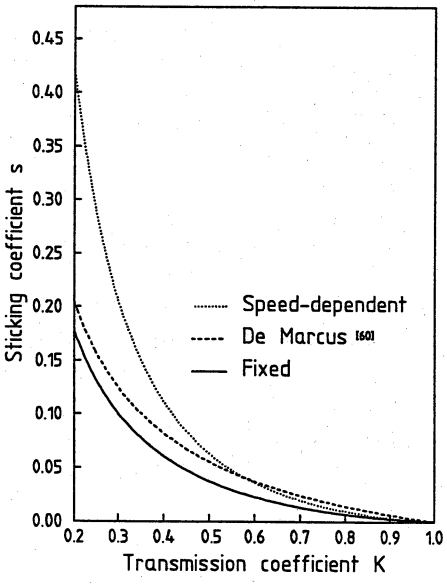

Figure 5.13:
The thermally averaged sticking coefficient s as a function of the transmission coefficient K according to: a) the De Marcus calculations (dashed line); b) our model with fixed atomic sticking coefficients (full line); c) our model with velocity dependent atomic sticking coefficients (dotted line).

empirical form

$$s = \frac{1-K}{1-K_C}\left[\frac{K_C}{K}\right]^{1/2} e^{(-3.915\Delta K)}(1+4.2\Delta K^2)\ , \tag{5.49}$$

where $\Delta K = K - K_C$.

The capillary-flow simulation was based on the assumption that after sticking the atom is desorbed from the surface in a random direction according to a cosine distribution:

$$P(\theta,\phi)\mathrm{d}\theta\mathrm{d}\phi = 2\cos\theta(\mathrm{d}\Omega/2\pi)\ . \tag{5.50}$$

In general, we should apply detailed balance to relate the velocity distribution of desorbing atoms $P_{\mathrm{out}}(T,\vec{v})$ to the atomic sticking probability as in Eq. (5.26). For $s(\vec{v}) \equiv s(T)$ this equation leads to $P_{\mathrm{in}}(T,\vec{v}) \equiv P_{\mathrm{out}}(T,\vec{v})$, *i.e.* the particles will desorb from the surface according to a cosine distribution. This assumption [Eq. (5.50)] leaves no room for a temperature dependence of $s(T)$.

The results of the capillary-flow experiment as published in an earlier report, based on the simulation assuming $s(\vec{v}) \equiv s(T)$ (the one-speed model), are summarized by the relation $s/T = 0.33(3)\ \mathrm{K}^{-1}$ for $145 < T < 526$ mK.[21] In view of the fact that the observed sticking coefficient is not temperature-independent, the assumption of a fixed atomic sticking probability for each atom independent of its velocity and angle of incidence became suspect. The linear dependence of $s(T)$ on T suggests an atomic sticking probability of the form $s(\vec{v}) \sim v^2\cos\theta$, with Eq. 5.24 resulting in

$$s(\vec{v}) = s(T)\left(\frac{3m}{8k_BT}\right)v^2\cos\theta\ . \tag{5.51}$$

The distribution of desorbing atoms after sticking then should be

$$P_{\mathrm{out}}(T,\vec{v})\mathrm{d}\vec{v} = \frac{3}{2\pi}\left(\frac{m}{2k_BT}\right)^3 \times v^3\cos^2\theta\exp\left(\frac{-mv^2}{2k_BT}\right)\mathrm{d}\vec{v}\ . \tag{5.52}$$

We resimulated the capillary flow based on this model (the velocity-dependent model). The above formula for $s(\vec{v})$ breaks down for atoms with a velocity in excess of $[\frac{\pi}{3}s(T)]^{1/2}\bar{v}$, as this leads to a sticking probability of more than unity. Therefore, for large ($s(T) > 0.25$) sticking coefficients we expect this model to be insufficiently accurate. The model is also suspect in the low-temperature limit, as theory predicts $s(\vec{v}) \sim v$. In fact, recent experiments have shown that for helium films $s(\vec{v})$ need not even be monotonous in T at low temperature,[33] possibly due to substrate effects.[45,46] Furthermore, the $\cos\theta$ angular dependence of $s(\vec{v})$ as suggested by simple theory is only approximately correct outside the low-temperature ($s(\vec{v}) \sim \sqrt{T}$) regime. The result of the new simulation therefore only indicates the influence of the particular model used to analyze our data.

The simulation starts with an atom placed at a random location in the entrance of the capillary having a speed generated with the relation $u_y = (y+1)\exp(-y)$ with $y =$

$(mv^2)/(2k_BT)$ and u_y a uniformly distributed random number in the range $0 < u_y < 1$. The direction of departure is chosen randomly according to a cosine distribution. When a wall collision occurs, the atom has the probability $s(\vec{v}) = \frac{3}{4}s(T)y\cos\theta$ to stick to the surface. After sticking, the speed of the atom is determined by $u_y = (\frac{1}{2}y^2 + y + 1)\exp(-y)$ to comply with the detailed balance. The result may be described to within 0.7% relative error in $s(K)$ in the range $0.03 < s < 0.25$ by the empirical formula

$$s(K) = 0.134e^{3.2(1-K)^4} + 1.17e^{0.075(1-K)} - 0.09(0.5 - K)^3 - 1.31525\ . \tag{5.53}$$

This formula may be extended to the interval $0 \leq s \leq 0.35$ while the relative error between this formula and the results of the simulation remains <1.5%. This result is also shown in Fig. 5.13.

The models on which the computer simulations are based clearly represent a simplified picture of the physics involved. The measurements are sensitive for any process that leads to momentum transfer in the direction along the axis of the capillary tube. This is most effectively done by atoms that stick some time to the surface, but more generally results from any inelastic scattering process or surface roughness. Hence our models tend to overestimate s. This is in particular the case for the velocity-dependent model in which the contribution to the transmission by atoms at grazing incidence is disproportionally large. In view of the theoretical assertion[23,39,47] that the sticking channel is most effective in exchanging energy and momentum between gas and surface it seems reasonable to assume that the effect of inelastic scattering is small compared to the experimental accuracy.

The results of the experiment, based on the one-speed model and those based on the velocity-dependent model are given in Fig. 5.14. For ^{4}He the results are shown by the open circles, obtained from pressure decay measurements, and the filled circles, obtained from flux decay measurements. Note the excellent agreement between both methods. Each data point represents the average of at least 4 measurements, the error bar being the standard deviation of the results, augmented by a small systematic error. The sticking coefficient, based on the velocity-dependent model, substantially differs from our previous analysis. It is still linear in temperature, but whereas the previous analysis resulted in a sticking coefficient which may be described as $s/T = 0.33(3)\ \mathrm{K}^{-1}$ for $145 < T < 526$ mK, the new analysis renders $s/T = 0.65(6)\ \mathrm{K}^{-1}$ in the same temperature range.

Due to the inherent shortcomings of both models to relate s to K it is hard to express a strong preference to one or the other. The uncertainty in the relation between K and s shows this type of experiment to be not very suitable to determine $s(T)$ with precision, although the linear temperature dependence of s appears to be well established. The enhancement in transmission of the velocity-dependent model with respect to the one-speed model is mainly due to the population of low-velocity particles and atoms striking the walls at grazing incidence. As discussed above, it is this population for which the velocity-dependent model

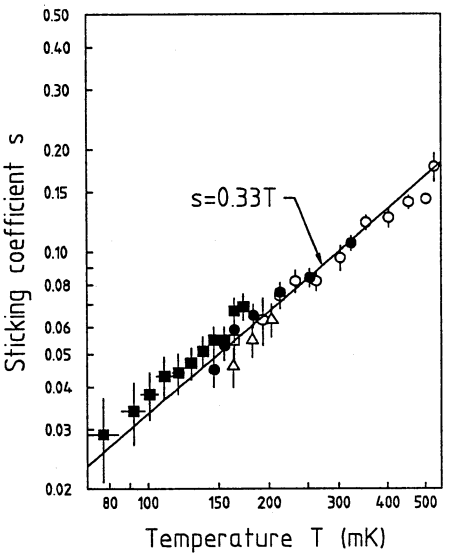

Figure 5.14:
The sticking coefficient as a function of temperature, based on a model with fixed atomic sticking coefficient. Drawn line: $s = 0.33T$. Open circles: pure ^{4}He surface, pressure decay measurements; Filled circles: pure ^{4}He surface, flux decay measurements; Open triangles: mixture with 0.2% ^{3}He, pressure decay measurements; Open square: mixture with 5% ^{3}He, pressure decay measurement; Closed squares: mixture with 5% ^{3}He, flux decay measurements.

is most unreliable. We therefore have a slight preference for the results of the one-speed model although this preference is somewhat speculative.

Adding a small amount of ^{3}He (0.2%) to the ^{4}He in our cell we noticed a clear reduction of the recombination rate, indicating a reduction of the binding energy and implying a definite change in adsorption potential and in ripplon dispersion (the surface tension falls from $\gamma = 3.54 \times 10^{-4}$ J m^{-2} to $\gamma = 1.53 \times 10^{-4}$ J m^{-2} when changing from pure ^{4}He to pure ^{3}He surfaces).[43,44,63] However within experimental error no effect was observed on s (open triangles in Fig. 5.14). Increasing the ^{3}He fraction to 5% a small (about 10%) increase in s was observed at 164 mK with the pressure gauge (open square). Under these conditions we estimate the local ^{3}He concentration in the cell to be at least 30% and hence expect the H$\downarrow$ to scatter from a ^{3}He-rich phase. Most of our 5% ^{3}He results, shown as closed squares in Fig. 5.14, were obtained with the pump plate and are in fair agreement (10%) with the 164 mK pressure gauge result. Adding 50% ^{3}He with the flux decay measurements no change was observed on s. No further pressure measurements could be done as bulk liquid started to collect in the pressure gauge. The results on ^{3}He–^{4}He mixtures in the cell are described by the same formula as those on pure ^{4}He substrates within the range of $73 < T < 174$ mK for our measurements. Although the reliability of our thermometry rapidly decreases below 100 mK the trend of decreasing sticking probabilities with decreasing temperatures clearly continues down to our lowest temperature.

To incorporate the effect of binary gas collisions in our one-speed model, we randomly generated collisions using a mean free path λ corresponding to the local density n in the cap-

illary according to $\lambda = (16\sqrt{2}n\sigma/9\pi)^{-1}$, where σ is a hard-sphere scattering cross section.[64] The local density was based on the wall-collision rate calculated with the same simulation, but neglecting gas collisions. After a gas collision, the test atom was restarted in a random direction, sampling an angular distribution chosen to be isotropic in the laboratory system. We may describe our simulation results for the density dependence of K by

$$K \approx K_0(1 - \sigma\lambda_0 K_0 n) \,. \tag{5.54}$$

Here K_0 is the transmission coefficient in the zero density limit and $\lambda_0 \equiv 6.1$ mm is a reference length provided by the simulation. Equation (5.54) only holds in the extremely rarefied limit. At higher densities K should show the Knudsen minimum before entering the viscous regime.[65] In our measurements $\lambda > 2$ cm, comparable to the length of the capillary. We thus find $c_1 \equiv K_0/\tau_0$ and $c_2 \equiv -\sigma\lambda_0 K_0^2/\tau_0 + K_{\rm rec}$, where $K_{\rm rec}$ is a rate constant accounting for recombination. These expressions show that gas collisions do not affect c_1. To look for effects of gas-phase collisions, we analyzed our pressure decays with pure ^{4}He surfaces to extract the c_2. Values for c_2 were obtained starting the fits at a fixed initial density $n_0 = 5\times10^{14}$ cm^{-3}. We found $c_2 = -A+B(T-T_{\rm ref})$, with $A = 6.2(15)\times10^{-17}$ cm^3/s, $B = 8(14) \times 10^{-17}$ cm^3 s^{-1} K^{-1} and $T_{\rm ref} = 270$ mK. We established experimentally that the contribution of $K_{\rm rec}$ to c_2 was negligibly small. Once σ is extracted from c_2 the coefficient of self-diffusion follows with $D = \frac{1}{3}\bar{v}\lambda$,[64] which is found to be temperature independent within experimental error. Averaging over all data we find $nD = 1.3(5) \times 10^{18}$ cm^{-1} s^{-1}, in good agreement with the theoretical value of Lhuillier $nD = 1.5 \times 10^{18}$ cm^{-1} s^{-1}.[66]

This agreement with theory is rather fortuitous. If we take into account some effect of the speed of the particle from which the atom collides by assigning the atom after collision a velocity according to a random distribution in the reference frame moving with the mean drift speed of the atoms in the capillary at the location of the collision, the results for the diffusion constant change by a factor of 10. Clearly the one-speed test particle method is not suited to accurately account for gas-collisional effects, although the origin of the c_2 term is well established. In view of the large experimental error in c_2 and the availability of high-quality NMR data for spin diffusion[67] we did not pursue the refinement of simulation methods for gas collisions any further.

5.5.2 Mirror reflection experiment

The aim of the MR experiment was to study the H-surface scattering at normal incidence with high angular resolution. The atoms escaping through the orifice in the bottom of the buffer volume give rise to a highly divergent atomic beam in the pumping volume. We observe the influence of the position of the mirror on the density decay time of the H gas in the buffer reservoir. If the center of the mirror coincides with the center of the orifice the

atoms in the beam will be specularly reflected back into the reservoir. The net flux through the diaphragm may be expressed as

$$\Phi = \tfrac{1}{4} n \bar{v} A \chi \,, \tag{5.55}$$

with A the area of the orifice and χ a loss factor representing the probability that the atoms are *not* scattered back into the buffer volume. This equation closely resembles Eq. (5.39), but with χ replacing K. For our setup 100% reflectivity of a perfectly aligned mirror would correspond to $\chi = 0.042$, as limited by geometrical factors and image aberrations such as coma. For densities up to $n = 10^{14}$ cm^{-3} interatomic collisions in the beam are completely negligible. This analysis implies that the leakage from the reservoir may be largely suppressed with the mirror. The total loss factor χ is due to several loss mechanisms, like surface roughness, coma, sticking etc. For N independent loss mechanisms with loss factors χ_i the total loss factor χ may be written as

$$\chi = 1 - \prod_{i=1}^{N} (1 - \chi_i) \,. \tag{5.56}$$

As in the CF-experiment, we assume the density decay is given by Eq. (5.41). The density at a time t is then given by

$$n(t) = \frac{c_1 n_0 e^{-c_1 t}}{c_1 + c_2 n_0 (e^{-c_1 t} - 1)} \,. \tag{5.57}$$

We assume the reduction of the density is only due to the escape of atoms from the buffer volume to the pump volume, so the flux is given by

$$\Phi(t) = -\mathrm{d}N(t)/\mathrm{d}t = -V_e \mathrm{d}n(t)/\mathrm{d}t \,. \tag{5.58}$$

As we no longer could neglect the influence of c_2, we use this exact equation, resulting in

$$\Phi(t) = \frac{c_1 V_e n_0 e^{-c_1 t}}{c_1 + c_2 n_0 (e^{-c_1 t} - 1)} \times \left[c_1 + \frac{c_1 c_2 n_0 e^{-c_1 t}}{c_1 + c_2 n_0 (e^{-c_1 t} - 1)} \right] \,. \tag{5.59}$$

We fit this formula to our data to obtain c_1 and c_2. The second order constant now represents the possible influence of gas collisions, recombination and a first order correction for the time constant (about 0.5 s) of the pump plate flux detector.

A typical measurement is shown in Fig. 5.15. We plot the observed loss factor,

$$\chi \equiv \tau_0 / \tau_1 \equiv c_1 \tau_0 \,, \tag{5.60}$$

as a function of the vertical position z of the mirror. Here τ_0 is the first order decay time in the absence of the mirror, defined in Eq. (5.46), and ranging from 5.1 s at 80 mK to 2.4 s at 400 mK. The results clearly demonstrate the occurrence of specular reflection of the atoms. With the mirror far from focusing conditions, the decay time is only slightly larger than

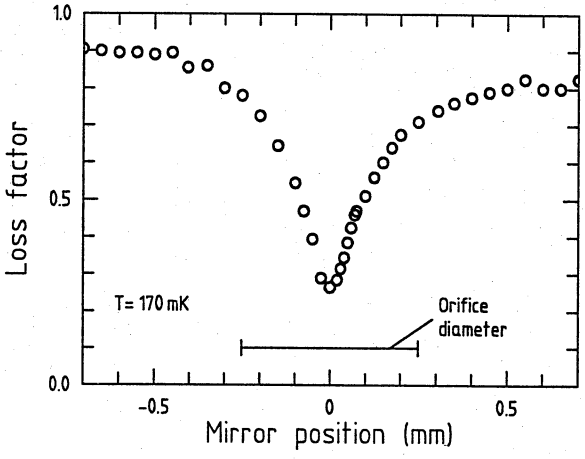

Figure 5.15:
A typical loss factor measurement.

that expected in the absence of a mirror. As the mirror is moved to bring the diaphragm into focus, the decay time starts to increase dramatically. As seen from the figure, the overall resolution of our apparatus is better than 300 μm (FWHM). From each position scan we may extract the minimal χ value ($\chi_{\min}$) for a given temperature and film thickness. The shape of the χ-curve is not exactly symmetrical with respect to the position of $\chi_{\min}$. We were able to devise a model which reproduced the observed lineshape. This model incorporates the effects of multiple scattering of the H atoms in the mirror compartment and the geometry of this compartment and the mirror itself. We refrained from using this model to fit our data. While the many assumptions on which this model was based were all plausible, as a whole it is rather speculative. Its value lies in the demonstration that the observed lineshapes are in principle understood. To obtain consistent results and reduce the influence of noise in the data we fitted each position scan to an empirical function in which the width of the observed curve Ω and the position of $\chi_{\min}$ were treated as free parameters, while for the loss factor far from focus we took the calculated χ_s. The function was chosen to result in a good fit to all measured scans and was of the form

$$\chi_s^{-1} + \frac{\chi_{\min}^{-1} - \chi_s^{-1}}{\{1 + [2\sqrt{3}(z - z_0)/\Omega]\}^{1/2}} \,. \tag{5.61}$$

We also analyzed our data with the same function, but treating τ_0 as an additional free parameter. The average of τ_0 over all data agrees within 1% with the calculated value as given by Eq. (5.45), while individual fits deviated on average about 7%. A summary of our results for $\chi_{\min}$ as a function of temperature is shown in Fig. 5.16. The triangles represent

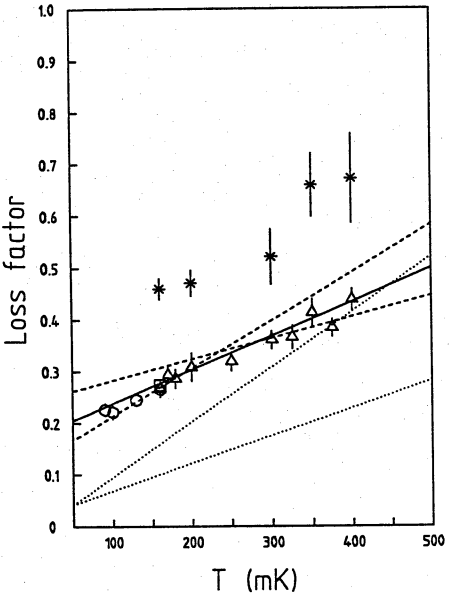

Figure 5.16:
Measured loss factors as a function of temperature. Crosses: results on thin pure ^{4}He films; Triangles: results on saturated ^{4}He films; Square: saturated ^{4}He film with partial ^{3}He monolayer coverage; Circles: results on saturated ^{4}He films with full ^{3}He monolayer coverage. Dotted lines: expected loss factors with perfect mirror alignment and $s(T) = 0.33T$ resp. $0.65T$; Dashed lines: fits to loss factors under assumption $s(T) = 0.33T$ resp. $0.65T$; Full line: fit to loss factors, resulting in $s(T) = 0.5T$.

our data for a saturated ^{4}He film of estimated thickness 115 Å.[68] We purified our ^{4}He with a superleak. The ^{3}He content is ≈ 0.2 ppm. As our measurements of s clearly show the linear dependence on T, the sticking at normal incidence according to theory is given by $s_\perp = \frac{3}{2}s(T) = \gamma_1 T$. The analysis of the CF-experiment based on the one-speed model therefore leads to $\gamma_1 = 0.50(5)$ K^{-1}, whereas the analysis based on the velocity-dependent model leads to $\gamma_1 = 1.0(1)$ K^{-1}. The specular reflectivity at normal incidence $R_\perp$ may be estimated using the ansatz $R_\perp = 1 - s_\perp$. For $\gamma_1 = 0.50(5)$ K^{-1} we thus calculate $R_\perp \approx 0.95$ at $T = 100$ mK. For ideal alignment of the optics ($\chi_g = 0.042$) and taking the loss factor due to sticking $\chi_s = s_\perp = \gamma_1 T$, the temperature dependence of $\chi_{\min}$ predicted is indicated by the dotted lines, the lower one assuming $\gamma_1 = 0.50(5)$ K^{-1} and the upper one assuming $\gamma_1 = 1.0(1)$ K^{-1}. Most of the discrepancy with the data may be explained by assuming a lateral misalignment of the mirror or by residual roughness due to surface imperfections of the quartz substrate. Both effects cause a temperature-independent loss χ_L from the specular beam,[69] implying that only a lower bound for $R_\perp$ may be extracted from the raw data. For instance, a lateral misalignment of 30 μm of an otherwise perfect mirror leads to $\chi_L = 15\%$. The large loss factors obtained for thin under-saturated films (crosses) may well be understood in terms of substrate roughness.

Assuming $s_\perp = \gamma_1 T$ and fixing $\gamma_1 = 0.5$ K^{-1}, a least squares fit to the saturated-helium-film data results in $\chi_L = 23\%$ (dashed lines), while fixing $\gamma_1 = 1.0$ K^{-1} results in $\chi_L = 13\%$. These fits poorly describe the data. Alternatively, assuming a linear temperature

dependence, $s_\perp = \gamma_1 T$ and treating γ_1 and χ_L as free parameters, fitting Eq. (5.56) to the data yields the full line characterized by $\chi_L = 17\%$ and $\gamma_1 = 0.74(5)$ K^{-1}. This fit satisfactorily describes our data. The value of γ_1 lies between the values resulting from our determination of s from both models.

In view of the high angular resolution of our experimental setup of 10 mrad even ripplons with wavelength as long as $\lambda = 3000$ Å carry sufficient momentum to deflect H atoms out of the specular beam as defined by the diaphragm. At wavelengths $\lambda \geq 500$ Å the dynamic surface roughness is dominated by thermal ripplons rather than by zero-point fluctuations which are responsible for the sticking process. If we assume that apart from the sticking/desorption process also direct (non-sticking) inelastic scattering by ripplons is of importance, an additional loss factor is present which we shall denote by χ_{in}. The direct inelastic scattering processes neither shows up in measurements of α, since they are quasi-elastic, nor in measurements of s by the capillary-flow method, as to first order the momentum along the capillary axis is conserved. The calculation by Hijmans and Shlyapnikov, based on the application of the perturbative scattering theory to direct inelastic scattering, result in $\chi_{in}(T) = \gamma_2 T^2$ with $\gamma_2 \approx 0.7$ K^{-2} for the probability at normal incidence to scatter out of the specular beam.[26] This result is independent of the exact shape of the H–He potential.[26,27] A least squares fit to the data, assuming $\chi_s = \gamma_1 T$ with fixed $\gamma_1 = 0.5$ K^{-1} (based on our one-speed model and supported by the measurements of the accommodation coefficient of Helffrich *et al.*[32]) and $\chi_{in} = \gamma_2 T^2$, yields $\gamma_2 = 0.5(1)$ K^{-2} and $\chi_L = 0.20$ (solid curve). This curve also satisfactorily describes our data. Given both fits discussed we are reluctant to use our data to prove or disprove the existence of another inelastic scattering channel, as reported earlier in our Letter.

Evidence for the absence of static surface roughness was obtained by increasing the film thickness by a factor 2, which had no effect on the observed loss factor. We therefore assume χ_L is due to a lateral misalignment of the mirror of about 40 μm. Remarkably, as in the capillary-flow experiment, no effect on the reflectivity was observed by adding up to 0.1% ^{3}He to the helium in the cell. Under these conditions the presence of a full monolayer of ^{3}He is to be expected on the surface of the mirror.

5.6 Conclusions

In the capillary-flow experiments we observe a strong enhancement of more than a factor 10 of the flow rate in comparison to ordinary Knudsen flow. This is related to a small sticking probability s for the temperature regime studied. For ^{4}He surfaces, using a fixed atomic sticking probability in our model, we find $s/T = 0.33(3)$ K for $145 < T < 526$ mK, while for a velocity-dependent atomic sticking probability we find $s/T = 0.65(6)$ K. We have a slight preference for the first model. In Fig. 5.17 the results of the one-speed model are compared with all other measurements in this temperature range. In particular the

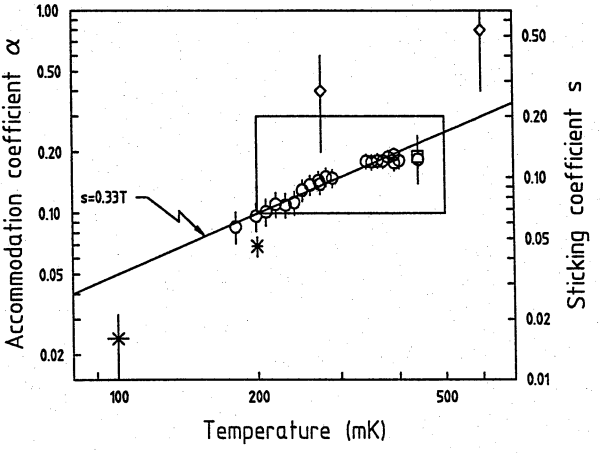

Figure 5.17:
Sticking probabilities and accommodation coefficients by various authors. Crosses: results of Jochemsen et al. (Ref. 28); big square: result of Salonen et al. (Ref. 30); little square: result of SJKTT (Ref. 31); diamonds: results of Bell et al. (Ref. 9); circles: results of Helffrich et al. (Ref. 32). The results of the CF-experiment based on the one-speed model is represented by the straight line $s(T) = 0.33T$.

agreement with the results of Helffrich *et al.* are striking. The experimental results of Doyle *et al.* are not included in this figure as they apply to a temperature regime starting one order of magnitude lower than our lowest results. Their results show an increasing sticking probability with decreasing temperature. Both sets of data need not be conflicting as a local minimum in $s(T)$ may result from substrate induced resonant enhancement of the sticking process as discussed by Goldman, Hijmans and Shlyapnikov and Carraro and Cole. Within experimental error the transmission through the capillary did not change by adding up to 50% ^{3}He at 150 mK. Results for ^{3}He–^{4}He surfaces were obtained for $73 < T < 174$ mK and are described by the same relations. Our results show that differences between sticking and accommodation coefficients observed in the early experiments are mainly due to differences in temperature of observation.

Surface roughness may also lead to non-specular reflection. In view of the remarkable smoothness of the inside of the capillary as shown by the scanning electron microscope, combined with the smoothing effect of the helium film, we do not believe surface roughness of the pyrex substrate influences our data.

In the mirror experiments we measure at normal incidence a lower limit of 80% for

the specular reflectivity. Mirror and diaphragm enable us to study the specularly reflected beam with an angular resolution of about 10 mrad. This resolution is sufficiently high to discriminate between specular and near-elastic scattering. However, the method is extremely sensitive for radial misalignment. The coefficient for the direct inelastic process may only be extracted with confidence, if precision data for the sticking coefficient is available.

5.7 Acknowledgements

The authors wish to thank O.H. Höpfner for his overall technical support, M. Groeneveld for the construction of the quartz mirror, J.M.V.A. Koelman for pointing out an inconsistency in our computer simulation, I.D. Setija, O.J. Luiten, T. Mizusaki, I. Lunding and J. Mosk for their assistance with the measurements and/or data analysis, and T. Hijmans for his help with the data analysis and the theoretical calculations for the MR experiment. We profited from discussions with H. Beijerinck, A. Lagendijk, M. Papoular and R. Sprik. This work is part of the research program of the Stichting voor Fundamenteel Onderzoek der Materie (FOM), which is financially supported by the Nederlandse Organisatie voor Wetenschappelijk Onderzoek (NWO).

References

[1] J.J. Berkhout and J.T.M. Walraven, in *Spin-Polarized Quantum Systems*, edited by S. Stringari (World Scientific, Singapore, 1989), p. 201.

[2] J.T.M. Walraven and J.J. Berkhout, in *Frequency Standards and Metrology*, edited by A. de Marchi (Springer-Verlag, Berlin, 1989), p. 102.

[3] J.T.M. Walraven, in *The Physics of Electronic and Atomic Collisions*, edited by A. Dalgarno, K.S. Freund, J.M. Koch, M.S. Lubell, and T.B. Lucatorno, AIP Conf. Proc. **205**, 599 (1990).

[4] J.T.M. Walraven, in *Excitations in Two-Dimensional and Three-Dimensional Quantum Fluids*, edited by A.F.G. Wyatt and H. Lauter (Plenum, New York, 1991) p. 511.

[5] I.F. Silvera and J.T.M. Walraven, in *Progress in Low Temperature Physics*, edited by D.F. Brewer (North-Holland, Amsterdam, 1986), Vol. **X**, p. 139.

[6] R. Sprik, J.T.M. Walraven, and I.F. Silvera, Phys. Rev. Lett. **51**, 479, 942(E) (1983).

[7] H.F. Hess, D.A. Bell, G.P. Kochanski, R.W. Cline, D. Kleppner, and T.J. Greytak, Phys. Rev. Lett. **51**, 483 (1983).

[8] R. Sprik, J.T.M. Walraven, and I.F. Silvera, Phys. Rev. B **32**, 5668 (1985).

[9] D.A. Bell, H.F. Hess, G.P. Kochanski, S. Buchman, L. Pollack, Y.M. Xiao, D. Kleppner, and T.J. Greytak, Phys. Rev. B **34**, 7670 (1986).

[10] T.J. Tommila, S. Jaakkola, M. Krusius, I. Krylov, and E. Tjukanov, Phys. Rev. Lett. **56**, 941 (1986).

[11] T.J. Tommila, E. Tjukanov, M. Krusius, and S. Jaakkola, Phys. Rev. B **36**, 6837 (1987).

[12] J.D. Gillaspie, I.F. Silvera, and J.S. Brooks, Phys. Rev. B **38**, 9231 (1988).

[13] H.F. Hess, G.P. Kochanski, J.M. Doyle, N. Masuhara, D. Kleppner, and T.J. Greytak, Phys. Rev. Lett. **59**, 672 (1987).

[14] R. van Roijen, J.J. Berkhout, S. Jaakkola, and J.T.M. Walraven, Phys. Rev. Lett. **61**, 931 (1988).

[15] N. Masuhara, J.M. Doyle, J.C. Sandberg, D. Kleppner, T.J. Greytak, H.F. Hess, and G.P. Kochanski, Phys. Rev. Lett. **61**, 935 (1988).

[16] J.M. Doyle, J.C. Sandberg, N. Masuhara, I.A. Yu, D. Kleppner, and T.J. Greytak, J. Opt. Soc. Am. B **6**, 2244 (1989).

[17] T.W. Hijmans, O.J. Luiten, I.D. Setija, and J.T.M. Walraven, J. Opt. Soc. Am. B **6**, 2235 (1989).

[18] R.V.E. Lovelace, C. Mehanian, T.J. Tommila, and D.M. Lee, Nature (London) **318**, 30 (1985).

[19] H.F. Hess, Phys. Rev. B **34**, 3476 (1986).

[20] T.J. Tommila, Europhys. Lett. **2**, 789 (1986).

[21] J.J. Berkhout, E.J. Wolters, R. van Roijen, and J.T.M. Walraven, Phys. Rev. Lett. **57**, 2387 (1986).

[22] J.J. Berkhout, O.J. Luiten, I.D. Setija, T.W. Hijmans, T. Mizusaki, and J.T.M. Walraven, Phys. Rev. Lett. **63**, 1689 (1989).

[23] Yu. Kagan, G.V. Shlyapnikov, and N.A. Glukhov, Pis'ma Zh. Eksp. Teor. Fiz. **40**, 287 (1984) [JETP Lett. **40**, 1072 (1984)].

[24] B. Castaing and M. Papoular, J. Phys. Lett. (Paris) **44**, L537 (1983).

[25] For a compilation of measurements of the binding energy of H on He see W.N. Hardy, M.D. Hürlimann, and R.W. Cline, in *Proceedings of the Eighteenth International Conference on Low Temperature Physics, Kyoto, Japan, 1987*, Jpn. J. Appl. Phys. **26**, Suppl. 26-3, 2065 (1987).

[26] T.W. Hijmans and G.V. Shlyapnikov, Phys. Lett. A **142**, 45 (1989).

[27] E. Tiesinga, H.T.C. Stoof, and B.J. Verhaar , Phys. Rev. B **41**, 8886 (1990).

[28] R. Jochemsen, M. Morrow, A.J. Berlinsky, and W.N. Hardy, Phys. Rev. Lett. **47**, 852 (1981).

[29] M. Morrow and W.N. Hardy, Can. J. Phys. **61**, 956 (1983).

[30] K.T. Salonen, I.F. Silvera, J.T.M. Walraven, and G.H. van Yperen, Phys. Rev. B **25**, 6002 (1982).

[31] K. Salonen, S. Jaakkola, M. Karhunen, E. Tjukanov, and T. Tommila, in *Proceedings of the Seventeenth International Conference on Low Temperature Physics, LT-17, Karlsruhe, West Germany, 1984*, edited by U. Eckern, A. Schmid, W. Weber, and H. Wühl (North-Holland, Amsterdam, 1984), p. 543.

[32] J. Helffrich, M.P. Maley, M. Krusius, and J.C. Wheatley, Phys. Rev. B **34**, 6550 (1986).

[33] J.M. Doyle, J.C. Sandberg, I.A. Yu, C.L. Cesar, D. Kleppner, and T.J. Greytak, Phys. Rev. Lett. **67**, 603 (1991).

[34] I.B. Mantz and D.O. Edwards, Phys. Rev. B **20**, 4518 (1979).

[35] W.C. Stwalley, Chem. Phys. Lett. **88**, 404 (1982).

[36] D.S. Zimmerman and A.J. Berlinsky, Can. J. Phys. **61**, 508 (1983).

[37] I.F. Silvera and V.V. Goldman, Phys. Rev. Lett. **45**, 915 (1980).

[38] Yu. Kagan and G.V. Shlyapnikov, Phys. Lett. **95A**, 309 (1983).

[39] B.W. Statt, Phys. Rev. B **32**, 7160 (1985).

[40] D.S. Zimmerman and A.J. Berlinsky, Can. J. Phys. **62**, 590 (1984).

[41] M.W. Cole, Phys. Rev. B **2**, 4239 (1970).

[42] G.D.L. Webster, M. Chester, E. Webster, and T. Oestereich, J. Low Temp. Phys. **40**, 207 (1980).

[43] M. Iino, M. Suzuki, and A.J. Ikushima, J. Low Temp. Phys. **61**, 155 (1985).

[44] D.O. Edwards and W.F. Saam, in *Progress in Low Temperature Physics*, edited by D.F. Brewer (North-Holland, Amsterdam, 1978), Vol. **VIIA**, p. 283.

[45] T.W. Hijmans, J.T.M. Walraven, and G.V. Shlyapnikov, Phys. Rev. B **45**, 2561 (1992).

[46] C. Carraro and M.W. Cole, Phys. Rev. B **45**, 12930 (1992).

[47] V.V. Goldman, Phys. Rev. Lett. **56**, 612 (1986).

[48] Oxford Instruments Limited, Osney Mead, Oxford OX2 0DX, England.

[49] The characteristics of the germanium of this bolometer are given in H.D. Drew and A.J. Sievers, Appl. Opt. **8**, 2067 (1969).

[50] G.H. van Yperen, J.T.M. Walraven, and I.F. Silvera, Phys. Rev. B **30**, 2386 (1984).

[51] R. Sprik, J.T.M. Walraven, G.H. van Yperen, and I.F. Silvera, Phys. Rev. B **34**, 6172 (1986).

[52] J.J. Berkhout, O.H. Höpfner, E.J. Wolters, and J.T.M. Walraven, in *Proceedings of the Eighteenth International Conference on Low Temperature Physics, Kyoto, Japan, 1987*, Jpn. J. Appl. Phys. **26**, Suppl. 26-3, 231 (1987).

[53] Emerson and Cuming, Inc.

[54] IMI Titanium, P.O. box 704, Witton, Birmingham B6 7UR, England.

[55] A.F. Harvey, *Microwave Engineering* (Academic, London, 1963).

[56] Certified grade according to ASTM f68/77, manufactured by Outokumpu Oy, Finland.

[57] P. Clausing, Ph.D. thesis, University of Leiden, Leiden, 1928.

[58] A.S. Berman, J. Appl. Phys. **36**, 3356 (1965).

[59] P. Clausing, Ann. Phys. (Leipzig) **12**, 961 (1932).

[60] W.C. De Marcus, in *Advances in Applied Mechanics*, edited by L. Tabbot (Academic, New York, 1961), Suppl. 1, p. 161.

[61] G.A. Bird, *Molecular Gas Dynamics* (Clarendon, Oxford, 1976).

[62] K. Yamamoto, J. Hara, and K. Hirose, J. Phys. Soc. Jpn. **51**, 3729 (1982).

[63] A.P.M. Matthey, J.T.M. Walraven, and I.F. Silvera, Phys. Rev. Lett. **46**, 668 (1981).

[64] J.O. Hirschfelder, C.F. Curtiss, and R.B. Bird, *Molecular Theory of Gases and Liquids* (Wiley, New York, 1954).

[65] M. Knudsen, Ann. Phys. (Leipzig) **28**, 75 (1908).

[66] C. Lhuillier, J. Phys. (Paris) **44**, 1 (1983).

[67] D.M. Lee, in *Proceedings of the Eighteenth International Conference on Low Temperature Physics, Kyoto, Japan, 1987*, Jpn. J. Appl. Phys. **26**, Suppl. 26-3, 1841 (1987).

[68] To estimate the film thickness we use the formula $m_{He}gh = V(d)$ with $V(d) = \alpha(d)d^{-3}$. For $d = 0$ we use $\alpha = 1.61 \times 10^{-50}$ kg m^5 s^{-2} (Ref. 42), while we assume $\alpha(115\ \text{Å}) \approx 0.75\alpha(0)$ [D.F. Brewer, in *The Physics of Liquid and Solid Helium*, edited by K.H. Bennemann and J.B. Ketterson (Wiley, New York, 1978), Part II, p. 584].

[69] As pointed out to us by dr. M. Papoular static roughness with a needle-like shape and a diameter comparable to the thermal wavelength of the atoms may also result in a temperature dependence. The presence of this type of surface roughness is unlikely in view of the employed polishing procedure.

Chapter 6

SENSITIVE BOLOMETRIC DETECTION OF ATOMIC HYDROGEN FLUXES

We developed a sensitive device to detect atomic hydrogen fluxes. The device is based on a measurement of the heating due to forced recombination of the atoms in the flux. We found that $60 \pm 10\%$ of the recombination heat is collected by the detector. The DC noise equivalent (1σ) flux Φ is 6×10^{10} atm/s at a bandwidth of 0.4 Hz and a dynamic range of 1000 ($\Phi_{max} = 6 \times 10^{13}$ atm/s). The device may be used at ambient temperatures below 450 mK. We discuss possible improvements of the design.

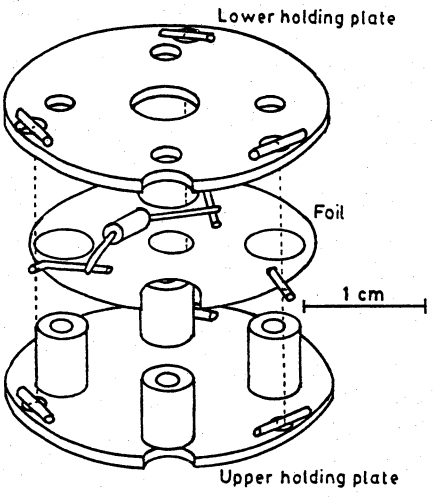

Figure 6.1:
Exploded view of the pumping plate assembly.

6.1 Introduction

Bolometric measuring techniques are widely used in both infra-red and nuclear physics.[1] In experiments with spin-polarized hydrogen bolometric detection has been commonly used as a simple and reliable method to monitor the presence of the gas.[2] Although the method is very sensitive due to the large heat of recombination its use for precision H flux detection has been limited by non-linearities in the bolometer response and large uncertainties in the fraction of collected recombination energy.

Here we report on a device in which we have overcome these limitations and to which we refer as "pumping plate". The device was developed for a capillary-flow experiment to measure the sticking probability of spin-polarized atomic hydrogen on liquid-helium surfaces, where we needed an efficient means of removing atomic hydrogen from a chamber with liquid-helium-covered walls.[3]

6.2 Principle of operation, construction

The pumping plate consists of a piece of copper foil with a total area of 7 cm^2 suspended with three tungsten wires of 16 micron diameter between an upper and a lower copper holding plate (Fig. 6.1). The tungsten wires are attached with Eccoshield VSM to copper poles that are glued with Stycast 2850 FT to the foil. These wires double as electrical leads to a 220 Ω Matsushita resistor which is also glued with Stycast 2850 FT to the foil. The complete assembly was found to be rather rugged. It is mounted with copper screws to the experimental cell (Fig. 6.2). The lower holding plate has a hole to permit entrance to the

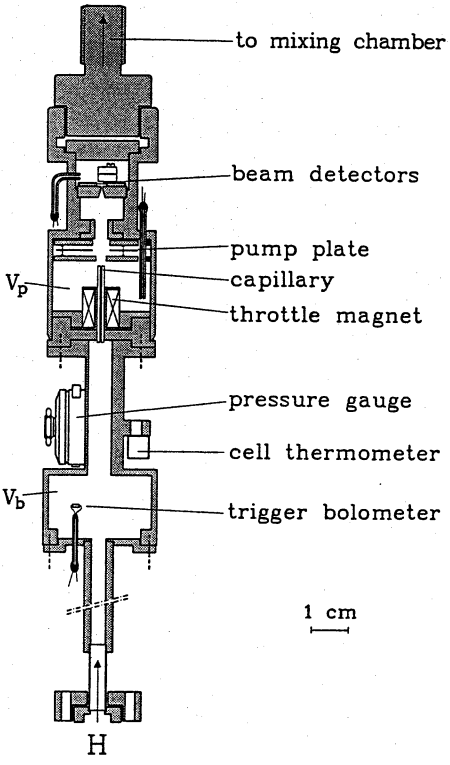

Figure 6.2:
The experimental cell

incident flux. Both holders were gold plated to reduce corrosion.

When the copper is heated, helium evaporates. The superfluid helium film then starts to flow towards the foil. This flow is limited by the critical velocity of the film, v_c. The maximum helium volume flux Φ_{max} is therefore[4]

$$\Phi_{max} = (\rho_s/\rho) p v_c d \ . \tag{6.1}$$

Here ρ_s/ρ denotes the superfluid density fraction, p is the minimum perimeter length for the flow, and d is the film thickness. For the temperatures of interest ($T < 1$ K) $\rho_s/\rho \approx 1$.

If the heating power $\dot{Q}$ is sufficiently high the helium film is completely desorbed from the foil, leaving a bare copper surface. For this one requires:

$$\dot{Q} > \Phi_{max} L \rho \ , \tag{6.2}$$

with[5] $L \approx (15 + T \times 5\mathrm{K}^{-1})\ 10^3$ J/kg the latent heat of evaporation.

The adsorption energy of atomic hydrogen on the bare copper surface is orders of magnitude larger than the binding energy of atomic hydrogen on liquid-helium surfaces and

than the temperature of the foil. Hydrogen atoms will therefore be adsorbed and will subsequently recombine to molecules, freeing the binding energy of $\sim$ 52000 K. This newly formed molecular hydrogen has a melting point of 14 K and thus will freeze out on any surface.

We measure the resistance of the resistor on the foil with a constant current of 10^{-6} A at 100 Hz, using a lock-in amplifier. The signal of this amplifier is fed to a proportional regulator regulating the amplitude of a voltage controlled oscillator at 30 kHz. The output of this oscillator is capacitively coupled to the resistor. In this way, the resistance (and thus the temperature of the pumping plate) is kept constant.

A second lock-in amplifier, measuring the 30 kHz voltage over the resistor, measures the heating voltage (typically 90 mV). The square of this voltage, divided by the resistance value, gives the electrically dissipated power (typically 15 μW).

The released binding energy from the recombined atoms is partly dumped into the pumping plate. By measuring the reduction of the necessary heating power compared to the power without flux the heat input due to the flux is determined. In this way no calibration is necessary for relative flux measurements.

If the cooling process of the pumping plate is effected by the flux, the assumption that the change in heating power corresponds to an equal change in the heating due to the flux is no longer valid. This puts an upper limit on the ambient temperature: at temperatures >450 mK the pumping plate is significantly cooled by the helium vapor. When operated with ^{3}He–^{4}He mixtures, this upper limit reduces to about 180 mK.

6.3 Measured performance

The response of the pumping plate has been calibrated using a pressure gauge. This was done by filling the buffer volume in the cell with atomic hydrogen, while the pumping plate was covered by a liquid ^{4}He film. After filling the pumping plate was heated, thereby removing the helium film. As a result, the density in the buffer, as measured by the pressure gauge, decreased because the flow through the capillary. The flow through this capillary depends on the density in the buffer volume according to

$$\Phi = nV_b/\tau \ , \tag{6.3}$$

with V_b the buffer volume and τ the time constant of the density decay.

By extrapolation of the decay as measured by the pressure gauge the flux at the start of the usable pumping plate signal could be calculated. This establishes the relation between the pumping plate signal and the flux. The noise equivalent (1σ) flux for the pumping plate turned out to be 6×10^{10} atm/s in a bandwidth of 0.4 Hz. The signal-to-noise ratio was limited by noise due to microphonic pick-up. At this setting, the maximum measurable

flux was about 6×10^{13} atm/s. The recombination energy dissipated in the pumping plate was 60 ± 10 % of the total recombination energy. In view of the geometry of the design this result gives support to the physical picture that after recombination the H_2 molecule bounces around many times before the recombination energy, stored as vibrational and rotational energy, is fully dissipated. The time constant of the plate and feedback system was 0.8 s. The calibration was done with the pumping plate stabilized at $T_{st} = 1.3$ K and was found to be insensitive to T_{st} within experimental error.

We also operated the pumping plate with varying amounts of helium in the cell. Depending on this amount the power $\dot{Q}$ to stabilize the pumping plate at $T_{st} = 1.3$ K varied from 0.7 to 15 μW. As such the device may be used to monitor variations in the helium-film thickness. Although a rough estimate of the film thickness d may be based on Eqs. (6.1) and (6.2), the use of the device as an accurate film thickness gauge requires careful calibration.

6.4 Conclusion

The pumping plate is a sensitive device for measuring the flux of atomic hydrogen. It does not need to be calibrated for relative measurements due to the feedback measuring system. The design might be improved by the use of a separate heater and thermometer resistor. The microphonic noise might be diminished by some means of maintaining the tension in the tungsten wires after cooling down. The financial support of the Stichting FOM is gratefully acknowledged.

References

[1] I.A. Khrebtov, Instr. & Exp. Tech. **27**, 781 (1984);
E.E. Haller, Infrared Phys. **25**, 257 (1985).

[2] T.J. Greytak and D. Kleppner, in *New Trends in Atomic Physics*, vol. 2, Les Houches 1982, edited by G. Grynberg and R. Stora (North-Holland, Amsterdam, 1984), p. 1125; I.F. Silvera and J.T.M. Walraven, in *Progress in Low Temperature Physics*, edited by D.F. Brewer (North-Holland, Amsterdam, 1986), Vol. **X**, p. 139.

[3] J.J. Berkhout, E.J. Wolters, R. van Roijen, and J.T.M. Walraven, Phys. Rev. Lett. **57**, 2387 (1986).

[4] J. Wilks, *The Properties of Liquid and Solid Helium* (Clarendon, Oxford, 1967).

[5] W.H. Keesom, *Helium* (Elsevier, Amsterdam, 1942) p. 230.

SUMMARY

In this thesis the scattering of atomic hydrogen, H, from the surface of liquid helium is studied. The linear dependence of the sticking coefficient s on temperature T is demonstrated for the temperature range of 73 mK to 526 mK for both ^{3}He and ^{4}He surfaces in an experiment using enhanced capillary flow to determine s. In a second experiment it is demonstrated for the first time how a widely divergent atomic beam (in our case H) may be focussed with a hemispherical concave mirror.

In Chapter 1 an introduction to these experiments is given. The origin of the quantum nature of atomic hydrogen is explained. A short overview of the development of the research on atomic hydrogen is given. The importance of the presence of liquid helium surfaces in experiments concerning atomic hydrogen is discussed.

In Chapter 2 the theory of sticking and accommodation of H on a ^{4}He surface is outlined, resulting in the expectation of low values for the sticking and accommodation coefficient. An overview is given of experimental work concerning the determination of these values.

Chapter 3 is a compact description of the capillary flow experiment. A strong enhancement of the flow of atomic hydrogen through a capillary with superfluid helium-film coated walls is observed. The flow rate is more than a factor 10 of the flow rate for ordinary Knudsen flow. This enhancement is used to extract the sticking coefficient s and show a linear decrease of this coefficient with decreasing temperature. No significant difference was found between the results using pure ^{4}He surfaces and surfaces with a layer of ^{3}He on top. Sticking coefficients as low as 4% were observed.

Chapter 4 describes the mirror reflection experiment. The use of a concave hemispherical mirror to focus a highly divergent 18-mm-wide beam of hydrogen atoms down to 0.5 mm is described. High reflectivity of at least 80% of this mirror is observed.

Both experiments are thoroughly discussed in Chapter 5. In this chapter the theoretical background is given, followed by a detailed description of the experimental setup. Particular attention is given to the determination of the roughness of the helium surfaces for both experiments, and to our thermometry. Then the results of the capillary flow experiments are thoroughly discussed. The determination of the sticking coefficient from the observed enhanced capillary flow is performed through the use of a computer simulation of this flow. We show that the result for the sticking coefficient is dependent on the exact model used

in this simulation. We analyze the results using two models, one a simple one-speed model and the other a model in which the effects of particle velocity is incorporated. While the results of the models differ by a factor 2, the linear dependence of s on T remains valid. The results of the mirror reflection experiment are reanalyzed on the basis of the results of the capillary flow experiment.

Chapter 6 contains a description of the main detection instrument used in these experiments. This atomic flux measuring device is based on a measurement of the heating due to forced recombination of the atoms in the flux. By stabilizing the temperature of the device, a large sensitivity is achieved.

SAMENVATTING

In dit proefschrift wordt de verstrooiing van atomair waterstof, H, aan het oppervlak van vloeibaar helium bestudeerd. Het lineaire verband tussen de plakkans s en de temperatuur T wordt aangetoond voor temperaturen van 73 mK tot 526 mK voor zowel ^{3}He als ^{4}He oppervlakken in een experiment dat gebruik maakt van de vergroting van capillairstroming om s te bepalen. In een tweede experiment wordt voor de eerste keer aangetoond hoe een sterk divergerende bundel van atomen (in ons geval H) kan worden gefocuseerd met behulp van een holle half-sferische spiegel.

In hoofdstuk 1 wordt een introductie tot deze experimenten gegeven. De oorsprong van de quantum-natuur van atomair waterstof wordt uitgelegd. Verder wordt een beknopt overzicht gegeven van de ontwikkeling van het onderzoek aan atomair waterstof. Het belang van de aanwezigheid van oppervlakken van vloeibaar helium wordt uitgelegd.

In hoofdstuk 2 wordt een schets gegeven van de theorie betreffende het plakken en de energie-accomodatie van H op een ^{4}He oppervlak, hetgeen resulteert in de verwachting van lage waarden voor de plakkans en de accomodatiecoëfficiënt. Verder wordt een overzicht gegeven van het experimentele werk betreffende de bepaling van de grootte van deze waarden.

Hoofdstuk 3 is een bondige beschrijving van het capillairstromingsexperiment. Er wordt een sterke vergroting van de stroming van atomair waterstof door een capillair waarvan de wanden bedekt zijn met een superfluïde heliumfilm waargenomen. De stroming is meer dan een faktor 10 hoger dan die van normale Knudsen stroming. Deze vergroting wordt gebruikt om de plakkans s te achterhalen. Het resultaat laat een lineaire afname zien van de plakkans met afnemende temperatuur. Er werd geen significant verschil gevonden tussen de resultaten die werden verkregen met gebruikmaking van puur ^{4}He en die waarbij de oppervlakken waren bedekt met een laag ^{3}He. Plakkansen tot 4% werden waargenomen.

Hoofdstuk 4 beschrijft het spiegelreflektie-experiment. Het gebruik van een holle half-sferische spiegel om een sterk divergerende 18 mm wijde bundel van waterstofatomen te focuseren tot op minder dan 0.5 mm wordt beschreven. Een hoge reflektie van ten minste 80% wordt hiermee waargenomen.

Beide experimenten worden uitvoerig besproken in hoofdstuk 5. In dit hoofdstuk wordt de theoretische achtergrond gegeven, gevolgd door een nauwkeurige beschrijving van de ex-

perimentele situatie. Bijzondere aandacht wordt geschonken aan de bepaling van de mate van ruwheid van het helium oppervlak in beide experimenten en aan onze thermometrie. Vervolgens worden de resultaten van het capillairstromingsexperiment uitvoerig besproken. De bepaling van de plakkans uit de waargenomen toegenomen capillairstroming wordt uitgevoerd door middel van computersimulaties van deze stroming. We laten zien dat het resultaat voor deze plakkans afhankelijk is van de details van het model dat bij deze simulaties wordt gebruikt. De resultaten van het experiment worden met twee verschillende modellen geanalyseerd. Het eerste model is een eenvoudig konstante-snelheids model, in het andere model worden de effekten van de snelheid en de hoek van inval van de atomen meegenomen. Hoewel de resultaten van beide modellen verschillen met een faktor 2, geven beide een lineaire temperatuurafhankelijkheid. De resultaten van het spiegelreflektie-experiment worden opnieuw geanalyseerd op basis van de resultaten van het capillairstromingsexperiment.

Hoofdstuk 6 bevat een beschrijving van de belangrijkste detektor die in deze experimenten wordt gebruikt. Dit instrument, dat de atomaire flux meet, is gebaseerd op meting van de warmte die vrijkomt als de atomen in deze flux worden gedwongen tot rekombinatie. Door de temperatuur van het instrument te stabiliseren wordt een grote gevoeligheid bereikt.

NAWOORD

Does anyone else have something further to add?

— R.A. Lafferty, *Does Anyone Else Have Something Further to Add?*.

Als sterrenkundestudent maakte ik in 1980 de fout om eerst mijn bijvakstage natuurkunde te doen. Na een rondleiding langs een aantal laboratoria koos ik hiervoor de groep Spectroscopie van de Verdichte Materie vanwege het enthousiasme van alle betrokkenen. Zoals uit het voorgaande proefschrift blijkt, is deze bijvakstage een beetje uit de hand gelopen. Desalniettemin wil ik alle personen, met wie ik in de loop van de tijd dat ik betrokken ben geweest bij het onderzoek aan atomaire waterstof heb samengewerkt, bedanken voor hun bijdrage aan het werk dat in dit proefschrift is beschreven.

Als eerste wil ik bedanken Jook Walraven. Vanaf mijn begin als student tot en met de totstandkoming van dit proefschrift heeft hij een bijzonder stimulerende uitwerking op mij gehad. Onze diskussies werden gekenmerkt door hardnekkige oppositie, respekt voor elkaar en een groot plezier in alle aspekten van het vak. Ik heb zeer veel van hem opgestoken. Bijzonder te waarderen is dat hij, gewaarschuwd als hij was door zijn ervaringen met mij als student, mij toch geheel uit vrije wil een promotieplaats aanbood. Dit is des te meer te prijzen, omdat ik op dat moment al ruim tien jaar ouder was dan andere pas afgestudeerde studenten. Ik hoop dat hij dit experiment net zo goed geslaagd vindt als zijn andere.

Aan Ike Silvera, die als hoogleraar de groep leidde tijdens mijn werk als student, bewaar ik zeer goede herinneringen. Zowel hij als de promovendus met wie ik toen begon samen te werken, Gert van Yperen, hebben een belangrijke invloed op mij gehad. Ook Stein Matthey, met wie ik de bij de in dit proefschrift beschreven experimenten gebruikte cryostaat in gebruik heb genomen, wil ik bedanken voor zijn samenwerking en vriendschap. Ad Lagendijk wil ik bedanken voor zijn begeleiding op afstand in de periode dat hij na Ike als hoogleraar de groep leidde, en voor de vele met hem gevoerde diskussies. Het doet mij genoegen dat ik hem tot het leren volkje heb kunnen bekeren.

Aan mijn experimenten hebben een groot aantal personen medegewerkt. Zonder de inzet en het technisch inzicht van onze 'eigen' instrumentmaker, Otto Höpfner, zouden onze ontwerpen nooit zijn omgezet in staal, koper en messing. Zijn eigenschap om te doen wat ik bedoelde in plaats van wat ik zei heeft het leven heel wat gemakkelijker gemaakt. Ook de studenten die hebben meegewerkt aan het capillairstromingsexperiment, Ib Lunding, Jos Mosk, Irwan Setija en Erik Wolters wil ik hier bedanken. Erik Wolters heeft op zijn eigen wijze enthousiast de simulaties van de capillairstroming voor zijn rekening genomen. Irwan Setija wil ik bedanken voor zijn inzet bij het verfijnen van de capillairstromingsimulaties. Hij en Jom Luiten hebben zich ook zeer sterk ingezet bij de metingen voor het spiegelexperiment, die daardoor op (voor mij) moeiteloze wijze verliepen. Michiel Groeneveld wil ik bedanken voor de konstruktie van de holle half-sferische spiegel die bij dit experiment het cruciale onderdeel was. I thank Takao Mizusaki for his contribution to the mirror reflection experiment, and for pointing out an error in the design of the mirror cell before it could do any harm. Ook de wetenschappelijke inbreng van Tom Hijmans bij de experimenten is van veel waarde geweest. Ik heb veel genoegen beleefd aan onze diskussies, ook op an-

der dan wetenschappelijk terrein. Computergebruik heeft door hem een nieuwe dimensie gekregen. Diskussies met Herman Beijerink, Maurice Papoular, Rudolf Sprik, Boudewijn Verhaar, Simo Jaakkola en Victor Goldman zijn zeer waardevol geweest. Ook de bijdrage van Vianney Koelman, die ons wees op een inkonsistentie in de capillairstromingssimulaties, is zeer waardevol geweest.

De wederzijdse samenwerking met mijn kollega-promovendus, Raymond van Roijen, heb ik op hoge prijs gesteld. Hij heeft bij al mijn experimenten mij met raad en daad bijgestaan. Dat deze samenwerking vruchtbaar was blijkt ook uit onze gemeenschappelijke (deels nog te publiceren) artikelen.

Tot het welslagen van de experimenten hebben ook de ondersteunende afdelingen van het laboratorium bijgedragen. Herman Pothoven en Nico Jonker wil ik bedanken voor hun inzet bij het beschikbaar maken van vloeibaar helium, ook buiten de normale werktijden. Ton Riemersma wil ik bedanken onder andere voor zijn hulp bij het vervaardigen van één van de detektoren in de capillairstromingscel. De technische en administratieve ondersteuning van Paul Langemeijer, Bert Zwart, Ron Manuputy, Ruud Scheltema, Hugo Schlatter, Eddie Inoeng, Bert Moleman en Willem Moolhuyzen, Hans Kragten, Klaas van Paasschen en Mariet Bos heb ik hogelijk op prijs gesteld. Verder wil ik Willem Mattens bedanken voor zijn steun bij het afronden van het schrijven van dit proefschrift. Albert Staalenhoef wordt bijzonder bedankt voor zijn tekening voor de omslag van dit proefschrift. Tenslotte wil ik Jeanette Bakker bedanken voor haar professionele redactie van de tekst.

Het doen van experimenteel onderzoek is altijd teamwork. Ook personen die niet direkt bij één van de in dit proefschrift genoemde experimenten zijn betrokken hebben de enthousiaste sfeer in de gehele groep bepaald. Het is goed om te zien hoe een verzameling uitgesproken individuen toch een samenhangende groep kunnen vormen. Deze goede sfeer bleek zeer duidelijk bij onze vrijdagmiddag bijeenkomsten, uit het geluidsniveau in de terminalkamer, bij diners tijdens congressen. Mick Baggen, inderdaad mijn kamergenoot, Raymond van Roijen met zijn levensblijheid, Martin van der Mark met zijn bescheiden opstelling, Ron Kroon met zijn genuanceerde uitspraken, Erik Wolters met zijn optimisme, Tom Hijmans met zijn geduld, Kees Mastenbroek als organisator van onze comfortabele zeiltochten, Erik (subtiel) Spaans, Martin (toetje) van Exter, Pedro de Vries, Han Saft, Rogier Groeneveld, Meint van Albada, Rob Vreeker, Johan de Boer, Peter Molenaar, zij allen hebben bijgedragen aan een onvergetelijke tijd.